Kathrin Müller

Organic Semiconductor Interfaces with Insulators and Metals
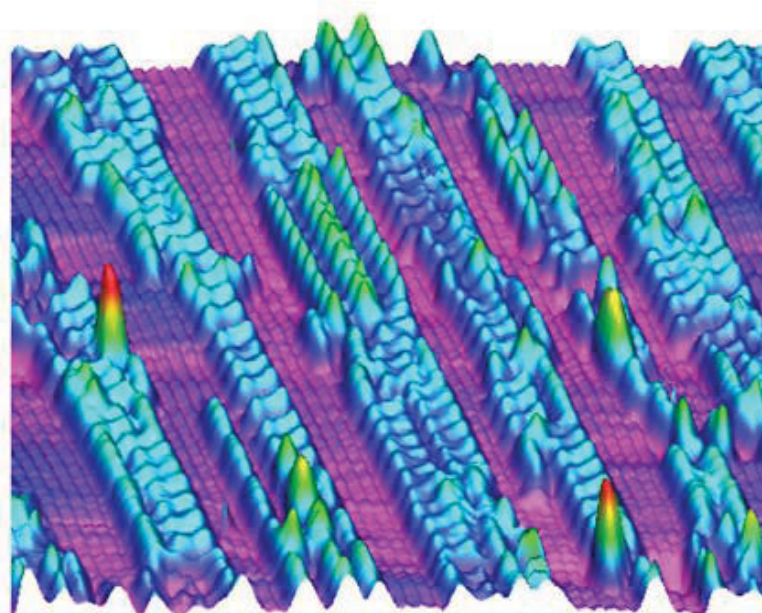
Organic Semiconductor Interfaces with Insulators and Metals

Dissertation

zur

Erlangung der naturwissenschaftlichen Doktorwürde

(Dr. sc. nat.)

vorgelegt der

Mathematisch-naturwissenschaftlichen Fakultät

der

Universität Zürich

von

Kathrin Müller

aus Deutschland

Promotionskomitee

Prof. Dr. Jürg Osterwalder (Vorsitz)
Dr. Thomas Jung (Leitung der Dissertation)
Dr. Gerhard Meyer

Zürich 2009

'If we knew what we were doing,
it wouldn't be called research,
would it?'
A. Einstein

Zusammenfassung

Die elektronischen Wechselwirkungen von organischen Halbleitern nach der Selbstanordnung auf Metallen, oxidierten Metallen und ultradünnen Isolatoroberflächen wurden mit Hilfe von komplementären Messmethoden wie Rastertunnelmikroskopie und -spektroskopie, Beugung niederenergetischer Elektronen, Röntgenphotoelektronen und Ultraviolett Photoelektronen Spektroskopie untersucht.

Zwei verschiedene Modellsysteme wurden ausgewählt und untersucht: Das erste Modellsystem umfasst die elektronischen Wechselwirkungen und die Selbstanordnung von Pentacen auf der Cu(110) sowie auf der oxidierten Cu(110) Oberfläche. In einem zweiten Modellsystem wurde die Grenzfläche zwischen Octaethylporphyrin und ultradünnen Isolatorschichten untersucht. Die Adsorption von Molekülen auf Isolatoroberflächen ist von besonderer Bedeutung, da diese sowohl die elektronischen als auch die chemischen Wechselwirkungen der Moleküle mit der Oberfläche deutlich reduzieren können.

Bei der Untersuchung von Pentacen auf Cu(110) konnte ein komplexes Phasen-Verhalten beobachtet werden, das durch Verbiegen der Moleküle, unterschiedliche Anordnung der Moleküle, unterschiedliche Bedeckungen und die Molekülmobilität charakterisiert ist. Weiterhin wurde der Einfluss der adsorbierten Pentacen-Moleküle auf den Shockley-Oberflächenzustand der Cu(110) Oberfläche untersucht. Durch ein komplexes Zusammenspiel mehrerer physikalischer Phänomene wie die Pauli Abstossung, Ladungstransfer, Hybridisierung von elektronischen Zuständen sowie die Polarisation der Adsorbate im Dipolfeld der Oberfläche wird der Oberflächenzustand zu grösseren Bindungsenergien verschoben. Bei der Adsorption einer Monolage Pentacen nimmt zusätzlich die Besetzung des Oberflächenzustandes zu. Ein ähnlich komplexes Verhalten von Struktur und elektronischen Wechselwirkungen wurde bislang für kein anderes Molekül/Metall System gezeigt. Das Adsorptionsverhalten von Pentacen auf der oxidierten Cu(110) Oberfläche zeigt, dass sowohl die elektronischen Wechselwirkungen als auch die Oberflächenkorrugation eine grosse Rolle bei der Selbstanordnung spielen.

Das zweite in dieser Dissertation studierte Modellsystem befasste sich mit den elektronischen Wechselwirkungen von Kupfer-Octaethylporphyrinen (CuOEP) mit ultradünnen Isolatorschichten. Die Hauptfragestellung bei diesem Projekt war, wie die elektronische Wechselwirkung zwischen Molekülen und Substrat mit zunehmender Isolatorschichtdicke abnimmt und ob es bei sehr geringen Schichtdicken (eine oder zwei Monolagen) möglich ist, die Moleküle vom Substrat elektrisch zu isolieren. Eine detaillierte Wachstumsstudie von NaCl auf unterschiedlichen Metallsubstraten führte zu homogenen, eine Monolage dicken NaCl Filmen, die mit nicht-lokalen Analyse-Methoden wie UPS und XPS untersucht werden können. Mittels Tieftemperatur STM und winkelaufgelöstem UPS konnte festgestellt werden, dass die Moleküle stark mit der Cu(111) und Ag(111) Oberfläche wechselwirken, was zu unbesetzten elektronischen Zuständen in der Bandlücke des Moleküls sowie zu einer Auslöschung des Shockley-Oberflächenzustandes führt. UPS- und XPS-Messungen an diesem System zeigten einen starken Einfluss der chemischen Umgebung, was zu einer Verschiebung der Bindungsenergien von CuOEP auf NaCl verglichen mit CuOEP auf der Metalloberfläche führt. Diese Verschiebungen können auf eine unterschiedliche Abschirmung des Photoloches zurückgeführt werden.

Abstract

The electronic interactions of self-assembled organic semiconductors with metals, metal-oxides and ultrathin insulator surfaces have been investigated by complementary analysis techniques comprising scanning tunnelling microscopy and spectroscopy, low energy electron diffraction, x-ray photoelectron spectroscopy and ultraviolet photoelectron spectroscopy.

Two model systems have been chosen and investigated: The first model system comprises the electronic interactions and the self-assembly of pentacene molecules on the Cu(110) as well as on the oxidized Cu(110) surface. In a second model system the interface of octa-ethyl porphyrins with ultrathin insulator films and metals has been investigated. The adsorption of molecules on insulator surfaces is especially interesting due to the strong reduction of the electronic and chemical interactions between the molecules and the substrate.

The investigation of pentacene on the Cu(110) surface revealed a multi-phase behaviour, which is characterized by molecular bending, molecular mobility, different relative orientation of the molecules and different packing densities. Furthermore, the influence of the adsorbate layer on the Shockley surface state of the Cu(110) has been investigated. A complex interplay of different phenomena, like Pauli repulsion, charge transfer, mixing and hybridization of electronic states as well as the polarization of the organic adsorbate in the surface dipolar field, lead to a shift of the surface state to higher binding energies. Additionally, the occupation of the surface state is increased for the adsorption of one monolayer of pentacene. This particular behaviour has not been reported for any other molecular/metal system so far. The adsorption of pentacene on the oxidized Cu(110) surface reveals that the electronic interactions and the surface corrugation determine the self-assembly of the molecular ad-layer.

The second project in this thesis comprises the electronic interactions of porphyrin molecules, another representative of molecular semiconductors, with ultrathin insulator layers. The main question here was how the electronic interactions between the molecules and the substrate change with increasing insulator thickness and whether it is possible to electronically decouple the molecules from the substrate for one or two monolayer thin insulator films. A detailed growth study of NaCl on different metal surfaces led to samples, which were homogenously covered with 1 ML of NaCl and thus could be investigated by non-local analysis techniques like UPS and XPS. Low temperature STS and angle-resolved UPS data showed that the CuOEP molecules strongly interact with the Cu(111) and Ag(111) substrate leading to unoccupied electronic states in the band gap of the molecule on Ag(111) and to quenching of the Shockley surfaces state for the adsorption of CuOEP on Cu(111). Further UPS and XPS measurements revealed a strong influence of the chemical environment on the binding energies, as identified by shifted peaks for CuOEP on NaCl compared to CuOEP on the metal surfaces. These peak shifts have been related to strong screening of the photoelectron hole.

List of acronyms

2D	Two-dimensional
3D	Three-dimensional
5C	Pentacene
AC	Analysis Chamber
ARPES	Angle-Resolved Photoelectron Spectroscopy
a.u.	Arbitrary Unit
CoOEP	Cobalt (II) octa-ethyl porphyrine
CuOEP	Copper (II) octa-ethyl porphyrine
DOS	Density of States
E_{bind}	Binding Energy
E_F	Fermi Energy
E_{kin}	Kinetic Energy
ESCA	Electron Spectroscopy for Chemical Analysis
(O)FET	(Organic) Field-Effect Transistor
FFT	Fast Fourier Transformation
HOMO	Highest Occupied Molecular Orbital
IPES	Inverse Photoelectron Spectroscopy
LEED	Low Electron Energy Diffraction
LiCl	Lithium Chloride
LT	Low Temperature
LUMO	Lowest Unoccupied Molecular Orbital
ML	Monolayer
NaCl	Sodium Chloride
NEXAFS	Near Edge X-ray Absorption Fine Structure
OEP	Octa-ethyl porphyrine
Pc	Phthalocyanine
PES	Photoelectron Spectroscopy
PTCDA	3,4,9,10-perylene tetracarboxylic dianhydride, $C_{24}H_8O_6$
QCMB	Quartz Crystal Microbalance
RHEED	Reflection High Energy Electron Diffraction
RT	Room Temperature
SIS	Surface/Interface Spectroscopy
SLS	Swiss Light Source
SPM	Scanning Probe Microscope/Microscopy
STM	Scanning Tunnelling Microscope/Microscopy
STS	Scanning Tunnelling Spectroscopy
TSP	Titanium Sublimation Pump
UHV	Ultra-High Vacuum
UPS	Ultraviolet Photoelectron Spectroscopy
XPS	X-ray Photoelectron Spectroscopy
Φ	Work Function

Contents

1 Introduction and outline

1.1 Organic molecular electronics

Organic molecular electronics can be divided into two fields: (i) *organic electronics* and (ii) *(single) molecular electronics*. In this thesis the latter term will be used in the context of single molecules in electronic devices as storage units or as single molecular switches. The first term – organic electronics – represents organic molecular thin films in electronic devices like photovoltaic[1] or organic light emitting diodes[2]. The exploration of organic materials for electronic applications has already started in 1963, when Weiss et al. reported first about a conducting polymer, namely Polypyrrole[3]. Organic electronic devices already found their way to applications like e.g. mobile phone displays and flexible displays, while the concept of molecular electronics is still a topic of basic research and remains far away from application, to date. The research reported in this thesis, which is based on the study of molecular/substrate interfaces, may lead to a deeper insight into both fields of organic molecular electronics.

Moore's law predicted that the number of transistors per area doubles every 18 to 24 months. Astonishingly, this prediction has been valid over several decades, but it is facing new challenges at the moment because fundamental physical properties lead to a minimum layer thickness of the silicon dioxide gate of five layers[4,5]. Muller et al. predicted the end of Moore's law in the year 2012 because the current gate oxide thickness is already getting close to its minimal value, which shall be reached by then[4]. This raises the attention of researchers and technologists and asks for new concepts and new materials to satisfy the continuously increasing demand for fast, highly integrated processors and devices.

Today, silicon transistors are made with photolithographic procedures by the *top-down* approach, starting from the homogenous surface of a silicon wafer. The photon energy used in photolithography techniques has been shifting to ever smaller wave lengths, to manufacture devices with ever smaller size of the minimal transistor channel length, which is at 32 nm today[6]. In spite of other predictions, optical lithography is used to date and alternative higher resolution lithography techniques like electron beam lithography are not yet established in device manufacturing. The particular disadvantages of this sequential technique result from the time consuming and therefore costly processes, which have so far always motivated the further development of optical methods. An alternative way to reproduce well defined and identical structures is by *bottom-up* self-assembly. This completely new approach, however, has so far failed to make structures large enough to allow for reliable top-down contacting and integration. However, this bottom-up approach may contribute to further decrease the size of well defined atomic or molecular structures in electronic devices. Ultimately, bottom-up self-

assembly and top-down manufacturing have to be combined in order to contact and integrate complex devices[7].

Next to the possibility to use bottom-up self-assembly, organic materials exhibit several advantages also for current day organic electronic devices. These advantages include their applicability to a huge variety of substrates including flexible layers[8]. In contrast, the silicon technology is restricted to hard crystalline solid substrates, which usually consist of SiO_2 on Si. Further advantages of organic materials for electronic applications are the low temperature processability, the fairly low-cost of materials and processes and the low specific weight[9]. Advancements in the fabrication of organic thin film devices led to charge carrier mobilities of more than $1\,cm^2V^{-1}s^{-1}$, which are comparable to those of amorphous silicon thin film transistors[10].

The performance of organic FET strongly depends on interface properties[11], which determine the charge carrier mobility, as well as the charge injection at the source and drain electrodes[12]. Lately, it has been shown that by specific design of the gate dielectric charge carrier mobilities of up to $5.5\,cm^2V^{-1}s^{-1}$ could be obtained for pentacene. These high charge carrier mobilities were related to the interface characteristics and not to different growth modes or different defect densities of the pentacene thin film[13]. For further improvements of organic electronic devices the fundamental characteristics of the interfaces – the organic/gate dielectric as well as the organic/metal drain and source interfaces – have to be studied and understood in detail. This research on interface properties may lead to specially designed active interfaces for organic electronic devices with characteristic performance.

1.2 Organic molecular self-assembly

The idea of reducing machines and computers down to the scale of atoms and molecules was already stated in 1959 by Richard P. Feynman's famous talk "*There's plenty of room at the bottom*" at the annual meeting of the American Physical Society at the California Institute of Technology[14]. Since then, many improvements in the formation as well as in the characterisation techniques of very small structures have been obtained. A decisive step towards the atomically precise positioning of atomic or molecular objects, which was already proposed by Feynman, was made by the invention of the scanning tunnelling microscope (STM) in 1982[15]. This very unique technique provides the possibility of imaging and manipulating atomic structures on surfaces[16]. For example, by atomic positioning of xenon atoms switching systems accessible by the STM tip have been realized[17]. However, it should be noted, that the piecewise arrangement of single atoms or molecules to complex electronic devices by means of an STM tip as realized by Heinrich et al. with CO adsorbates on Cu(111)[18] is time consuming and thus seems to be hardly feasible for technological application.

To avoid piecewise assembly of individual atomic and molecular components, self-assembly, as demonstrated in supra-molecular chemistry[19], provides an alternative. In a more technological sense, self-assembly has been introduced for the design of nanostructures by tuned physical growth processes in semiconductors. More recently, the definition of molecular self-assembly as the "spontaneous association of molecules under equilibrium conditions into stable, structurally well-defined aggregates joined by noncovalent bonds"[20] has been brought about. This definition is used to differentiate self-assembly from self-organization, which requires external energy from an open system and is usually far away from equilibrium. Although self-assembly and self-organization can be clearly distinguished on the basis of thermodynamics[21] they are also often used as synonyms by some authors and in some scientific communities. The patterns obtained with both processes can be quite similar, but usually the time and length scales required for assembly of the structures are different[22].

Self-assembly at surfaces crucially depends on intermolecular and molecular/substrate interactions and on the registry or corrugation felt by the particular adsorbate on the particular surface. The deposition of organic molecules on low-reactivity metals or semiconductor substrates leads to a higher degree of ordering by self-assembly than on reactive metals or highly corrugated surfaces. On reactive or highly corrugated surfaces the diffusion is insufficient to allow for self-assembly, as the molecular adsorbate cannot find the position with minimal energy before immobilization.

On ultrathin insulator films on the other hand, the typical adsorbate/substrate interaction is quite low, which leads to mobile molecules at room temperature for low coverage. Therefore, molecular/insulator/metal systems in comparison to molecular/metal interfaces provide very good model systems to study the electronic interaction of the adsorbate with substrates of different characteristic properties. By using ultrathin insulators with their thickness varying from one to some monolayers, the relevant interactions for self-assembly and electronic interactions can be tuned and studied in detail[23].

The work presented in this thesis is the result of a step by step approach to obtain detailed insight into the specific properties at the molecular/substrate interface. Surfaces with different reactivity and different electronic structure have been used to study the self-assembly as well as the electronic adsorbate/substrate interaction.

In the first step the highly interacting system of pentacene on Cu(110) has been studied. In detail, the influence of the molecular adsorbate on the substrate electronic states in different self-assembled phases[24] and vice-versa the influence of the substrate on the self-assembly has been investigated. For the first time a complex multi-phase behaviour of pentacene in the first molecular layer has been observed by a systematic study on this very intensely studied system[25].

In the second step the molecular/substrate interactions have been modified by oxidation of the Cu(110) substrate prior to pentacene deposition, which changes the molecular/substrate interaction considerably[26]. Additionally, it was possible to reduce the intermolecular interactions by separating molecular chains with CuO adsorbates.

In the last step a series of experiments has been performed, where octa-ethyl porphyrins have been adsorbed on ultrathin insulators, which are used for a further reduction of the molecular/substrate interaction. This approach was especially challenging because it required a suitable system, which could be analysed by local and non-local techniques like STM, LEED, UPS and XPS. The application of non-local surface analysis techniques like XPS and UPS asks for homogenous surfaces, which can usually not be provided by evaporation of insulators on metal substrates because these typically grow in a Volmer-Weber (island) growth mode. This task has been successfully accomplished and homogenous layers of NaCl have been grown on the stepped Cu(311) surface.

1.3 Outline

The presented work is organized as follows: After the introduction to organic molecular electronics and molecular self-assembly the most important aspects on thin film growth will be reviewed. This part serves as a basis for the discussion of the growth phenomena and their optimization towards homogenous ultrathin alkali halide films on metal surfaces; reported about in chapter 5.2. The experimental techniques and details including the sample preparation are described in chapter 3. In the fourth chapter the monolayer self-assembly of pentacene on Cu(110) as well as on the oxidized Cu(110) will be described. At the beginning of this chapter a brief motivation is provided, which is then followed by two full papers published in Physical Review B[24,25]. The first paper covers the influence of pentacene adsorption on the Cu(110) Shockley surface state. The second paper reports about monolayer multimorphism for pentacene on Cu(110). Chapter 4.4 reports about the interaction of pentacene with the p(2x1)O reconstructed Cu(110) surface and chapter 4.5 about the influence of oxygen exposure on the self-assembly of pentacene.

The fifth chapter deals with the interaction of octa-ethyl porphyrins (OEPs) with metals and ultrathin insulator surfaces. After an introduction to ultrathin insulators and organic molecules on insulators the self-assembly and growth of LiCl on Cu(001) and NaCl on different metal surfaces is described. Results on the electronic interaction of OEPs with NaCl and metal substrates by scanning tunnelling spectroscopy (STS), ultraviolet photoelectron spectroscopy (UPS) and x-ray photoelectron spectroscopy (XPS) are shown and discussed in chapter 5.3. The final chapter with concluding remarks will complete the main part of this thesis.

2 Thin film growth

2.1 Nucleation and epitaxy

Epitaxy is the deposition of a single crystalline film on a single crystal substrate[27]. Thin films are layers of material on a substrate with thicknesses ranging from a fraction of a nanometre to some micrometers[28]. Thin film properties often differ from bulk properties due to different defect structures, their quasi two-dimensionality (ultrathin films) and the strong influence of surface and interface effects. Thin film growth is influenced by a large variety of physical effects like thermodynamics and kinetics, crystallography, as well as electronic, mechanic and magnetic properties. The grain size of the thin film or the domain size of the first layer is mostly determined by the deposition rate and the substrate temperature, which affect the nucleation and diffusion of the adsorbates[29]. High temperature and/or low deposition rate result in large crystal grains/domains, while low temperature and/or high deposition rate lead to small grains/domains.

In UHV conditions, three steps in the deposition of material on a surface can be distinguished: (i) emission of the material (e.g. atoms, molecules or ion pairs) by sublimation, (ii) collision free transfer of the material to the surface, (iii) condensation on the surface. The third step mostly determines the thin film growth and can be viewed as a multi step process[29]: (i) energy loss of the impinging particles to stay on the surface, (ii) binding to the surface (either physisorption or chemisorption), (iii) surface diffusion and cluster formation, (iv) nucleation, (v) island growth, (vi) coalescence of the islands, (vii) continued three-dimensional growth of the islands. During the nucleation small numbers of particles meet and arrange in a crystalline pattern. Thereby, they form sites where additional particles can be trapped and initiate the growth process[30]. The initial nucleation usually takes place at defects like steps, kinks or dislocations due to the lower coordination sites, which exhibit a higher desorption barrier of the particles at these defects.

2.2 Growth modes of thin films

In general, there exist three different growth modes of epitaxial films as illustrated in Figure 1. These growth modes depend on the lattice misfit, on the differences in the binding energies between the particles and between particles and the surface, on diffusion and on the surface tension. For the Volmer-Weber (island) growth mode (cf. Figure 1, right) the interaction between the particles is stronger than the interaction between particles and surfaces. In contrast, in the Frank van der Merwe growth mode the adsorbates bind more strongly to the surface which results in a layer by layer growth (cf. Figure 1, left). The

Stransky-Krastanov growth mode is an intermediary process, where a layer-by-layer growth, i.e. the formation of a wetting layer with thicknesses up to several monolayers, is followed by island growth on top of the wetting layer (cf. Figure 1, centre). Stransky-Krastanov growth usually results from the strain, induced in the fist monolayers, due to the lattice misfit.

Frank van der Merwe   Stransky-Krastanov   Volmer-Weber

Figure 1: Different thin film growth modes as described in the text.

3 Experimental techniques and set-up

3.1 Experimental techniques

In this thesis several complementary surface sensitive techniques, like STM and STS, XPS, UPS and LEED have been used. This chapter provides an introduction into these techniques and into some particularities, which are necessary for the interpretation of the data.

3.1.1 Scanning tunnelling microscopy and spectroscopy

The scanning tunnelling microscope (STM) was invented in 1982 by Binnig and Rohrer[15], who were honoured with the Noble prize in 1986. The invention of a microscope, which provides a three-dimensional real space image of a surface with atomic resolution, allowed spatially localized investigation of the electronic and geometric properties of surfaces. The invention of the STM gave rise to several further scanning probe techniques like atomic force microscopy, magnetic force microscopy and chemical force microscopy, which expanded the field of surface science. With the wide parameter-sets possible for all scanning probe techniques, like variable temperature and variable pressure, different physical and chemical information can be acquired. SPMs are used (i) to access electronic states of surface adsorbates with a very good lateral resolution[31], (ii) to directly investigate chemical reactions at the solid liquid interface[32] and (iii) to laterally and chemically manipulate[33] adsorbates on surfaces. For a detailed description of the various scanning probe techniques the reader is referred to several text books[34,35].
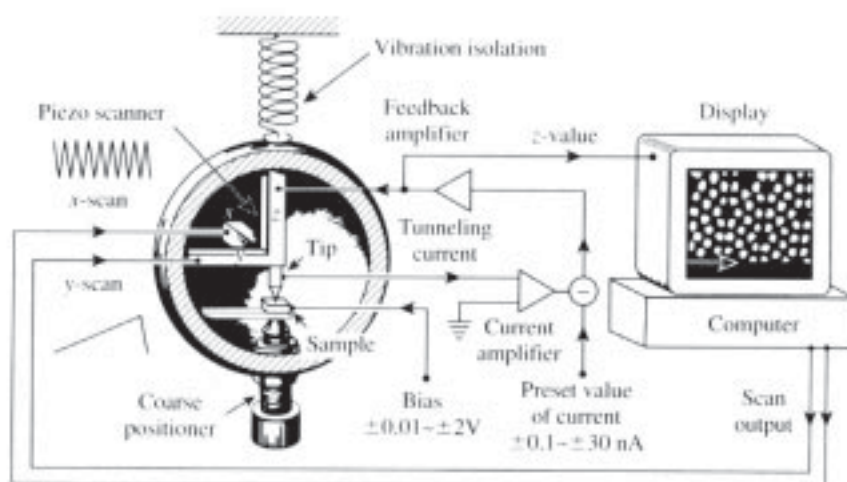

Figure 2: Set-up of an STM from[34].

3 EXPERIMENTAL TECHNIQUES AND SET-UP

The set-up of a scanning tunnelling microscope is shown in Figure 2. An STM tip usually made of electrochemically etched W or wire-cut PtIr is attached to a three-piezo scanner (x, y and z) or a piezo tube. A bias voltage is applied between the tip and the sample to establish a tunnelling current, when the tip is in close proximity to the surface (~1 nm). By using piezoelectric actuators the tip scans the surface line by line with a very high local accuracy. The tunnelling current measured at each point is amplified and compared to a reference value. Using the z-piezo actuator to adjust the tip elevation above the substrate the tunnelling current can be kept constant. Thus, a topographic image of the surface can be acquired by plotting the z-position in dependence of the x- and y- position of the tip, as seen in the display in Figure 2. This measurement technique is called constant current mode. Another measurement method is the so called constant height mode. Here the z-position of the tip is kept constant and the current in dependence on the x- and y-position is displayed directly. For the latter technique higher scanning speeds can be achieved because the z-displacement does not need to be adjusted via the feedback loop. Therefore, a higher resolution can be obtained, but it is limited to very flat surfaces otherwise the tunnelling contact may be lost or the tip may crash into the surface. For atomic resolution a sufficient damping and vibration isolation between the microscope and the environment is necessary.

In the following, a brief overview of the electronic nature of the tunnelling process will be given. Figure 3 shows schematically the energy diagram of a vacuum tunnelling barrier between an STM tip (T) and the sample (S). The density of states (DOS) of the tip is assumed to be featureless near the Fermi energy whereas the density of states of the sample varies with energy, which is usually the case for semiconducting samples or organic adsorbates. In Figure 3a the absolute value of two wave functions with different energies are displayed and both decay exponentially in the vacuum with the decay length of the lower lying states being smaller (cf. equation 1). When the tip and the sample are separated the vacuum levels of both are equal; the position of the Fermi level (E_{Fermi}) is given by the work function (Φ) of the tip and the sample, respectively. When both are brought to close contact (usually 0.5-5 nm distance between the tip and the sample for STM measurements), tunnelling of electrons between both materials is possible and the Fermi levels in the thermal equilibrium are aligned, resulting in a change of the vacuum level of the sample with respect to the vacuum level of the tip (Figure 3b). When a negative voltage V is applied to the tip a rigid shift of the energy states of the tip with respect to the energy states of the sample by approximately eV occurs. This results in a net tunnelling current from the occupied states of the tip into the unoccupied states of the sample (Figure 3c). When a positive voltage is applied to the tip a tunnelling current in the opposite direction, i.e. out of occupied states of the sample into unoccupied states of the tip occurs (Figure 3d). The arrows in Figure 3c and d indicate the tunnelling probability depending on the energy of the electrons according to equation 1. Thus, the main contribution to the tunnelling current results from the highest lying states due to the energy dependent decay length of the electron wave functions as indicated in Figure 3a.

$$\Psi \approx \exp(-\kappa d) \qquad\qquad \kappa = 2\sqrt{-2mE}/\hbar \qquad\qquad \textbf{(1)}$$

8

By changing the applied bias it is possible to spectroscopically measure the occupied and unoccupied states of the sample. Figure 3d shows that it is difficult to detect the lower lying occupied states (HOMO–1, HOMO–2) of the sample because the biggest amount of the tunnelling current results from the states near the Fermi energy and the contribution of lower lying states to the tunnelling current is comparably small. In consequence, the unoccupied states can be easier detected with scanning tunnelling spectroscopy (STS) than the occupied states. To directly acquire the DOS of the sample scanning tunnelling spectroscopy can be performed by placing the tip on top of the point of interest, switching off the feedback loop and measuring a current/voltage curve. Due to the dependence of the tunnelling spectra on the DOS of the tip it is often advantageous, if not essential, to compare the scanning tunnelling spectra with complementary analysis methods like UPS, NEXAFS and/or IPES.
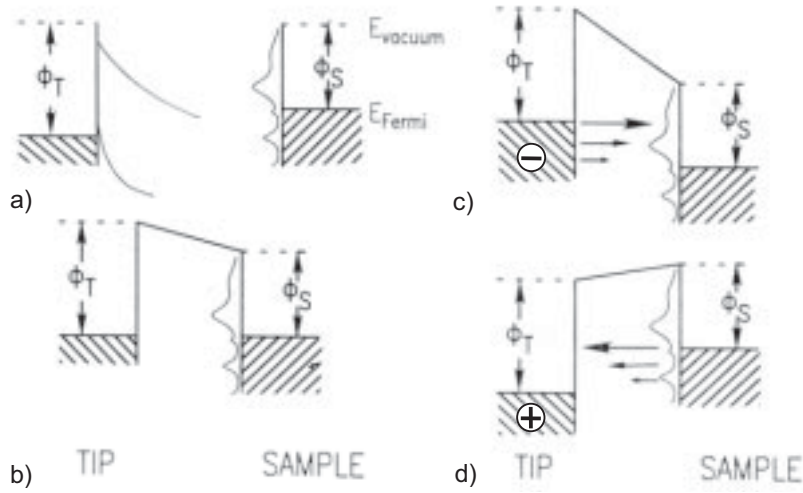
Figure 3: Energy diagram of the vacuum tunnelling barrier between the STM tip and the sample a) tip and sample separated, b) tip and sample in close contact, c) negative voltage applied to the tip, d) positive voltage applied to the tip; from[35].

To estimate the tunnelling current the Wentzel–Kramers–Brillouin (WKB) approximation can be applied as shown in equation 2: d is the distance between the tip and the sample, m is the electron mass and V is the applied tunnelling voltage.

$$i(d,V) \cong \frac{2\pi e}{\hbar}\left(\frac{\hbar^2}{2m}\right)^2 \int_0^{eV} \rho_s(E)\rho_t(E-eV)T(d,V,E)dE \qquad \textbf{(2)}^{36}$$

Thus, the tunnelling current density depends on the DOS of the sample (ρ_s), on the DOS of the tip (ρ_t) and on the transmission function T, which is given in equation 3.

$$T(d,eV,E) = \exp\left(-\frac{2d\sqrt{2m}}{\hbar}\sqrt{\frac{\Phi_s + \Phi_t}{2} + \frac{eV}{2} - E}\right) \qquad \textbf{(3)}^{36}$$

Equation 2 shows that the tunnelling current directly depends on the DOS of the sample, as already discussed in the previous paragraph. Thus, to study the DOS of a sample one can differentiate the tunnelling current. Assuming a constant DOS of the tip and a slowly changing transmission function the derivative of the tunnelling current can be approximated according to equation 4. The tip quality and the density of states of the tip is usually controlled by measuring tunnelling spectra on the clean well-known substrate.

$$\frac{\partial i(d,V)}{\partial V} \approx \rho_t(0)\rho_s(E)T(d,V,eV) \qquad \textbf{(4)}^{36}$$
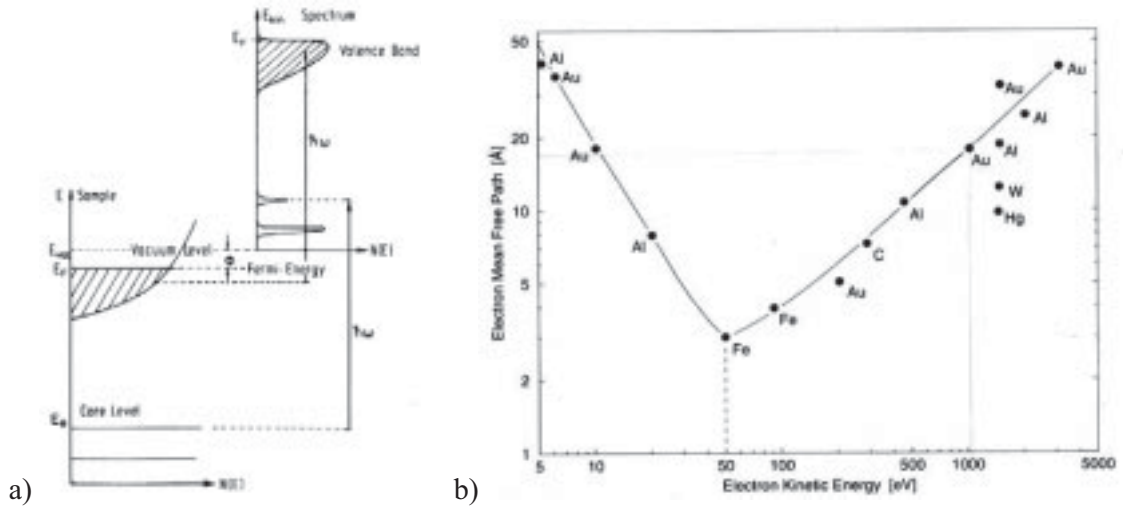
3.1.2 Photoelectron spectroscopy

Figure 4: a) relation between the energy levels of a solid and the resulting electron energy distribution; b) electron mean free path depending on the electron kinetic energy; from[37].

The phenomenon of photoemission of electrons from materials was already discovered in 1887 by Hertz[38] and in 1905 Einstein delivered the explanation of this so called photoelectric effect using the quantum nature of light[39]. The photoemission process and the resulting photoemission spectrum is schematically depicted in Figure 4a. A sample is irradiated with photons with a well defined energy $\hbar\omega$. The energy is transferred to the electrons of the material and as a consequence the electrons can leave the material with a kinetic energy (E_{kin}) which is given in equation 5, where E_{bind} is the binding energy of the electron with respect to the Fermi energy and Φ is the work function of the sample. Due to the relatively small electron mean free path for electron kinetic energies between 50 and 1000 eV (cf. Figure 4b) this technique is highly surface sensitive and thus very well suited for studying adsorbates on surfaces. Due to the element specific binding energy of the electrons this technique is also called Electron Spectroscopy for Chemical Analysis (ESCA). One main application area for

ESCA is the determination and quantification of the elemental composition of unknown materials.

$$E_{kin} = h\nu - E_{bind} - \Phi \tag{5}$$

The photoemission process can be described by a three step model. In the first step the photo-ionization takes place, i.e. the electron is excited. In a second step this electron is transported to the surface and finally the electron escapes from the surface into the vacuum in the third step. During the transport of the electron to the surface inelastic scattering of the electron can take place resulting in a decrease of the kinetic energy. This results in an increasing background with increasing binding energy of the photoemission spectra. The three step model is a rather simple picture and the photo-ionization, i.e. the first step of this model is actually more complex because it has to be viewed as a many-body process. After removal of the electron from the *N*-electron system a positively charged hole remains which leads to a (*N-1*)-final state. Usually the binding energy of the emitted electron calculated by equation 5 is smaller than the real binding energy due to the different energy of the (*N-1*)-system compared to the *N*-system. During the relaxation of the excited system the relaxation energy is released and can be transferred to the photoelectron to increase its kinetic energy. In consequence one has to rewrite equation 5 like it is done in equation 6:

$$E_{kin} = h\nu - (E_f^{N-1} - E_i^{N}) - \Phi \tag{6}$$

The measured effective binding energy ($E_{b,eff}$) depends on several terms as shown in equation 7[40]:

$$E_{b,eff} = E_b(atom) + \Delta E_{chem} + \Delta E_{Mad} + \Delta E_{r,int} + \Delta E_{r,ext} \tag{7}$$

The chemical shift ΔE_{chem} describes the effective charge of the atom and the influence of the nearest neighbours to the binding energy of the electron. If the atom is surrounded by electronegative neighbours, the electrons are attracted by the neighbouring atoms which results in a higher binding energy of the core electrons. This effect can be well seen for halide-containing molecules. For example, the binding energy of the C1s electron of CF_4 is 296.7 eV compared to CHF_3 which has a binding energy of 294.7 eV[41]. The chemical shift is a very important factor for determining the chemical composition of unknown materials, especially for polymers and organic molecules.

The Madelung term ΔE_{Mad} is only valid for ionic crystals and describes the electric potential of all lattice components at the central atom. For ionic crystals the Madelung term can often completely compensate the chemical shift.

The relaxation energies consider the multi-particle effects which lead to a larger kinetic energy of the photoelectrons. Generally, the relaxation can be divided into two factors the internal relaxation $\Delta E_{r,int}$ and the external relaxation $\Delta E_{r,ext}$. The latter term considers the polarizability of the medium surrounding the atom. The local positive charge of the photohole can be screened by attraction of the surrounding electrons. The internal relaxation ($\Delta E_{r,int}$) results from a shifting of the electronic orbitals towards the core as well from relaxation of the

exited system by filling of the photohole with an electron from a higher orbital. Parts of this relaxation energy can be transferred to the photoelectron which results in a higher kinetic energy and in consequence in a smaller binding energy.

3.1.3   *Low energy electron diffraction*

Low energy electron diffraction (LEED) is a very valuable tool to determine the surface structure of a sample[40,42]. Electrons with a kinetic energy of 20 to 500 eV are used, which results in a de Broglie wavelength in the range of atomic distances ($\lambda = 0.05$ to 0.3 nm). Electrons with low kinetic energy interact strongly with the surface atoms. As a consequence they penetrate only 1-5 nm into the surface (cf. Figure 4b, page 10), which renders this technique highly surface sensitive. In the special case of ad-layers on surfaces the adsorbate unit cell can be determined with respect to the known substrate unit cell provided that the adsorbates show a long-range periodic ordering on the surface.

Figure 5a shows the set-up of a LEED system consisting of an electron gun, which emits electrons with variable energy, the grounded sample and the detection unit (four grids and a fluorescent screen). The first grid (counted from the sample) is grounded to insure a free field region around the sample. Grid two and three are held at slightly smaller biases than the kinetic energy of the electrons to repel the inelastically scattered electrons. Thus, only the elastically scattered electrons can pass the fourth grid and are then accelerated to the fluorescent screen, which is set to a high positive bias. Behind the screen a window in the UHV system equipped with a video camera allows direct recording of the diffraction pattern.
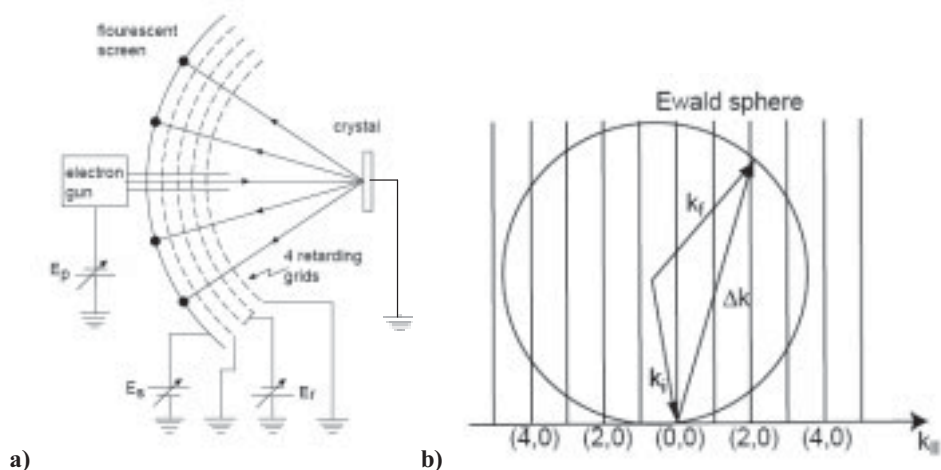

Figure 5: a) LEED system with the electron gun the crystal, the four retarding grids and the fluorescent screen; b) Ewald's sphere construction for diffraction from a 2D lattice; from[42].

Due to its very high surface sensitivity we can consider the LEED pattern as a diffraction from a two-dimensional (2D) lattice. When this 2D lattice in real space is transferred to the reciprocal space, which is actually displayed in the LEED pattern, the reciprocal space consists of lattice rods because an infinite distance in the third dimension in real space leads to an infinitesimal distance in the reciprocal space. The Ewald construction to find the Laue conditions for constructive interference for a 2D reciprocal lattice is shown in Figure 5b. The initial wave vector k_i, which is given by the wave length of the incident beam ($k_i = 2\pi/\lambda$) defines the radius of the Ewald sphere. Constructive interference is given, if the scattering vector $\Delta k = k_i - k_f$ coincides with the reciprocal lattice rods, which is always fulfilled when the initial wave vector is large enough to intersect with a rod. The fact that for different electron energies some diffraction spots disappear and reappear for other energies can be related to the simplification of the third dimension being infinitive, which is effectively not the case.

3.2 Sample preparation and experimental details

All single crystals were purchased from Mateck[43] and the initial preparation was carried out by Ar^+ sputtering/annealing cycles with increasing annealing temperature for each cycle. After the successful initial preparation of the single crystals three sputtering/annealing cycles with decreasing sputtering energy were performed as shown in Table 1, until neither carbon nor oxygen were found in the XPS spectra and the samples exhibited flat surfaces with big terraces as imaged in the STM. Before evaporation of organic molecules or oxygen exposure the samples have been cooled to approximately room temperature with a gaseous nitrogen stream. For evaporation of the insulators, which was most times carried out at elevated sample temperatures, the annealing temperature was reduced after the last annealing step and the samples have not been cooled to room temperature.

Table 1: Single crystal preparation procedure.

Sample:	1st sputtering	2nd sputtering	3rd sputtering	Annealing
Ag(111)	1.5 keV, 20 min	1.0 keV, 20 min	0.8 keV, 20 min	770 K 20 min
Cu(111)	1.5 keV, 20 min	1.0 keV, 20 min	0.8 keV, 20 min	770 K 20 min
Cu(100)	1.5 keV, 20 min	1.2 keV, 20 min	1.0 keV, 20 min	810 K 30 min
Cu(311)	1.2 keV, 20 min	1.0 keV, 20 min	0.8 keV, 20 min	770 K 30 min
Cu(110)	1.5 keV, 20 min	1.2 keV, 20 min	1.0 keV, 20 min	810 K 20 min

Both, organic molecules and insulators were evaporated with a rate of 0.2 - 0.5 ML/min. The evaporation time was estimated by the frequency change of a water-cooled quartz crystal microbalance (QCMB) before evaporation. For molecular deposition the frequency was also controlled after the evaporation to view possible changes of the evaporation rate during the

deposition. The coverage was calculated by the main XPS peak of the adsorbate (C1s and/or Na1s, Cl2p, O1s) and the substrate XPS peak (Cu2p or Ag3p) as well as by the STM images. 1 ML refers to the amount of material necessary to produce the most densely packed monolayer. The oxygen exposure was accomplished at oxygen partial pressures of 2.5-7.5*10^{-10} mbar in the STM chamber.

After the sample preparation, the STM measurements were usually performed before the LEED and XPS studies. This analysing sequence was chosen to reduce electron and/or photon beam-damage before the STM images were taken.

The XPS and UPS data were recorded with a PHOIBOS hemispherical electron energy analyser from Specs. The acceptance angle was 16° for both UPS and XPS measurements. All XPS spectra were recorded with a non-monochromatized Al Kα-source and the UPS spectra were taken with a non-monochromatized HeI source. For the determination of the secondary electron cut-off the samples were biased with 9 V, whereas the other UPS measurements were performed without sample biasing.

The room temperature STM measurements were performed in a commercial Omicron UHV STM/AFM with electrochemically etched and in-situ sputtered tungsten tips. The bias voltage was applied to the sample. All STM data were analysed with the WSxM free software[44].

The LT-STS measurements shown in chapter 5.3.1 were performed at the University of Basel using an Omicron UHV LT-STM (Omicron NanoTechnology GmbH) at 5 K. The STM was operated by the Nanonis SPM control system (Nanonis GmbH), which also provides an internal lock-in amplifier. For the measurements wire-cut PtIr tips were used. The bias voltage was applied to the tip, but all voltages given in this thesis refer to a grounded tip i.e. negative bias voltage indicates the occupied states, to keep the usual sign convention. The differential conductance spectra (dI/dV vs V) are directly recorded with the lock-in amplifier. The sample preparation was carried out as described above, with slightly different sputtering and annealing parameters. The NaCl was evaporated from a home-built evaporator, while the samples were kept at room temperature. The CuOEP was evaporated with a commercial three crucible evaporator with the samples kept at liquid nitrogen temperature (approx. 78 K). The quality of the tip was controlled by scanning tunnelling spectra recorded on the clean metal surface state.

3.3   Experimental set-up – the Nanojunction Laboratory

Most of the experiments were performed in a multi chamber ultra-high vacuum (UHV) system, called the Nanojunction Laboratory, which is schematically depicted in Figure 6a. The UFO (1) has two major functions. First it serves for the storage of all transportable parts, which are needed in the UHV system, like samples, STM tips, AFM cantilevers and

evaporators filled with organic molecules or insulators. The second task is the distribution of this material into the different vacuum chambers with the UFO manipulator arm. The UFO is equipped with a quadrupole mass spectrometer for leakage detection. The samples can be heated on the UFO manipulator arm, which can be rotated by 180°, so that the samples are facing downwards during the evaporation procedure.


a)   b)
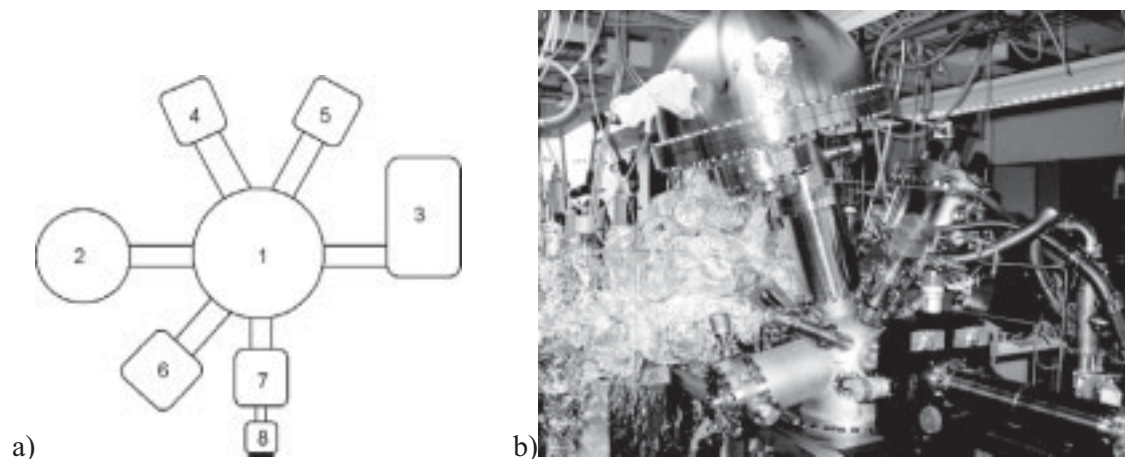
Figure 6: a) Sketch of the UHV system of the Nanojunction Laboratory: 1) UFO, 2) analysis chamber, 3) STM chamber, 4) molecule evaporation chamber, 5) salt/metal evaporation chamber, 6) electron beam evaporation chamber, 7) transfer chamber, 8) portable vacuum chamber. b) photograph of the analysis chamber with x-ray monochromator on the right back side.

The sample preparation was carried out in the analysis chamber (AC) (2), which is equipped with an Ar^+-sputtering gun for sample cleaning, as well as for sputtering the electrochemically etched tungsten tips. The samples can be heated via a filament attached to the sample holder and cooled via gaseous nitrogen. Additionally, the AC is equipped with an x-ray gun (Mg Kα and Al Kα) and a UV lamp (HeI and HeII), for photoelectron spectroscopy (PES). Since beginning of 2009 an x-ray monochromator (SPECS) with a twin anode providing Al Kα and Ag Lα radiation is attached to the chamber. The electron energy analyser is a nine channeltron SPECS PHOIBOS HSA 3500 hemispherical deflection analyser (HDA). In Figure 6b the electron energy analyser, the manipulator and the x-ray monochromator (right in the back) are visible. A LEED optics completes the instrumentation of the analysis chamber.

The STM chamber (3) consists of a transfer part for the samples, a tip storage carousel and the Omicron UHV STM/AFM. It is decoupled from the rest of the system via a bellow which is fixed with spacers made of a special silicon material called α_{GEL}[45] to reduce vibrations. With this decoupling system it is possible to obtain molecular resolution while the turbomolecular pump of the STM is running. The STM chamber is additionally equipped with a dosing valve.

3 EXPERIMENTAL TECHNIQUES AND SET-UP

The molecular evaporation chamber (4) is separated from the salt/metal (S/M) evaporation chamber (5) to prevent contaminations of the high melting point materials with low melting point organics. Both chambers are home-built and the chimney evaporators can be transferred in and out of the chamber via the UFO manipulator without breaking the vacuum. Figure 7a shows a photograph of the molecule evaporation chamber equipped with four chimney evaporators. Both evaporation chambers are equipped with a quartz crystal microbalance (QCMB) for calibrating the evaporation rate. The molecular evaporation chamber can host up to four different evaporators, the S/M chamber can host two different evaporators and is additionally equipped with an electron bombardment heating stage and a gas inlet for sample preparation at high temperature in oxygen atmosphere. The home-built molecule evaporator can be exchanged by a commercial three crucible evaporator (KENTAX TCE-CS) with temperature control, cooling system and shutter. This evaporator is mainly used for synchrotron measurements, where homogenous, reproducible adsorbate layers are necessary, or for co-evaporation of different molecules because it is possible to determine the evaporation rate of each molecule separately by using the shutter.
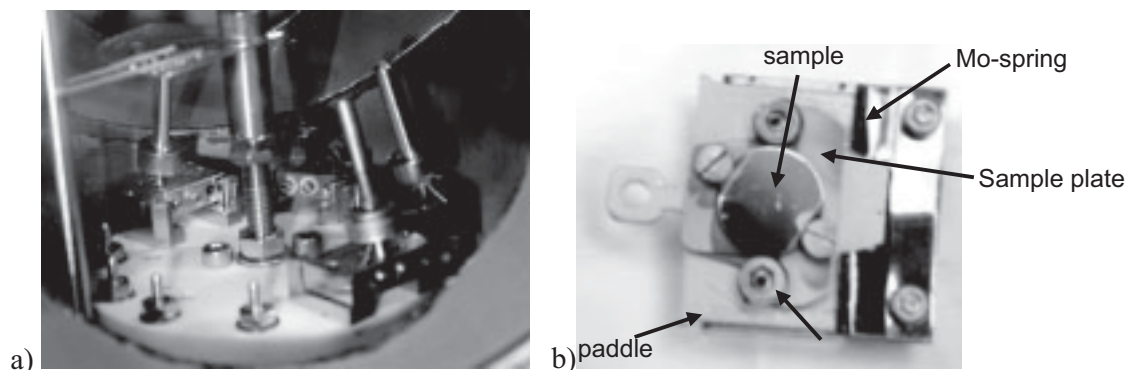
Figure 7: a) photograph of the molecule evaporation chamber equipped with four chimney evaporators; b) photograph of the sample and sample holder as used in the Nanojunction Laboratory.

For the evaporation of metals with high melting points like cobalt the UHV system has been equipped with an additional electron beam evaporation chamber (6) with a commercial four crucible e-beam evaporator (EGCO4 from Oxford Applied Research) with integrated shutter and flux control. This chamber also contains a QCMB. During the evaporation in all three evaporation chambers the samples are on the UFO manipulator and can be heated by the sample holder filament.

The transfer part (7) was in former times used as a portable vacuum chamber but is now replaced by a smaller one (8), which can be easier transferred between the SLS and the Nanojunction Laboratory. The transfer part is equipped with a load-lock were samples, STM tips and evaporators can be transferred into the vacuum system.

All single crystal samples are attached to commercial Omicron sample holders, called "paddles", either by means of a small sample plate which can be fixed on the paddle via two screws (cf. Figure 7b) or by direct spot-welding to the paddle. The single crystals which are attached to the paddle via the sample plate are 8 mm in diameter whereas the samples directly spot-welded on the paddle are 10 mm in diameter. The small 8 mm samples can be unscrewed from the paddle and can be fixed to a Swiss stub in the transfer chamber (7) for measurements at the beamline of Surface and Interface Spectroscopy (SIS) of the Swiss Light Source (SLS). The Omicron paddle is attached to a sample holder called "Klötzli" by means of a molybdenum spring (cf. Figure 7b). The Klötzli and therewith the sample can be resistively heated by a tantalum filament, which is placed below the molybdenum spring.

Most UHV chambers of the system are equipped with several vacuum pumps. For pumping after venting each chamber has a turbomolecular pump, which can be started by a scroll pre-vacuum pump. After starting the turbomolecular pump its pre-vacuum can be switched to the main vacuum line, which is additionally pumped with a turbomolecular pump. This leads to a very good pre-vacuum pressure ($1*10^{-5}$ mbar) which can lead to pressures below $1*10^{-10}$ mbar after bake-out of the chambers. Most of the turbomolecular pumps are separated from the chambers by gate valves, such that they can be switched off and vented for regular operation of the chambers. This venting of the turbomolecular pumps has several advantages e.g.: (i) it reduces noise in the lab and consequently leads to reduced noise for STM measurements (ii) the maintenance time of the turbomolecular pumps can be increased. Additionally, most of the chambers are equipped with ion getter pumps, to pump the chambers, when the turbomolecular pumps are switched off. Most chambers are pumped once a day via a titanium sublimation pump (TSP). The base pressure in the analysis chamber is below $1*10^{-10}$ mbar. The pressure in the other chambers is below $1*10^{-9}$ mbar also during evaporation. Thus, the cleanliness of a sample covered with a monolayer of adsorbates can be guaranteed for several days.

4 Pentacene on Cu(110) and oxidized Cu(110)

4.1 Motivation

The fact that more than 3160 publications containing the word pentacene could be found in the Web of knowledge[46], is a sign of the importance of this molecular semiconductor for basic research as well as device application. Pentacene has several advantageous properties like a high chemical stability and a comparably high hole mobility which can be up to 5.5 $cm^2V^{-1}s^{-1}$ [13]. Without doping, hole transport (p-transistor) dominates in pentacene devices due to the higher hole mobility compared to the electron mobility[10]. However, by doping the pentacene/gate dielectric interface with calcium, an n-type transistor could be realized with electron mobilities of 0.19 $cm^2V^{-1}s^{-1}$ [47]. The possibility to use pentacene either as p- or as n-type semiconductor is another important property of this molecule, which is not very common for other organic semiconductors.

For pentacene it was shown that the performance of thin film devices strongly depends on the pentacene/gate interface[13], on the metal contact interface[12], on the structure of the pentacene thin films[11] and on defects like gas inclusions[48]. Since the growth and the thin film structure are determined by the pentacene/gate interface as well as by the pentacene/metal contact interface, the study of the interface properties plays a crucial role for understanding the relation between the interface structure and the resulting transistor performance.

The alignment of pentacene on the surface strongly depends on the DOS of the substrate near the Fermi energy. Thus, pentacene molecules are lying flat on metal surfaces whereas they are standing upright on insulators or semiconductors[49]. A more detailed overview of the growth of pentacene on different surfaces as well as on the Cu(110) surface can be found in the corresponding Introduction sections in the following chapters.

Up to now pentacene has been studied on different substrates with respect to the following points: (i) the self-assembly on different metal surfaces like Cu(110)[50,51,52], stepped Cu surfaces[53], Ag[54] and Au[55,56,57], (ii) the modified electronic structure of pentacene by adsorption on metal surfaces[58,59] and (iii) the device performance depending on charge injection and charge carrier mobility[10,13]. In contrast, we investigated the influence of the pentacene molecules on the metal surface, i.e. the changes induced by the adsorbate/substrate interaction in the metal electronic structure. This new approach together with the study of molecular orbitals can lead to a more detailed understanding of the pentacene/metal interface. For this purpose we used the Cu(110) Shockley surface state as a direct probe for the changes of the electronic states of the metal surface induced by pentacene. We found a strong interaction between the pentacene molecules and the Shockley surface state, which results in a shift of the surface state away from the Fermi energy. Additionally, we also studied the influence of the coverage on the surface state and found that the occupation of the surface state depends on the adsorption structure and the coverage. This observation of the

dependence of the surface state on the adsorbate structure has not been reported yet for any system and shows that a detailed investigation of the adsorption structure depending on the coverage is necessary to understand the adsorbate/substrate interaction. Although there are already several publications on the adsorption of pentacene on Cu(110) we found two additional mobile phases and three different condensed phases, which have not been described in detail, yet.

A major aim of this research is to study and control the electronic adsorbate/surface interaction by using substrates with different reactivity and different density of electronic states near the Fermi energy, like e.g. different noble metals, semiconductors and insulators. Towards this aim, specifically to reduce the interaction of pentacene with the Cu(110) substrate, we also studied the adsorption of pentacene molecules on the oxidized Cu(110) substrate. A different adsorption behaviour of the molecules in the context of self-assembly, mobility and interface interactions has been observed. A possibility to change the intermolecular interactions is the separation of molecular rows by oxygen exposure. This leads to a reduced intermolecular interaction and is an alternative way to discriminate between substrate mediated intermolecular and molecular/substrate interactions.

4.2 Modification of the Cu(110) Shockley surface state by an adsorbed pentacene monolayer

The following chapter is a copy of a full paper, published in Physical Review B[24].

Modification of the Cu(110) Shockley surface state by an adsorbed pentacene monolayer

A. Scheybal,[1] K. Müller,[1] R. Bertschinger,[1] M. Wahl,[2] A. Bendounan,[3] P. Aebi,[4] and T. A. Jung[1]

[1]Laboratory for Micro- and Nanotechnology, Paul Scherrer Institut, CH-5232 Villigen PSI, Switzerland
[2]Institut für Physik, Universität Basel, Klingelbergstrasse 82, CH-4056 Basel, Switzerland
[3]Synchrotron Soleil, L'Orme des Merisiers, Saint-Aubin, BP 48, F-91192 Gif-sur-Yvette Cedex, France
[4]Institut de Physique, Université de Neuchâtel, Rue A.-L. Breguet 1, CH-2000 Neuchâtel, Switzerland

(Received 13 January 2009; published 5 March 2009)

The modification of the Cu(110) Shockley-type surface state by an adsorbed pentacene layer was determined using high-resolution angle-resolved photoelectron spectroscopy. It was found that the surface state is shifted by 80–120 meV to higher binding energies, depending on the pentacene coverage. In addition, an increase in the surface-state population is measured for the sample adsorbed with one monolayer of pentacene. The modification of the surface state by the adsorption of pentacene is put into relation to a complex interplay of different phenomena such as the hybridization and mixing of electronic states, the polarization of the adsorbate in the surface dipole, and the Pauli repulsion. Thus, this observation of a molecular adlayer shifting a surface state away from the Fermi energy sheds more light on the adsorbate-adsorbent interactions.

I. INTRODUCTION

In general, the chemistry and physics of metal surfaces is modified by the presence of surface and interface states which emerge from the discontinuation of the periodic bulk potential.[1] Such states have been studied spectroscopically and have also been visualized by standing-wave patterns in scanning-tunneling microscopy (STM).[2,3] Surface states can influence adsorbate-adsorbent interactions resulting in a modification of, e.g., the adsorption potential and the barriers for diffusion and dissociation.[4,5] Other effects which arise from the scattering of surface-state electrons are the stabilization of stepped surfaces[6] and the modification of adsorbate self-assemblies via Friedel charge-density oscillations.[7,8]

Organic molecular semiconductors such as pentacene ($C_{22}H_{14}$) with their intrinsically high charge-carrier mobility and their controllable electronic properties by doping are interesting materials for studying the interaction of molecules and metallic surfaces, also with relevance to organic electronic and optoelectronic devices.[9] In a recent study of the self-assembly of pentacene on Cu(110) Lukas et al.[10] observed long-range self-ordering by the formation of widely spaced rows of close-packed molecules. They proposed that this particular adsorbate structure is also mediated by Friedel charge-density oscillations produced by a surface state.

On the other hand, the presence of the adsorbates modifies the surface electronic structure of the substrate. Examples are the adsorption of rare gases discussed in the context of Pauli repulsion,[11,12] alkali metals discussed in the context of charge transfer,[13,14] and other more complex cases such as noble metals[15–17] on noble-metal surfaces.

Up to today only little has been published on the modification of surface states by the adsorption of large organic molecules. For example, a combined scanning-tunneling and photoelectron spectroscopy study of the PTCDA/Au(111) interface (PTCDA=3,4,9,10-perylene tetracarboxylic dianhydride, $C_{24}H_8O_6$) demonstrated that the Shockley surface state shifts about 40 meV to lower binding energy, i.e., closer to the Fermi energy.[18] Very recently, high-resolution angle-resolved photoelectron spectroscopy (ARPES) measurements at low temperatures showed a shifted surface state of about 160 meV toward the Fermi level after adsorption of PTCDA or 1,4,5,8-naphthalene tetracarboxylic dianhydride (NTCDA) on Au(111).[19] In another study it was shown that for the adsorption of a characteristically different system, C_{60} on Cu(111), the surface state was also shifted toward the Fermi energy.[20]

The here presented paper deals with the modification of the $\bar{Y}$-localized Shockley state of the Cu(110) surface by pentacene adsorbed in two different adlayer structures, a slightly disordered (7×2) phase and a $(6 -1, 1\ 4)$ phase. In contrast to the case of PTCDA on Au(111)[18] and C_{60} on Cu(111),[20] the adsorption of pentacene on Cu(110) leads to a shift of the surface state to higher binding energies. Different mechanisms for the modification of the surface state by adsorbates, such as Pauli repulsion, mixing and hybridization of electronic states, charge transfer, and polarization, will be discussed in the context of the large organic adsorbate pentacene. Notably, our study aims to reveal the role of the surface state in the pentacene on copper adsorption, which has been recently unraveled to deviate from the simple chemisorption/physisorption schemes for pentacene on Cu(110).[21] The modification of surface states depends on the properties of both the organic molecules and the metallic substrates and strongly relies on the nature and the strength of the bonding and the electronic coupling at the interface.

II. EXPERIMENT

The ARPES measurements have been performed at the high-resolution photoelectron spectroscopy (HRPES) end station of the surface/interface spectroscopy (SIS) beamline at the Swiss Light Source (SLS), Paul Scherrer Institut, Villigen, Switzerland. The data have been recorded with a Scienta SES 2002 electron energy analyzer in the angular mode with the sample kept at room temperature. The analyzer was oriented in such a way that the angular dispersive direction was perpendicular to the polar rotation axis of the sample

manipulator (i.e., the theta axis). Therefore, a full two-dimensional (2D) Fermi-surface (FS) map of the surface state was obtained by performing subsequent theta scans with the azimuth of the sample kept fixed along the $\bar{\Gamma}$-$\bar{Y}$ direction. All data presented in this paper were obtained with a photon energy of 40.8 eV using p-polarized light. This particular photon energy was selected for optimum signal-to-background ratio of the surface state. The energy and angular resolution were estimated to be about 20 meV and 0.3°, respectively.

The Cu(110) single crystals were cleaned by repeated cycles of Ar$^+$ sputtering and subsequent annealing to 750 K until no carbon and no oxygen were found in photoemission spectra. The pentacene was thermally evaporated onto the Cu(110) crystals while they were kept at room temperature. After preparation and characterization by low-energy electron diffraction (LEED) and STM, the pentacene-covered samples were transferred in a portable vacuum chamber to the HRPES end station. Typical transfer times were 5–6 h, during which the pressure stayed in the low 10^{-10} mbar range.

During the ARPES measurements the exposure time of the sample to the synchrotron light was optimized in order to avoid radiation damage. Additionally, for each new theta value the sample was moved by 0.1 mm along the theta axis to always provide a fresh sample surface. After the ARPES measurements the sample quality was checked again by STM and LEED, which confirmed the absence of significant sample degradation. Further, laboratory-based x-ray photoelectron spectroscopy (XPS) and ultraviolet photoelectron spectroscopy (UPS) measurements were performed to determine the pentacene coverage and the work function.

III. PHASE BEHAVIOR OF PENTACENE ON Cu(110)

The here reported STM study on the adsorption of pentacene on Cu(110) agrees well with earlier results[22,23] and discloses a complex multiphase behavior at room temperature, described in more detail elsewhere.[24] In contrast to earlier studies on pentacene on Cu(110) the samples have always been kept at room temperature, both during and after the pentacene deposition. For coverages below 0.6 monolayers (ML), STM reveals a disordered phase of highly mobile pentacene molecules. At 0.8 ML coverage extended, ordered molecular layers with limited long-range order can be identified in which the molecules are oriented with their long axis parallel to the [1$\bar{1}$0] direction. The side-by-side distance of the molecules is twice the substrate lattice spacing, which is confirmed by sharp LEED half-order spots. Along the [1$\bar{1}$0] direction the spacing of the molecules shows some variation with an average distance of 7 Cu-Cu atom distances. Hence, LEED shows a (7×2) structure where the superstructure spots along [1$\bar{1}$0] are smeared out along [0 0 1]. At higher coverage (1 ML), a well-ordered (6 −1, 1 4) structure is formed, which appears in two mirror domains tilted by ±9° with respect to the [0 0 1] direction. The STM and LEED data as well as the corresponding structural models of these two phases are shown in Fig. 1.
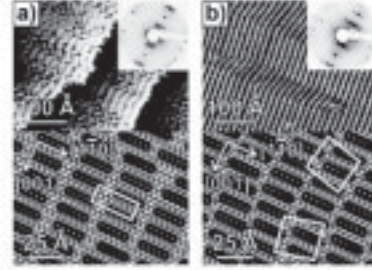

FIG. 1. (Color online) Observed adlayer structures for submonolayer and monolayer coverages of pentacene on Cu(110): (a) 0.8 ML; (b) 1.0 ML. Top: STM images 30×40 nm^2. Insets: corresponding LEED patterns taken at (a) 53.5 and (b) 63.0 eV. Bottom: structural models with unit cells marked in pale gray (yellow).

IV. Cu(110) SURFACE-STATE MAPPING AS A FUNCTION OF PENTACENE PHASE

In Fig. 2 we present the ARPES data of the surface state around the $\bar{Y}$ point of the surface Brillouin zone (SBZ) obtained on the clean Cu(110) surface. A parabolic shape of the surface-state band is observed along both high-symmetry directions $\bar{\Gamma}$-$\bar{Y}$ and $\bar{Y}$-$\bar{S}$ with a binding-energy minimum of $E_0 \approx 400$ meV. Different effective masses were measured in the two high-symmetry directions: $m^*_Y/m_e = 0.40 \pm 0.01$ and $m^*_{\Gamma}/m_e = 0.28 \pm 0.01$ along $\bar{Y}$-$\bar{S}$ and $\bar{\Gamma}$-$\bar{Y}$ directions, respectively (see Fig. 2). These values are in good agreement with data available in the literature[25] and reveal an anisotropy in the FS contour appearing in elliptical shape with the long axis along $\bar{Y}$-$\bar{S}$, which was also confirmed by STM studies.[26] The FS anisotropy is closely related to the Cu(110) surface
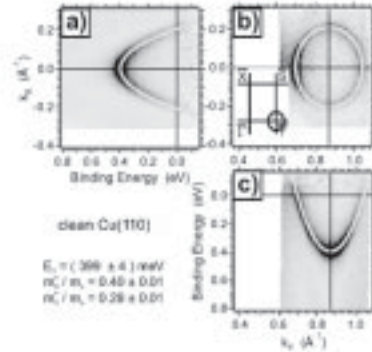

FIG. 2. (Color online) Dispersion of the $\bar{Y}$ surface state of the clean Cu(110) surface. (a) Dispersion along $\bar{Y}$-$\bar{S}$. (b) Cut through the $\bar{Y}$ surface state at the Fermi energy. Inset: sketch of the upper-right quadrant of the surface Brillouin zone with the Fermi line of the surface state marked in gray (red). (c) Dispersion along $\bar{\Gamma}$-$\bar{Y}$. The grayscale plots represent the photoelectron intensity after normalization by a Fermi step function and conversion to k-vector scale (dark corresponds to high intensity). The pale gray (yellow) lines mark the fit of a paraboloid to the experimental data.
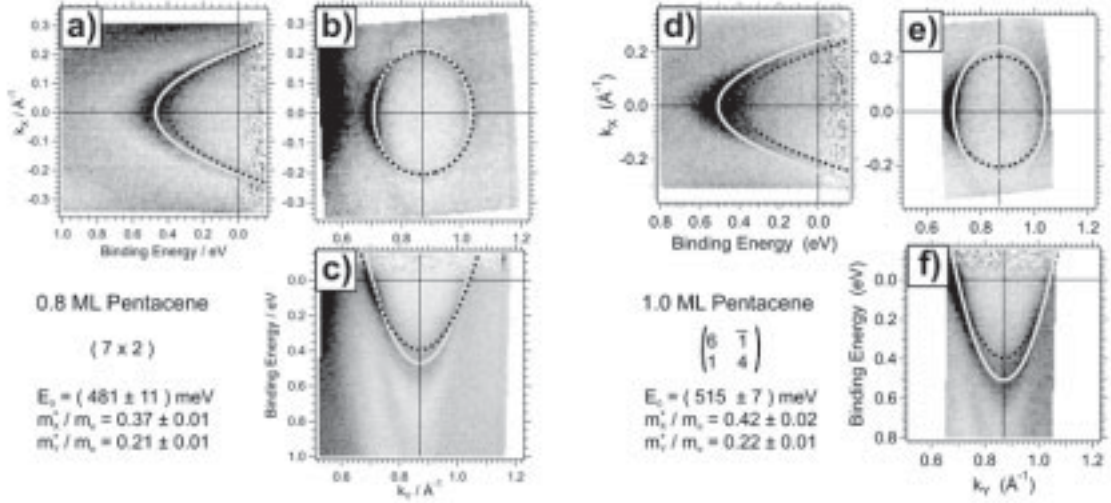
21

FIG. 3. (Color online) Dispersion of the $\bar{Y}$ surface state of a Cu(110) surface, covered with (a)–(c) 0.8 ML pentacene and (d)–(f) 1.0 ML pentacene. The straight lines marked in pale gray (yellow) mark the fit of a paraboloid to the experimental data. The dotted lines marked in gray (red) correspond to the paraboloid fitted to the experimental data of the clean Cu(110) surface from Fig. 2.

geometry presenting a twofold symmetry. Indeed, the bulk band gap projected on the (110) SBZ results in anisotropic behavior, i.e., a gap diameter shorter in the $\bar{\Gamma}$-$\bar{Y}$ direction than in the $\bar{Y}$-$\bar{S}$ direction.[25]

Adsorption of pentacene at coverages of 0.8 and 1 ML leads to a shift of the surface-state band to higher binding energies and to a change in the effective masses of the surface-state electrons. In Fig. 3 the corresponding ARPES data are presented. The bottom band energy was found at 481 meV for the (7×2) phase and at 515 meV for the (6 −1, 1 4) phase. While the effective mass in the $\bar{\Gamma}$-$\bar{Y}$ direction decreases for both the (7×2) and the (6 −1, 1 4) phases, the effective mass in the $\bar{Y}$-$\bar{S}$ direction decreases for the (7×2) phase and increases for the (6 −1, 1 4) phase. As a consequence, the Fermi wave vectors of the Shockley surface state are similar for the (7×2) phase compared to the ones obtained on clean surfaces, whereas for the (6 −1, 1 4) phase the Fermi wave vector increases along the $\bar{Y}$-$\bar{S}$ direction, leading to a higher anisotropy of the FS. Thereby the Fermi line for the (6 −1, 1 4) phase encloses a larger fraction of the SBZ than for the clean surface [Fig. 3(e)], which means that the population of the surface state is increased. These results are also confirmed by Martínez-Blanco et al.[27,28]

Provided that the area of the whole surface Brillouin zone corresponds to two electrons per surface copper atom (spin up and spin down), this increase corresponds to 0.034 ± 0.016 electrons per surface copper atom. Assuming for the pentacene surface density the value of 0.08 pentacene molecules per surface copper atom taken from the presented model [Fig. 1(b)], this would correspond to 0.43 ± 0.20 electrons per pentacene molecule.

In addition to the ARPES measurements on the surface-state modifications, the change in the work function has been

measured, by measuring the positions of the cutoff in the secondary electrons' background in the UPS spectra before and after adsorption of a pentacene monolayer. We observed a reduction in the work function of about 0.9 eV,[29] which is confirmed in Ref. 30 and indicates the formation of a surface dipole, likely induced by a charge transfer from the molecule to the substrate.

V. DISCUSSION

Only few systems have been reported yet where the surface state survives upon deposition of an adsorbate with considerable (e.g., π-metal) interaction, at the submonolayer up to the highly packed monolayer coverage. For example, it has recently been reported that adsorption of a PTCDA monolayer on Ag(111) leads to a huge shift of the surface state up to 0.6 eV above the Fermi level, induced by the strong bonding at the interface.[31] In contrast, the case of pentacene/Cu(110) shows a smaller shift, which indicates that the metallic electronic states are not strongly affected by the presence of the pentacene layer. On the other hand, the modification of the surface-state properties (binding energy and effective mass) implies that the interaction at the interface cannot be considered weak and therefore suggests a complex interaction between the metallic states and the molecular orbitals, being neither pure physi- nor chemisorption.

For the here presented experiments of pentacene on Cu(110) the modification of the surface state emerges from the complex interplay of different phenomena. In fact, when an adsorbate is resting on a surface, the surface dipole can be modified by (i) the different charge distributions of positive core and negative electronic charges (jellium model),[32] (ii) charge transfer,[13,14] (iii) mixing and hybridization of electronic states,[20,21,33] (iv) Pauli repulsion,[31,12] and (v) "mutual

22

4.2 Modification of the Cu(110) Shockley surface state by an adsorbed pentacene monolayer

polarization."[34,35] These are all simplified interaction schemes which are interdependent and therefore difficult to separate. Additionally, coupling between neighboring adsorbates, which can influence the electronic states, may originate from (vi) the increasing delocalization of molecular states with increased molecular packing and (vii) band alignment and band bending.[36,37] The complex interplay of the different phenomena affecting both the geometry and the electronic structure in a large unit cell makes calculations very complex and time consuming. The relative importance of the factors influencing the surface state in our experiments is therefore discussed qualitatively in the following paragraphs.

In the first part of the discussion we are going to concentrate on the influence of the coupling between neighboring adsorbates on the surface state. The data presented in Fig. 3(e) exhibit an increase in the anisotropy in the Fermi-surface shape (increase in k_F along the $\bar{Y}$-$\bar{S}$ direction). This increase appears more significant at the full monolayer coverage than at 0.8 ML, an observation which can be related to the packing of the molecular adlayer. Specifically, as shown in Fig. 1(b), a well-ordered, long-range periodic structure is obtained at maximum packing density of the first pentacene monolayer. Along the [0 0 1] direction the distance between the pentacene molecules, i.e., the packing density, is the same for the (7×2) phase and the $(6 -1, 1\ 4)$ phase, which corresponds to the separation of two Cu atoms in this direction. In the $[1\bar{1}0]$ direction, which corresponds to the $\bar{Y}$-$\bar{S}$ direction in SBZ instead, the packing density increases with increasing coverage, i.e., the distance between two neighboring molecules is 15.76 Å for the $(6 -1, 1\ 4)$ structure compared to 17.9 Å for the (7×2) structure.

In a recent calculation for two adjacent pentacene molecules held in the vacuum, the onset of intermolecular interaction in vacuum is found at a separation of 16.5 Å between the two molecules.[38] Thus, intermolecular interaction along the $[1\bar{1}0]$ direction has to be expected also for surface-supported molecules within the $(6 -1, 1\ 4)$ layer and potentially leads to the formation of an electronic band. Such an electronic band may modify the electronic potential felt by the surface-state electrons and may thus affect the occupation of the surface state. The correspondence of the close-packed direction ($[1\bar{1}0]$) of strongest interaction with the induced change in the Fermi wave vector in the $\bar{Y}$-$\bar{S}$ direction provides support for such a relation.

Three distinct mechanisms have been proposed for the modification of noble-metal surface states by adsorbed rare gases (Pauli repulsion), alkali metals (charge transfer), and other noble metals (change of the noble-metal character).[39] For adsorbed rare gases on noble-metal (111) surfaces the Shockley surface state shifts to lower binding energy, which has been attributed to the Pauli repulsion between the surface-state electrons and the closed shell of the rare-gas atoms. This repulsion pushes the surface-state electrons toward the bulk, thereby destabilizing the surface state and thus lowering its binding energy.

For alkali metals adsorbed on (111) and (110) noble-metal surfaces, the surface state shifts to higher binding energies as long as there is no adsorbate-induced surface reconstruction

formed.[14] The highly electropositive character of the alkali metals leads to an electron transfer from the adsorbate to the substrate, thereby decreasing the electrostatic potential in the surface region. Consequently, the electrons of the surface state are pulled toward the surface so that the surface state is stabilized and its binding energy increases.

Similar to the case of rare-gas adsorption, the surface-state electrons are repelled by the valence electrons of the pentacene adsorbed on Cu(110). However, this is not the main contribution to the modification of the surface state in this case, as it shifts to higher binding energies instead toward the Fermi level as is the case for rare gases. In contrast to rare-gas adsorption, the frontier orbitals in organic molecules are energetically closer to the Fermi level, which enables interaction with the electronic states of the substrate. Therefore, charge transfer, mixing of electronic states near the Fermi level, and covalent bonding between the adsorbate and the substrate are possible.

Our observation of an increased population of the surface state for the $(6 -1, 1\ 4)$ phase may indicate a charge transfer between the pentacene molecules and the surface state. On the other hand, the population increase could also be induced by the highly packed molecular layers, which may only affect the mixing between surface and bulk states. Notably, the fact that the population of the surface state is not increased for the (7×2) phase with respect to the clean surface, although the binding-energy shift is almost as high as for the $(6 -1, 1\ 4)$ phase, can be an indication that the shift of the surface state is more probably due to the mixing of the electronic states than due to pure charge transfer.

The direction of a possible charge transfer between the molecule and the surface can be estimated from the chemical potential of the adsorbate and the substrate as reported by Lindell *et al.*[40] This estimate, however, does not consider local surface physical properties, such as the surface and step states. The chemical potential of metals is the opposite of the work function, i.e., in the case of Cu(110) $\mu_{Cu(110)} = -4.5$ eV.[29] For organic molecules the chemical potential can be estimated by $\mu = -(IP + EA)/2$. For pentacene the ionization potential (IP) ranges from 5.9 to 6.6 eV.[41–43] The electron affinity (EA) is reported to be between 1.1 and 1.5 eV.[41,42] For these values the chemical potential of pentacene ranges between -4.05 and -3.50 eV. A possible electron transfer will occur in the direction from the species with higher chemical potential to the one with lower chemical potential, in our case in the direction from the pentacene to the Cu(110) substrate.

It is important to note that the charge transfer between the adsorbate and the substrate does not exclusively involve the surface state. Some charge could also be transferred directly to the bulk states; e.g., Baldacchini *et al.*[44] showed that there is a strong interaction of the pentacene π orbitals with Cu(100) and Cu(119) d bands. But this is a phenomenon which is only to be assessed in a detailed numerical study which goes far beyond the scope of this experimental report on a rather novel electronic interaction.

In the following we compare the case of PTCDA on Ag(111) and on Au(111) with our observations. In contrast to pentacene adsorption on Cu(110), for PTCDA adsorption on Au(111) the surface state is shifted to the opposite direction,

23

i.e., to lower binding energy, and remains occupied.[18,19] For PTCDA adsorption on Ag(111) the surface state is strongly shifted above the Fermi level.[31] This shows that our observation of a binding-energy increase after adsorption of a large organic molecule is unexpected. For PTCDA on Au(111), LEED,[45] work-function measurements,[18] and x-ray standing-wave experiments[46,47] indicate that PTCDA is weakly physisorbed. Therefore, the interaction between the molecules and the substrate is considerably different compared to the pentacene/Cu(110) system. In contrast, PTCDA is strongly chemisorbed on Ag(111) via the central carbon ring,[48] which results in an electron transfer from the substrate to the molecule.[48,49] Notably, the UPS spectrum of PTCDA adsorbed on Ag(111) reveals an additional band near the Fermi level arising from the partially filled lowest unoccupied molecular orbital (LUMO) of the adsorbed molecules due to an electron transfer from the substrate to the molecules.[49] Moreover, it has been reported that free-electron-like unoccupied states are developed in the PTCDA overlayer mediated by the valence electrons of the Ag(111) substrate.[50] Later, these electronic states have been identified to be the Shockley states modified upon the adsorption of the PTCDA monolayer.[31] Thus, we conclude that the interaction strength of the pentacene with Cu(110) is stronger than the one of PTCDA/Au(111) and weaker than the one of PTCDA/Ag(111).

The complex interaction mechanisms of the pentacene with the Cu(110) surface make it difficult to classify the adsorption in terms of physisorption or chemisorption. On one hand, if there is a charge transfer between the molecule and the substrate or mixing of the substrate and adsorbate electronic states, this is typically associated to weak chemisorption. On the other hand, if the modification of the surface state is induced by mixing and hybridization of electronic bulk states with the surface state in the presence of the adsorbate, this may be associated to strong physisorption.

Besides direct measurements of the local density of states within the surface state by STM,[47] ARPES is an ideal probe for learning about the interaction at the interface and provides featured information. For PTCDA/Au(111), the major factor for the modification of the surface state is the Pauli repulsion leading to a shift of the bottom band by about 40 meV to lower binding energy. This energy shift is much higher for a PTCDA monolayer on the Ag(111) surface (of about 660 meV) due to the strong interaction at the interface.

In the case of pentacene on Cu(110) the complex substrate-molecule and intermolecular interactions lead to a shift of the binding energy as well as to an increase in the occupation of the surface state for the 1 ML covered sample.

VI. CONCLUSION

In conclusion, the pentacene/Cu(110) interface provides a model system exhibiting a shift of the Cu(110) Shockley surface state to higher binding energies upon adsorption of a well-ordered molecular monolayer. Besides this binding-energy increase we also observe an increase in the population of the surface state for the (6 −1, 1 4) phase, which we associate either to an electron transfer to the substrate or to surface state/bulk state mixing.

The complex interplay of surface and molecular states has been related to the combination of a number of phenomena: Pauli repulsion, charge transfer, mixing and hybridization of electronic states, and polarization as well as coupling of neighboring molecules. The interrelation of these phenomena as they manifest themselves in the here presented experiments motivates *ab initio* calculations to deepen the understanding beyond the current discussion.

Furthermore, the measurement of surface-state modifications upon adsorption is a complementary and direct probe of the electronic processes occurring at the organic-metal interface compared to the more common investigations of molecular orbitals at surfaces by STM,[51] STS,[52] and (inverse) photoemission techniques.[53,54] The behavior of the surface state can thus be used as a probe for the adsorbate/substrate interaction, thereby providing additional information about the properties of electronic interfaces toward applications in organic electronic devices.

[1] W. Shockley, Phys. Rev. **56**, 317 (1939).

[2] M. F. Crommie, C. R. Lutz, and D. M. Eigler, Nature (London) **363**, 524 (1993).

[3] Y. Hasegawa and P. Avouris, Phys. Rev. Lett. **71**, 1071 (1993).

[4] N. Memmel and E. Bertel, Phys. Rev. Lett. **75**, 485 (1995).

[5] E. Bertel and N. Memmel, Appl. Phys. A: Mater. Sci. Process. **63**, 523 (1996).

[6] F. Baumberger, M. Hengsberger, M. Muntwiler, M. Shi, J. Krempasky, L. Patthey, J. Osterwalder, and T. Greber, Phys.

Rev. Lett. **92**, 016803 (2004).

[7] P. Hyldgaard and M. Persson, J. Phys.: Condens. Matter **12**, L13 (2000).

[8] N. Knorr, H. Brune, M. Epple, A. Hirstein, M. A. Schneider, and K. Kern, Phys. Rev. B **65**, 115420 (2002).

[9] J. Zaumseil and H. Sirringhaus, Chem. Rev. **107**, 1296 (2007).

[10] S. Lukas, G. Witte, and Ch. Wöll, Phys. Rev. Lett. **88**, 028301 (2001).

[11] T. Andreev, I. Barke, and H. Hövel, Phys. Rev. B **70**, 205426

4.3   Multimorphism in molecular monolayers: pentacene on Cu(110)

The following chapter is a copy of a full paper, published in Physical Review B[25].

Multimorphism in molecular monolayers: Pentacene on Cu(110)

Kathrin Müller,[1] Abdelkader Kara,[2] Timur K. Kim,[3] Rolf Bertschinger,[1] Andreas Scheybal,[1] Jürg Osterwalder,[4] and Thomas A. Jung[1]

[1]Laboratory for Micro- and Nanotechnology, Paul Scherrer Institut, CH-5232 Villigen PSI, Switzerland
[2]Department of Physics, University of Central Florida, Orlando, Florida 32816, USA
[3]Leibniz Institute for Solid State Research, IFW-Dresden, D-01171 Dresden, Germany
[4]Institute of Physics, University of Zürich, CH-8057 Zürich, Switzerland
(Received 21 January 2009; revised manuscript received 1 May 2009; published 18 June 2009)

The architecture of the contacting interface between organic molecular semiconductors and metallic or insulating substrates determines its cooperative properties such as the charge injection and the charge-carrier mobility of organic thin-film devices. This paper contributes a systematic approach to reveal the evolution of the different structural phases of pentacene on Cu(110) while using the same growth conditions. Complementary measurement techniques such as scanning tunneling microscopy and low-energy electron diffraction together with ab initio calculations are applied to reveal the complex multiphase behavior of this system at room temperature. For coverages between 0.2 and 1 monolayer (ML) a complex multiphase behavior comprising five different phases is observed, which is associated to the interplay of molecule/molecule and molecule/substrate interactions. Multimorphism critically depends on the thermodynamics and kinetics determined by the growth parameters as well as the system itself and arises from shallow energy minima for structural rearrangements. In consequence, the multimorphism affects the interface structure and therefore the interface properties.

I. INTRODUCTION

Organic semiconductors have been attracting increasing attention recently due to their application in organic electronic devices such as organic light-emitting diodes and organic field-effect transistors.[1,2] Compared to amorphous silicon, which is often used in thin-film transistors, these devices have several advantages such as low-temperature processability, low-cost fabrication, and the compatibility with a wide variety of substrates including flexible layers.[3,4] For high quality organic electronic devices, high charge-carrier mobility, and good conductivity are required. A promising organic semiconductor showing these characteristics is pentacene which shows high intrinsic charge-carrier mobility without doping.[4]

The organic/inorganic interfaces between the organic semiconductor and the gate dielectric as well as the contacting electrodes play a crucial role for the performance of organic electronic devices.[5,6] Specifically, the adsorbate/substrate interaction during the initiation of growth affects the structure of the first molecular layer and thus influences cooperative properties such as the charge injection at the metal/semiconductor interface and the charge-carrier mobility. Hence, it is an important task to understand the interaction between metallic or insulating substrates and the first layer of the adsorbate in dependence of growth parameters by studying the interface structure. For example, Thayer et al.[7] have reported that the orientation of adsorbed pentacene strongly depends on the electronic structure of the substrate. Pentacene molecules prefer to lie flat on metallic substrates due to their π electrons interacting with the near Fermi-level electronic states of the metal. In contrast, the molecules stand upright on insulators and semiconductors such as SiO$_2$,[8] organically terminated Si,[9] or Bi(001).[10]

The (110)-oriented face-centered-cubic single-crystal surfaces are particularly interesting substrates because their twofold symmetry prohibits the formation of rotational domains for adsorbates which also exhibit a twofold symmetry such as polyacenes. For example, Lukas et al.[11] have observed long-range self-ordering by the formation of widely spaced rows of close packed pentacene molecules on Cu(110) after annealing the pentacene covered sample to 400 K.

More recently Söhnchen et al.[12] and Lukas et al.[13] have reported the coexistence of a $p(6.5 \times 2)$ structure with a $c(13 \times 2)$ structure of a pentacene monolayer (ML) on Cu(110), by annealing the sample during evaporation to 430 K. At these temperatures the second layer formation is thermodynamically less favorable than the nucleation of a highly ordered monolayer with few defects. Pentacene layers with a similar structure have been shown by Chen et al.[14] For multilayers evaporated on the monolayer preassembled as described above, the molecules are tilted around the long axis by an angle of 28° with respect to the Cu(110) substrate for thicknesses below 2 nm. With increasing pentacene coverage this orientation becomes unstable and a new phase with molecules standing upright exhibiting a tilt angle of 73° develops, which is observed consistently for multilayers and thin films up to at least 50 nm thickness.[12]

The characteristically different two-dimensional (2D) arrangements observed for pentacene in the monolayer—the widely spaced rows of closed packed molecules[11] and the $p(6.5 \times 2)$ structure[12]—show that the phase behavior of pentacene on Cu(110) is so far not well understood. Thus, the study reported here contributes a systematic approach to reveal the growth of pentacene on Cu(110) from the nucleation at a few percents of a monolayer to the evolution of the different structural phases up to the most densely packed monolayer while using the same growth conditions. Specifi-

245421-1

27

cally, the study reported here has been carried out at room temperature without annealing of the pentacene adlayer. Therefore, this study provides an essential basis to understand how the molecule/substrate and the intermolecular interaction affect the layer structure at this technologically relevant interface.

II. EXPERIMENTAL SECTION

The experiments were carried out in a multichamber UHV system with a base pressure of less than 5×10^{-10} mbar. Cu(110) single crystals purchased from Mateck[15] were cleaned by repeated cycles of argon-ion sputtering and subsequent annealing to 750 K. The quality and cleanliness of the single crystals were checked with x-ray photoelectron spectroscopy (XPS), low-energy electron diffraction (LEED), and scanning tunneling microscopy (STM). After the final annealing step, the samples were cooled to room temperature and then the pentacene was thermally evaporated on the samples kept at room temperature. The evaporation rate (0.2–0.5 ML/min) was controlled by a quartz crystal microbalance. For rates in this range it was found that the adsorbate structure does not depend on the deposition rate. After evaporation of the molecules, the samples were examined by STM, LEED, and XPS. STM images were recorded with an Omicron UHV-STM/AFM at ambient temperature in constant current mode using electrochemically etched and *in situ* sputtered tungsten tips.

The x-ray photoelectron spectra were used to determine the chemical composition of the organic adlayer (e.g., no oxygen contamination was found in the XPS spectra) and to quantify the molecular coverage. One ML coverage in this paper corresponds to the most densely packed monolayer we observed during our studies, i.e., the (6 −1, 1 4) layer as specified and shown below.

III. COMPUTATIONAL METHOD

A comprehensive study of energetics and electronic structure was made by solving Kohn-Sham equations[16,17] in a plane-wave basis set using the Vienna *ab initio* simulation package (VASP).[18–20] Exchange-correlation interactions are included within the generalized gradient approximation (GGA) in the Perdew-Burke-Ernzerhof form.[21] The electron-ion interaction is described by the projector augmented wave method in its implementation of Kresse and Joubert.[22,23] A plane-wave energy cutoff of 400 eV was used for all calculations and is found to be sufficient for these systems. The bulk lattice constant for Cu was found to be 3.655 Å using a k-point mesh of $10 \times 10 \times 10$. This value is by about 1.1% larger than the experimental one (3.615 Å), a typical trend when using GGA. The slab supercell approach with periodic boundaries is employed to model the surface and the Brillouin-zone sampling is based on the technique devised by Monkhorst and Pack.[24] The slab consists of five layers of Cu(110) each containing 14 atoms (7 × 2). The choice of five layers was made on the assumption that the adsorbed molecule might introduce substantial structural perturbations to the substrate, hence only the bottom layer was kept fixed as

in bulk copper. In all our calculations we used a k-point mesh of $2 \times 6 \times 1$.

Initially, the unperturbed flat pentacene molecule was placed at about 3.5 Å above the substrate at an arbitrary lateral position. A few lateral positions of the molecules have been tried as starting positions and the minimum energy was found to be the same for all configurations.

IV. RESULTS AND DISCUSSION

Figure 1(a) (bottom) shows an STM image of a sample covered with 0.5 ML of pentacene. Molecular adsorbates are rarely resolved individually due to their high mobility relative to the scanning speed of the STM tip (approx. 0.5 s/line). The characteristic lines extending along the $[1\bar{1}0]$ direction which are visible in the STM image correspond to pentacene molecules anisotropically diffusing along the grooves of the Cu(110) crystal. At step edges or kinks of the substrate individual pentacene molecules are observed in a pinned state. This shows that the pentacene diffusion generally does not proceed across the substrate steps. The pinned molecules are oriented with their long axis along the [110] direction, which agrees well with earlier studies of pentacene on Cu(110).[11–14] LEED data [Fig. 1(a), top left] taken on this sample covered by 0.5 ML of pentacene exhibits oval halos around the [0 0 1] spots. These ovals cross the [0 0 1] direction at 1/3 of the substrate reciprocal lattice vector which corresponds to an average distance of three Cu-lattice constants between $[1\bar{1}0]$ diffusion channels occupied with pentacene. Thus, this structure will be called a mobile ($n \times 3$) phase. The three Cu-lattice constants spacing and the direction of the highest mobility are also presented in the scheme of the adsorption structure in Fig. 1(a), top right. This mobile adlayer structure was observed for pentacene coverages up to 0.5 ML. A weak long-range ordering as well as tip induced mobility were also shown for tetracene on Cu(110).[14]

Differences in the diffusion constants depending on the relative substrate crystallographic direction and the molecular orientation were also shown for other organic molecules on the Cu(110) surface such as decacyclene and hexa-tert-butyl-decacylene,[25] azobenzene,[26] as well as the so-called "violet lander" molecule ($C_{108}H_{104}$).[27] For all these molecules no diffusion along the [0 0 1] direction has been observed, whereas they are diffusive along the $[1\bar{1}0]$ channels. Specifically, Linderoth *et al.*[26] showed that at low temperatures (120–170 K) the diffusion in the $[1\bar{1}0]$ direction for azobenzene oriented with the long axis parallel to the $[1\bar{1}0]$ direction is six times faster than for molecules oriented perpendicular to the diffusion channel. In the case of pentacene reported here, the molecules are also oriented with their long axes parallel to the $[1\bar{1}0]$ direction, which is a similar situation to the azobenzene orientation with highest diffusion. This explains the considerable diffusion along the $[1\bar{1}0]$ direction for low coverages of pentacene at room temperature.

This high degree of diffusion for low-molecular coverage shows that the diffusion barrier of an individual molecule along the $[1\bar{1}0]$ direction is rather low at room temperature.
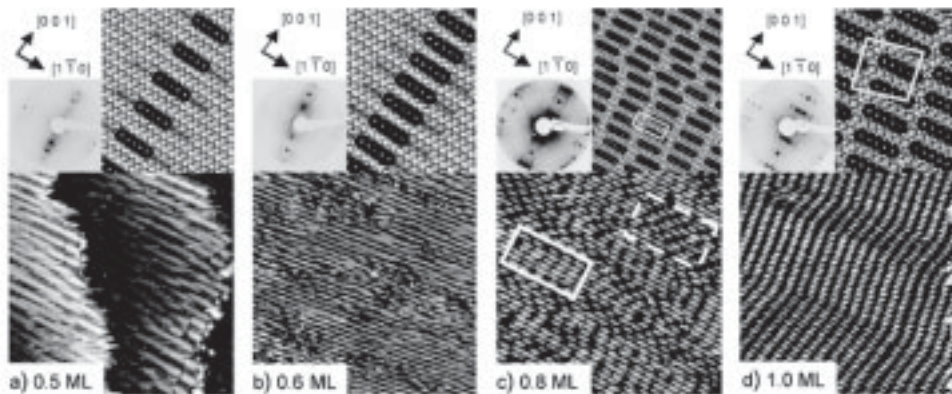
FIG. 1. (Color online) Structures of the pentacene adlayers on Cu(110). Bottom: STM images 25×25 nm^2. Top right: schemes of the adsorption structure; the scheme in (c) covers a larger area to show the degree of disorder; for clarity only one mirror domain (domain 1) is shown in scheme (d). Top left: LEED patterns at (a) and (b) 48 eV, (c) 53 eV, (d) 63 eV. (a) 0.5 ML of pentacene; STM image reveals diffusive molecules in the adatom channels and some molecules pinned at the step edges, the adsorption structure shows the three Cu-atoms distance between the neighboring diffusion channels; (b) 0.6 ML of pentacene: the diffusion channels are closer together (two Cu-atoms spacing) than in (a); (c) 0.8 ML of pentacene: the STM image shows two different adsorption structures marked with white rectangles (see discussion in the text), LEED reveals a slightly disordered (7×2) structure; (d) 1 ML of pentacene: STM image showing nicely ordered molecules in two mirror domains, indicated by the white numbers, revealing a $(6 -1, 1 4)$ structure, each row of pentacene molecules is shifted by one Cu atom along the [0 0 1] direction.

Our calculations showed a diffusion barrier of 150 meV. Additionally, we can conclude that the interaction between the pentacene molecules adsorbed in the same [$1\bar{1}0$] row is small and no such linear condensation is induced. The separation of the diffusion channels by three Cu-atoms spacing reduces the interaction between the molecules in the [0 0 1] direction and indicates a weak interaction between the adsorbates in neighboring diffusion channels. In contrast, C$_{60}$ forms ordered 2D arrays also for coverages below 1 ML on noble metal surfaces[28,29] and one-dimensional arrays at step edges,[30] due to its considerable cohesive energy. For the case of pentacene on Cu(110), the interaction between the pentacene molecules after adsorption is too small to immobilize the molecules on the surface for low coverages. The existence of a higher density mobile phase (see below) leads to the conclusion that the intermolecular interaction between molecules in neighboring diffusion channels is repulsive. The mobility of the molecules in the diffusion channels of the Cu(110) substrate can be reduced by additional exposure to oxygen, which serves as pinning centers for the molecules and as nucleation sites for the condensed phase.[31]

A second mobile phase exists for coverages between 0.5 and 0.6 ML [cf. Fig. 1(b)]. Here, the LEED pattern also shows oval halos but these cross the [0 0 1] direction at $\frac{1}{2}$ of the substrate reciprocal lattice vector [cf. Fig. 1(b), top left]. This indicates that due to the higher coverage the distance between occupied diffusion channels decreases to two Cu atoms instead of three Cu atoms as shown in Fig. 1(a). Thus, this adsorption structure can be called a mobile $(n \times 2)$ phase. In the STM image in Fig. 1(b) the diffusive molecules are closer together in the [0 0 1] direction than in Fig. 1(a). This is also indicated in the schematic representation of the adsorption structure (Fig. 1, top right). Additionally, few in-

dividually condensed molecules can be observed not only at defects such as step edges and kinks but also on the flat terraces indicating the onset of molecular nucleation. The fact that the occupied diffusion channels move closer together while maintaining the mobility of the molecules in the [$1\bar{1}0$] channels indicates that the repulsive interactions between the molecules in neighboring channels are comparably low.

For coverages higher than 0.6 ML the diffusion of the pentacene molecules decreases due to the higher occupancy of the available adsorption sites and due to site blocking of nearest neighbors within the adatom rows. Consequently, single molecules are mostly resolved in the STM images [Fig. 1(c), bottom] while few still exhibit a limited mobility. The layer structure at this coverage is characterized by a distance corresponding to twice the Cu-lattice constant along the [0 0 1] direction. This observation in the STM data is also confirmed by the spots observed at $\frac{1}{2}$ of the substrate reciprocal-lattice vector in the [0 0 1] direction in the LEED pattern [Fig. 1(c), top left]. In this coverage range—0.6 to 0.8 ML—different arrangements of the molecules can be identified. On some parts of the STM image the molecules tend to form rows along the [0 0 1] direction [highlighted by the white continuous rectangle in Fig. 1(c)]; on other parts they do not show a specific ordering [highlighted by the white dashed rectangle in Fig. 1(c)]. The presence of differently arranged molecules marked in the STM image demonstrates the lack of long-range order, which is also well represented in the LEED data which exhibits diffraction stripes along the [0 0 1] direction [cf. Fig. 1(c), top left]. The six stripes in between the fundamental spots in the [$1\bar{1}0$] direction indicate that the average distance between neighboring molecules in this direction is corresponding to seven Cu at-
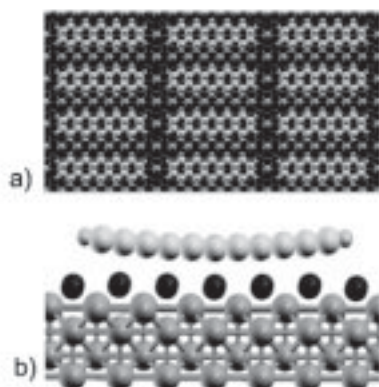
FIG. 2. (Color online) Calculation of the pentacene adsorption sites on Cu(110) for the (7×2) structure; light gray (yellow): C atoms, small and darker gray (blue): H atoms, dark gray (red): surface Cu atoms; (a) top view: C atoms of the molecule adsorb on top of the Cu atoms of the first layer; (b) side view indicating bending of the molecule by approximately 0.4 Å.

oms, therefore we call this structure a (7×2) structure despite the absence of long-range order. A sketch of the arrangement of the pentacene molecules for coverages between 0.6 and 0.8 ML is shown in the top right of Fig. 1(c).

DFT calculations for a single molecule on Cu(110) show that the pentacene molecules adsorb preferably with the C atoms on top of the Cu atoms of the first layer [cf. Fig. 2(a), the first layer atoms are colored dark gray (color online; red) for clarity]. Because of the good match between the Cu-lattice constant and the phenyl spacing in the pentacene molecules each phenyl ring is in the same position with respect to the Cu lattice. The calculations additionally show that the molecules are bent out of the surface plane by 0.4 Å; i.e., the center of the molecule is closest to the metal substrate [cf. Fig. 2(b)]. The adsorption energy was calculated to be 1.59 eV. For the slightly different (6.5×2) adsorption structure reported in Ref. 12 an adsorption energy of 2.1 eV has been determined by thermal desorption. This considerable difference probably results from the fact that our calculations have been performed for a single molecule while the adsorption energy was experimentally determined for 1 ML of pentacene, i.e., also including the intermolecular interaction. For comparison the adsorption energy of adenine on Cu(110) is calculated to 0.34 eV (Ref. 32) and the adsorption energy of NTCDA [1, 4, 5, 8-naphtalene-tetracarboxylic-dianhydride on Ag(110) and Ag(100) is 0.9 eV and 1.0 eV, respectively].[33] This shows that the molecules interact more strongly with the Cu substrate than in the case of weakly physisorbed systems. An additional indication for the strong molecule/substrate interaction is that all molecules seem to lie flat on the Cu(110) surface while it has been reported that a mixed layer of flat lying and tilted (by 90° around the long axis) molecules can be observed for pentacene on Au(110).[34] This strong interaction between the molecules and the substrate is also observed in angle-resolved photoelectron spectroscopy measurements of pentacene on Cu(110).[35,36] The calculated bending of the molecules is also consistent with
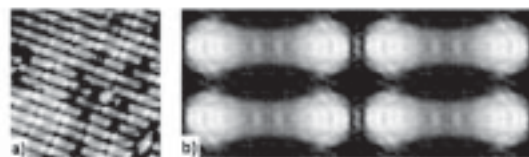

FIG. 3. (Color online) (a) 0.7 ML pentacene on Cu(110): STM image 8×8 nm² indicating the bending of the pentacene molecules by the white ends of the molecules; (b) calculated STM image.

the STM data shown in Fig. 3(a) where the ends of the molecules are imaged brighter than the centers; an observation which fits well with the calculated STM image in Fig. 3(b).

The (7×2) structure reported here shows a slightly lower packing density compared to the previously reported $p(6.5\times2)$ structure.[12] The small difference in the packing density along the [1$\bar{1}$0] direction (6.5 vs 7 Cu atoms) and the lower degree of long-range ordering of the (7×2) structure is attributed to the slightly smaller coverage of our samples and to the different parameters used during sample preparation. From the described observations it is plausible that a number of (z×2) phases [z=6,[34] 6.5,[12] and 7 (this work)] can be prepared due to the expected small energy difference between such phases and in dependence of preparation parameters such as coverage, annealing temperature, and evaporation rate. Different annealing temperatures and evaporation rates lead to a change in the mobility of the molecules, which consequently may change the spacing of the molecules in the [1$\bar{1}$0] direction. We have to point out that the distance of seven Cu atoms is an average and the molecular separation is varying around six to eight Cu atoms in our data.

Coverage of a full monolayer leads to a characteristically different highly ordered structure with very few defects. The molecules are oriented in rows which are tilted by ±9° out of the [0 0 1] direction leading to two mirror domains, while maintaining the molecular orientation of the long axis parallel to the [1$\bar{1}$0] direction [cf. Fig. 1(d)]. The neighboring pentacene rows are shifted by one Cu atom along the [0 0 1] direction, which results in an oblique unit cell. The LEED pattern shows discrete spots forming rows, which are tilted out of the [1$\bar{1}$0] direction [cf. Fig. 1(d), top left]. This observation, together with the molecular resolution STM data, suggests an adsorption structure like the one shown in Fig. 1(d), top right, which can be described by a (6 −1, 1 4) matrix, each unit cell containing two molecules. Occasionally, but on comparably smaller surface areas a coexisting phase was observed. Here the neighboring molecular rows are not shifted with respect to the Cu substrate leading to aligned molecules with respect to the short axis of the molecules (cf. Fig. 4, in between the white lines of the STM image). This structure, which has the same packing density as the (6 −1, 1 4) structure can be described by a (6.25 −1, 0 4) matrix.

These two structures, which we observed for 1 ML coverage, exhibit a slightly higher packing density than the previously reported $p(6.5\times2)$ and $c(13\times2)$ phases.[12,13] Note that the packing density for the (6 −1, 1 4) structure is
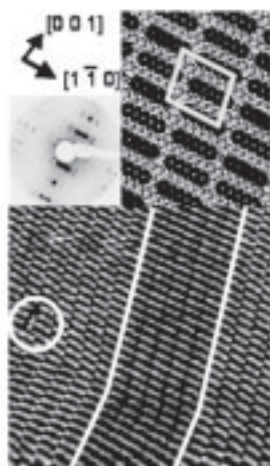
FIG. 4. (Color online) 1 ML of pentacene. Bottom: STM image 20×20 nm^2; top left: LEED pattern at 63 eV. Top right: scheme of the adsorption structure; in between the white lines of the STM image an area of molecular rows not shifted along the [0 0 1] direction is visible which can be described by a (6.25 −1, 0 4) matrix.

0.87 molecules/nm^2, while the packing density of the $p(6.5 \times 2)$ phase is 0.83 molecules/nm^2. Beside this small difference in the packing density, the main difference between the structures is the tilt of the molecular rows out of the [0 0 1] direction, which is clearly visible in the STM image and in the LEED pattern shown in Figs. 1(d) and 4. Additionally, it has to be emphasized that the $p(6.5 \times 2)$ and the $c(13 \times 2)$ structures were obtained by annealing of the sample at 430 K during pentacene deposition, while our sample preparation was performed at room temperature. Noteworthy, Chen *et al.*[14] mentioned that the intermolecular rows are slightly diverted away from the [0 0 1] direction due to interdigitation of the CH bonds.

Additionally, in Fig. 4 one defect consisting of a molecule oriented perpendicular to the [1$\bar{1}$0] direction can be seen (white circle). Due to the high packing density this molecule is sterically hindered to rotate back into the preferred orientation, which is along the [1$\bar{1}$0] direction. These defect sites, however, are very rarely observed in the STM images. This fact emphasizes the high quality of the self-assembled molecular layer.

Diffusing adatoms can influence the orientation of molecular adsorbates as it was shown for benzoate species on Cu substrates.[37] On the other hand it has been demonstrated that porphyrine adsorbates can change the surface reconstruction of a Au(110) surface.[38] Even weakly physisorbed glycine induces a reconstruction of the Au(110) surface.[39] Since the diffusion barrier along the channels is comparable for Au(110) (0.28 eV)[40] and Cu(110) (0.24 eV),[41] it is also important to briefly discuss the influence of the Cu adatom diffusion on the pentacene diffusion and adsorption structures shown in this paper. The diffusion barrier of pentacene along the [1$\bar{1}$0] direction is slightly smaller (0.15 eV) than

the diffusion barrier of the Cu adatoms, but still both—Cu adatoms and pentacene molecules—show a considerable diffusion along the [1$\bar{1}$0] channels at room temperature. It is difficult to determine how exactly the diffusion of the metal adatoms influences the diffusion of the molecules and vice versa. The investigation of this complicate interaction would require additional temperature-dependent studies combined with *ab initio* calculations, which would lead far beyond the scope of this paper. However, both diffusing species compete for the same space in the channels. In our data, the horizontal streaks near the left step in the STM image in Fig. 1(a) indicate that there is considerable Cu diffusion even after adsorption of pentacene. At higher molecular coverages, after the molecular diffusion has been blocked by the occupancy of neighboring sites, the steps and kinks appear much sharper. This is consistent with the expectation that the Cu adatom diffusion is reduced at higher pentacene coverages.

On the other hand, there is no evidence for the formation of a pentacene-induced surface reconstruction as observed for pentacene on Au(110) (Refs. 42 and 43): (i) the STM data and the models presented in Figs. 1 and 4 agree well and do not indicate a modification of the surface reconstruction. (ii) The Cu(110) Shockley surface state is still present after adsorption of 1 ML of pentacene.[35] This observation excludes considerable surface reconstruction, which would probably lead to a quenching of the surface state.

For all coverages between 0.6 and 1 ML, where the mobility of the molecules is sufficiently reduced to determine the layer structure by STM and LEED studies, the growth of pentacene is commensurate with the Cu(110) lattice in both directions. For the adsorption of 1 ML of pentacene the adsorption sites differ in their relative position with respect to the [1$\bar{1}$0] direction. Specifically, four different adsorption sites shifted by 1/4 of a Cu-lattice spacing in the [1$\bar{1}$0] direction exist for the (6.25 −1, 0 4) structure. In contrast this shift is inexistent for the (7×2) structure as shown in the STM image in Fig. 1(c) and in the calculations in Fig. 2. Notably, at lower coverages up to 0.6 ML LEED and STM indicate commensurability along [0 0 1] direction and diffusivity along [1$\bar{1}$0] direction.

V. CONCLUSIONS

In conclusion, we have shown five different adsorption structures of pentacene on Cu(110) to occur after deposition at room temperature (295 K) without annealing. By the comprehensive STM and LEED studies and by comparison to *ab initio* calculations, we have demonstrated that the substrate/molecular interaction is stronger than the intermolecular interaction leading to a complex multiphase behavior. The different stages of this phase behavior before nucleation of the second layer are characterized by molecular mobility, molecular bending, their structure modified, e.g., by their relative position of neighboring molecules and different packing densities of the linear pentacene molecules.

McCrone[44] stated for the crystal structures of organic molecules, that "every compound has different polymorphic forms, and that, in general, the number of forms known for a

given compound is proportional to the time and money spent in research on that compound." We realized the same for the 2D adsorption polymorph of pentacene on Cu(110): although a lot has already been published about this system, we have shown two diffusive adsorbate phases and three different condensed phases to occur at different coverages but with the same preparation parameters. The latter helped to refine already mentioned adsorbate structures.

The observation of five distinctively different adlayer phases in the monolayer for the comparably simple shape and adsorption geometry of the pentacene on Cu(110) system suggests that the phase behavior may be even more featured for more complex molecular adsorbates. Complex phase evolutions like in the demonstrated case will only be revealed by detailed studies—using complementary techniques—of the molecular packing with consistent parameter sets in a wide coverage range. The fact that the molecular packing and orientation at the interface influences any cooperative behavior such as charge injection, charge-carrier mobility, and the emergence of intermolecular and interface electronic states motivates the detailed comparison of experiment and theory also for other interfaces relevant

for organic electronics. The fabrication of specific organic/inorganic interfaces by controlling the first layer growth may offer a way to control the cooperative electronic and optoelectronic behavior of such interfaces, also within devices.

Note added in proof. J. Martínez-Blanco *et al.* have reported three stages of the phase behavior described here, i.e., one mobile phase and two condensed phases for different coverages of pentacene on Cu(110).[45]

[1] G. Horowitz, Adv. Mater. **10**, 365 (1998).

[2] B. Crone, A. Dodabalapur, Y.-Y. Lin, R. W. Filas, Z. Bao, A. LaDuca, R. Sarpeshkar, H. E. Katz, and W. Li, Nature (London) **403**, 521 (2000).

[3] G. H. Gelinck, H. E. A. Huitema, E. van Veenendaal, E. Cantatore, L. Schrijnemakers, J. B. P. H. van der Putten, T. C. T. Geuns, M. Beenhakkers, J. B. Giesbers, B.-H. Huisman, E. J. Meijer, E. M. Benito, F. J. Touwslager, A. W. Marsman, B. J. E. van Rens, and D. M. de Leeuw, Nature Mater. **3**, 106 (2004).

[4] M. Daraktchiev, A. von Mühlenen, F. Nüesch, M. Schaer, M. Brinkmann, M.-N. Bussac, and L. Zuppiroli, New J. Phys. **7**, 133 (2005).

[5] S. Y. Yang, K. Shin, and C. C. Park, Adv. Funct. Mater. **15**, 1806 (2005).

[6] S. F. Alvarado, L. Rossini, P. Müller, and W. Rieß, Synth. Met. **122**, 73 (2001).

[7] G. E. Thayer, J. T. Sadowski, F. Meyer zu Heringdorf, T. Sakurai, and R. M. Tromp, Phys. Rev. Lett. **95**, 256106 (2005).

[8] R. Ruiz, B. Nickel, N. Koch, L. C. Feldman, R. F. Haglund, A. Kahn, and G. Scoles, Phys. Rev. B **67**, 125406 (2003).

[9] F.-J. Meyer zu Heringdorf, M. C. Reuter, and R. M. Tromp, Nature (London) **412**, 517 (2001).

[10] J. T. Sadowski, T. Nagao, S. Yaginuma, Y. Fujikawa, A. Al-Mahboob, K. Nakajima, T. Sakurai, G. E. Thayer, and R. M. Tromp, Appl. Phys. Lett. **86**, 073109 (2005).

[11] S. Lukas, G. Witte, and Ch. Wöll, Phys. Rev. Lett. **88**, 028301 (2001).

[12] S. Söhnchen, S. Lukas, and G. Witte, J. Chem. Phys. **121**, 525 (2004).

[13] S. Lukas, S. Söhnchen, G. Witte, and C. Wöll, ChemPhysChem **5**, 266 (2004).

[14] Q. Chen, A. J. McDowall, and N. V. Richardson, Langmuir **19**, 10164 (2003).

[15] http://www.mateck.de

[16] P. Hohenberg and W. Kohn, Phys. Rev. **136**, B864 (1964).

[17] W. Kohn and L. J. Sham, Phys. Rev. **140**, A1133 (1965).

[18] G. Kresse and J. Furthmüller, Phys. Rev. B **54**, 11169 (1996).

[19] G. Kresse and J. Furthmüller, Comput. Mater. Sci. **6**, 15 (1996).

[20] G. Kresse and J. Hafner, Phys. Rev. B **47**, 558 (1993).

[21] J. P. Perdew, K. Burke, and M. Ernzerhof, Phys. Rev. Lett. **77**, 3865 (1996).

[22] G. Kresse and D. Joubert, Phys. Rev. B **59**, 1758 (1999).

[23] P. E. Blöchl, Phys. Rev. B **50**, 17953 (1994).

[24] H. J. Monkhorst and J. D. Pack, Phys. Rev. B **13**, 5188 (1976).

[25] M. Schunack, T. R. Linderoth, F. Rosei, E. Lægsgaard, I. Stensgaard, and F. Besenbacher, Phys. Rev. Lett. **88**, 156102 (2002).

[26] J. A. Miwa, S. Weigelt, H. Gersen, F. Besenbacher, F. Rosei, and T. R. Linderoth, J. Am. Chem. Soc. **128**, 3164 (2006).

[27] R. Otero, F. Hümmelink, F. Sato, S. B. Legoas, P. Thostrup, E. Lægsgaard, I. Stensgaard, D. S. Galvão, and F. Besenbacher, Nature Mater. **3**, 779 (2004).

[28] G. Costantini, S. Rusponi, E. Giudice, C. Boragno, and U. Valbusa, Carbon **37**, 727 (1999).

[29] W. W. Pai, C.-L. Hsu, M. C. Lin, K. C. Lin, and T. B. Tang, Phys. Rev. B **69**, 125405 (2004).

[30] M. T. Cuberes, R. R. Schlittler, and J. K. Gimzewski, Appl. Phys. Lett. **69**, 3016 (1996).

[31] K. Müller, A. Kader, J. Osterwalder, and T. A. Jung (unpublished).

[32] W. G. Schmidt, K. Seino, M. Preuss, A. Hermann, F. Ortmann, and F. Bechstedt, Appl. Phys. A **85**, 387 (2006).

[33] A. Alkauskas, A. Baratoff, and C. Bruder, Phys. Rev. B **73**, 165408 (2006).

[34] G. Bavdek, A. Cossaro, D. Cvetko, C. Africh, C. Blasetti, F. Esch, A. Morgante, and L. Floreano, Langmuir **24**, 767 (2008).

[35] A. Scheybal, K. Müller, R. Bertschinger, M. Wahl, A. Ben-

32

[illegible bibliography text]

4.4 Interaction of pentacene with a partly and fully oxidized Cu(110) surface

The following chapter is a manuscript, which will be submitted soon.

4.4.1   Introduction

Organic molecular semiconductors and their contacting interfaces have been attracting increasing attention recently due to their application in organic electronic devices, such as organic light-emitting diodes (OLEDs)[2], organic field-effect transistors (OFETs)[60,61] and solar cells[1]. Their main advantages compared to silicon technology are low temperature processability, low-cost fabrication and the compatibility with a wide variety of substrates including flexible layers[8,62]. One promising organic molecule showing high intrinsic charge carrier mobility and good conductivity is pentacene[62].

The performance of electronic semiconductor devices, like thin film transistors consisting of pentacene, crucially depends on the structure of the molecular layer[11] as well as on inclusions of impurities like water[63,64], oxygen[65,66] or other gases[48,67]. It was shown that water and oxygen do not react noticeably with the pentacene molecules but that they form trap states in the pentacene layer, thus reducing the charge carrier mobility and increasing the contact resistance[65,68]. Hence, oxygen and water inclusions lead to a significant degradation of the pentacene electronic device.

Unfortunately, cross-sectional scanning tunnelling microscopy (STM) and spectroscopy (STS) as they have been established for the visualization and characterisation of dopants and defects in GaAs[69] and GaAs/$Al_x Ga_{1-x}$As[70] cannot be applied in a straightforward way to organic materials. This motivates the search for model systems of organic semiconductors in contact with metal or insulator interfaces to investigate the interaction of defect states and surface adsorbates also in the context of the interface.

Ideal model-systems consist of large π-conjugated molecules on single-crystal metal surfaces[71,72], on ultrathin insulators[23,73] and on nano-structured templates[74,75,76]. A lot of research has been performed to study the physical[71] and chemical[72] properties of organic/inorganic interfaces. Chemisorbed oxygen on Cu(110), which forms the so called p(2x1)O reconstruction, provides an ideal template for the investigation of the interactions between the molecules and the substrate and can additionally be used to control the orientation of large organic molecules[77].

For all organic molecules studied so far on the p(2x1)O surface at room temperature it was shown that the molecules preferably adsorb on the bare metal and they only adsorb on the

oxygen reconstructed Cu(110) surface after the remaining bare metal patches have been covered with molecules[75,76]. Furthermore, significant changes in the adsorption geometry of organic molecules on the p(2x1)O sample compared to the clean Cu(110) have been reported[75,76].

Very recently, the growth of 30 nm thick films of pentacene on the p(2x1)O surface has been investigated[78]. Interestingly, the growth of the first monolayer of pentacene on the p(2x1)O Cu(110) surface has not been studied, yet. Here, we report that the pentacene molecules interact strongly with the p(2x1)O surface, in spite of their preferential adsorption on the clean Cu(110). The molecules do not show long-range ordering on the p(2x1)O surface. We assume that the highly corrugated p(2x1)O surface leads to reduced diffusion and hinders the close packing of the molecules. The lack of long-range ordering may also affect the structure and properties of interfaces within devices.

4.4.2 The p(2x1)O reconstruction of Cu(110)
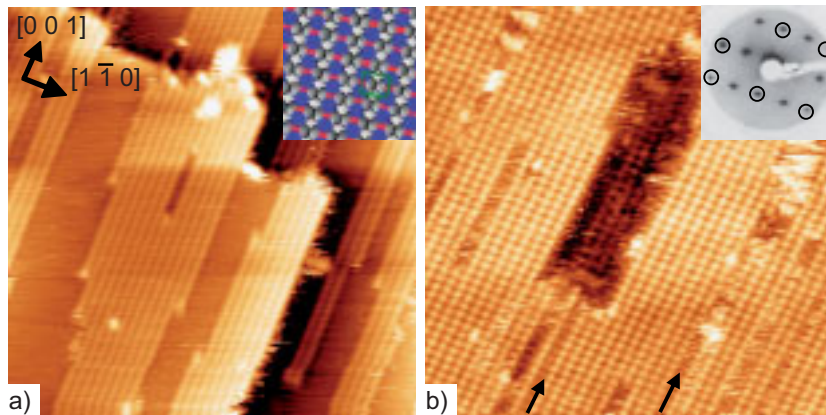
Figure 8: a) 0.6 ML oxygen on Cu(110), inset: scheme of the adsorption structure, red: Oxide ions, blue: additional Cu-atoms, p(2x1) unit cell marked in green ($U_{bias} = -1.7$ V, I = 0.11 nA, 20 x 20 nm^2). b) 1 ML oxygen on Cu(110); the vacancy island in the centre shows the depletion of Cu-atoms due to the added-row reconstruction ($U_{bias} = -1.1$ V, I = 0.18 nA, 15 x 15 nm^2); inset: LEED pattern taken at 71 eV.

Figure 8 shows the partly and fully oxidized Cu(110) surface. The LEED inset in Figure 8b clearly shows the diffraction spots at ½ of the Cu reciprocal lattice in the $[1\bar{1}0]$-direction, which correspond to the well-known p(2x1) reconstruction of oxygen on Cu(110)[79]. For clarity the substrate diffraction spots are marked with black circles in the LEED pattern. The inset in Figure 8a indicates the adsorption structure of the p(2x1)O added-row reconstruction. The oxygen superstructure patterns in Figure 8a differ by their width and their spacing. This is a consequence of the limited diffusion and equilibration due to the oxygen exposure being carried out at room temperature. Performing the deposition at elevated temperatures can lead to a more regular distribution of the reconstructed areas[77,80].

On the sample fully covered with oxygen some rows with a wider spacing can be observed (cf. black arrows in Figure 8b). At these positions two areas of the p(2x1)O reconstruction converge resulting in a domain boundary, which is characterized by a distance of three Cu-atoms spacing between adjacent CuO rows instead of two. The white, streaky areas in Figure 8b indicate some residual mobility due to Cu and oxygen ad-atom diffusion.

The STM image in Figure 8b displays a 1 ML deep vacancy island. This indicates that the additional copper atoms, which are required to form the added-row p(2x1)O reconstruction are not only supplied from the steps but also from the flat terraces. For each p(2x1)O unit cell one additional Cu-atom is necessary which is usually supplied from the steps due to the high ad-atom mobility of Cu on Cu(110)[81,82]. There are two reasons for the supply of copper atoms from the flat terraces, which we suggest for the system studied here: (i) The reduced mobility and reduced number of copper ad-atoms at room temperature compared to the usual annealing temperature during fabrication of the oxygen added-row reconstruction (> 450 K)[83,84] leads to the need for additional Cu sources on big terraces. (ii) For increasing CuO coverages the diffusion from the steps is blocked by the CuO rows, which also results in reduced mobility of the Cu ad-atoms and in the need for an additional Cu source[84]. Also, in this vacancy island in Figure 8b the oxygen reconstruction is present.

4.4.3   *Pentacene on a partly oxygen covered sample*

Figure 9a shows the adsorption structure of 0.5 ML of pentacene on a partly oxygen covered sample. The pentacene molecules preferably adsorb on the bare metal (no clean metal was visible anymore after the pentacene adsorption) and only after complete filling of the free metal the molecules start to assemble on the p(2x1)O reconstructed areas. An analogue behaviour has been shown for porphyrins on insulating NaCl layers[23] as well as for various molecules on the partly p(2x1)O covered sample[75,85]. Thus, we conclude that the adsorption energy of pentacene on Cu(110) is higher than the one on the p(2x1)O surface. To prove this assumption DFT ab-initio calculations are currently in progress.

Two different geometrical orientations of the pentacene molecules can be observed in Figure 9a: Most of the molecules are oriented with their long axis parallel to the $[1\bar{1}0]$-direction (cf. blue and red rectangle in Figure 9a). They form rows of close-packed molecules aligned along the [0 0 1]-direction. The other molecules are oriented perpendicular to this direction. Comparing the STM image of pentacene on the partly oxygen covered surface with STM images of 0.8 ML of pentacene on the clean Cu(110) (cf. chapter 4.3, Figure 1c), where all molecules are oriented parallel to the $[1\bar{1}0]$-direction, we can conclude that the molecules oriented with the long axis parallel to this direction are adsorbed on the bare Cu(110). The orientation of pentacene adsorbed on clean Cu(110) with the long axis parallel to the $[1\bar{1}0]$-direction was also reported in earlier studies[50,51,52].

Figure 9b was recorded after a sudden tip change, which led to a different contrast. The metal areas covered with pentacene appear dark whereas the p(2x1)O areas still appear bright. All molecules which are still visible in Figure 9b are most likely adsorbed on the p(2x1)O and are oriented with the long axis parallel to the [0 0 1]-direction. Thus, we conclude that the molecules on the p(2x1)O surface are rotated by 90° around the axis perpendicular to the surface compared to pentacene on clean Cu(110). Noteworthy, most of the molecules in a 30 nm thick film also grow with the long axis parallel to the CuO rows[78]. Relative orientation changes for molecular adsorption on Cu(110) and p(2x1)O reconstructed areas have also been reported for other organic molecules, like α-Quinquethiophene[75] and para-Sexiphenyl[76]. The appearance of the pentacene molecules on the p(2x1)O surface in Figure 9a is the same as on the clean metal surface, which leads to the assumption that the pentacene molecules are still lying flat on the p(2x1)O area. This flat orientation of the molecules indicates a rather high interaction between the molecules and the substrate.
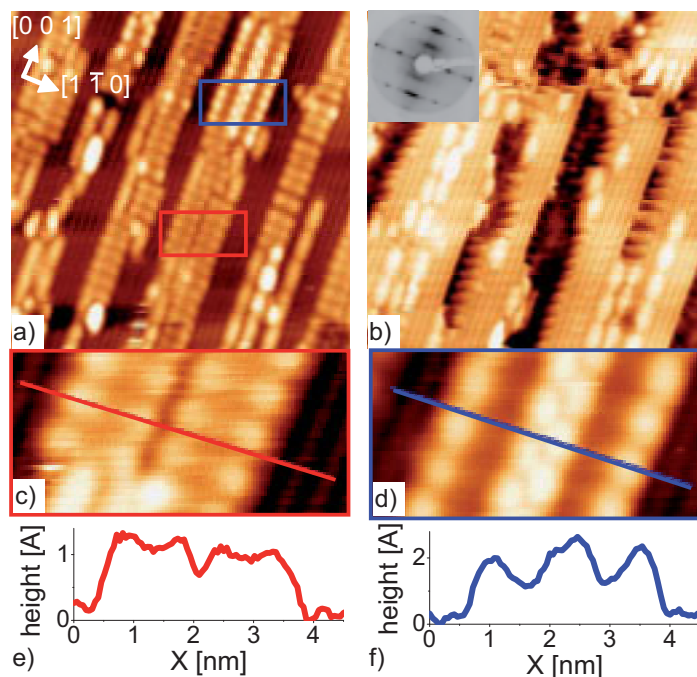
Figure 9: 0.5 ML of pentacene on Cu(110) covered with 0.6 ML of p(2x1)O; a) and b) are taken at the same area; the different contrast results from a sudden tip change between both images (a) $U_{bias} = -1.4$ V, $I = 0.21$ nA, b) $U_{bias} = -0.37$ V, $I = 0.10$ nA; 20 x 20 nm². inset in b): LEED 48 eV. c) and d) are zoom-ins of the areas marked with red and blue rectangle in a. e) and f) show the height profiles of c) and d).

In the LEED pattern in Figure 9b diffraction spots at ½ of the substrate reciprocal lattice vector in the [1$\bar{1}$0]-direction corresponding to the p(2x1)O reconstruction can be clearly recognized. The elongated diffraction spots at ½ along the [0 0 1]-direction correspond to the average spacing of the molecules on the bare metal in this direction, which is equal to the spacing of two Cu-atoms in this direction and thus, the same as for pentacene on the clean

Cu(110) surface (cf. LEED pattern in chapter 4.3, Figure 1c). The smearing out of the (0 1) spots along the $[1\overline{1}0]$-direction can be related to the pentacene molecules adsorbed on the p(2x1)O surface.

It is important to note that the molecules on the p(2x1)O surface do not show any mobility, whereas they are highly mobile on the clean Cu(110) surface for coverages below 0.6 ML, as can be seen in chapter 4.3, Figure 1a and b. The high mobility of pentacene on the clean Cu(110) is visible by the streaks corresponding to molecules diffusing along the $[1\overline{1}0]$-direction in the STM image i.e. parallel to the corrugation of the Cu(110) surface (cf. arrows in chapter 4.3, Figure 1a and b top right, indicating the direction of high mobility). A more detailed investigation on diffusion of pentacene on the different substrates is presented in the next subsection.

The zoom-in section marked by the blue rectangle in Figure 9a and displayed in Figure 9d shows two neighbouring molecular rows with a comparably high packing density in the $[1\overline{1}0]$-direction. The pentacene molecules in this rectangle exhibit a reduced spacing of six Cu-atoms compared to the usual spacing of seven copper atoms on the clean Cu(110). For both adsorption structures (the blue and the red rectangle) the molecules in neighbouring rows are shifted by one lattice constant of Cu along the [0 0 1]-direction. The higher affinity of the pentacene molecules to the metal than to the oxidized surface and the narrow patch of the free metal surface leads to this high packing density in the $[1\overline{1}0]$-direction, which we did not observe for pentacene on the clean Cu(110) surface. In comparison, the molecules are less densely packed in the area marked by the red rectangle and shown in Figure 9c because there is more free space for the molecules due to the discontinuation of one CuO row along the right border of the metallic substrate patch. The higher packing density of the pentacene molecules as shown in the area highlighted by the blue rectangle results in molecules bent out of the surface by 1.1 Å along the $[1\overline{1}0]$-direction with respect to the centre of the molecules (cf. blue line profile in Figure 9f). This bending is well visible in the STM topographs by the bright edges of the molecules. The bending of the molecules in the red rectangle in contrast is only 0.26 Å (cf. red line profile in Figure 9e), which is comparable to the calculated bending of the molecules on the (7 x 2)-structure, which is 0.4 Å, as shown in chapter 4.3. It seems that the squeezed adsorption of pentacene as visible in Figure 9d is energetically more favourable than the adsorption of molecules with the long axis perpendicular to the $[1\overline{1}0]$-direction or a tilted orientation.

4.4.4   *Pentacene on a fully oxygen covered sample*

In addition to the adsorption of pentacene on the partly oxygen covered surface, we also investigated the adsorption of the pentacene molecules on the fully oxygen covered surface. On this surface almost all the molecules are oriented with the long axis along the [0 0 1]-

direction (Figure 10) – an orientation already described for the partly oxygen covered sample (cf. Figure 9a). Few molecules are found which are adsorbed with the long axis perpendicular to the [0 0 1]-direction (cf. grey square in Figure 10). We assume that this orientation change is due to a local oxygen deficiency giving way to pentacene adsorption on the bare metal where this orientation is favoured.

The LEED pattern (inset in Figure 10) shows the p(2x1)O diffraction spots at ½ of the Cu reciprocal lattice along the [1$\bar{1}$0]-direction, which are marked with black circles. There are no additional spots or lines visible in the LEED pattern which can be related to a superstructure of the molecules on the p(2x1)O surface. The smearing out of the (0 1) spots along the [1$\bar{1}$0]-direction, which we also found for the molecules on a partly oxygen covered surface (cf. inset in Figure 9b) is a hint for the disordered adsorption of pentacene on the p(2x1)O surface. The diffraction spots at ½ of the Cu reciprocal lattice along the [0 0 1]-direction as shown for the partly oxygen covered sample in Figure 9b are not visible for the fully oxygen covered surface. This is a clear indication that these spots are resulting from the pentacene molecules on the bare metal as shown in Figure 9.
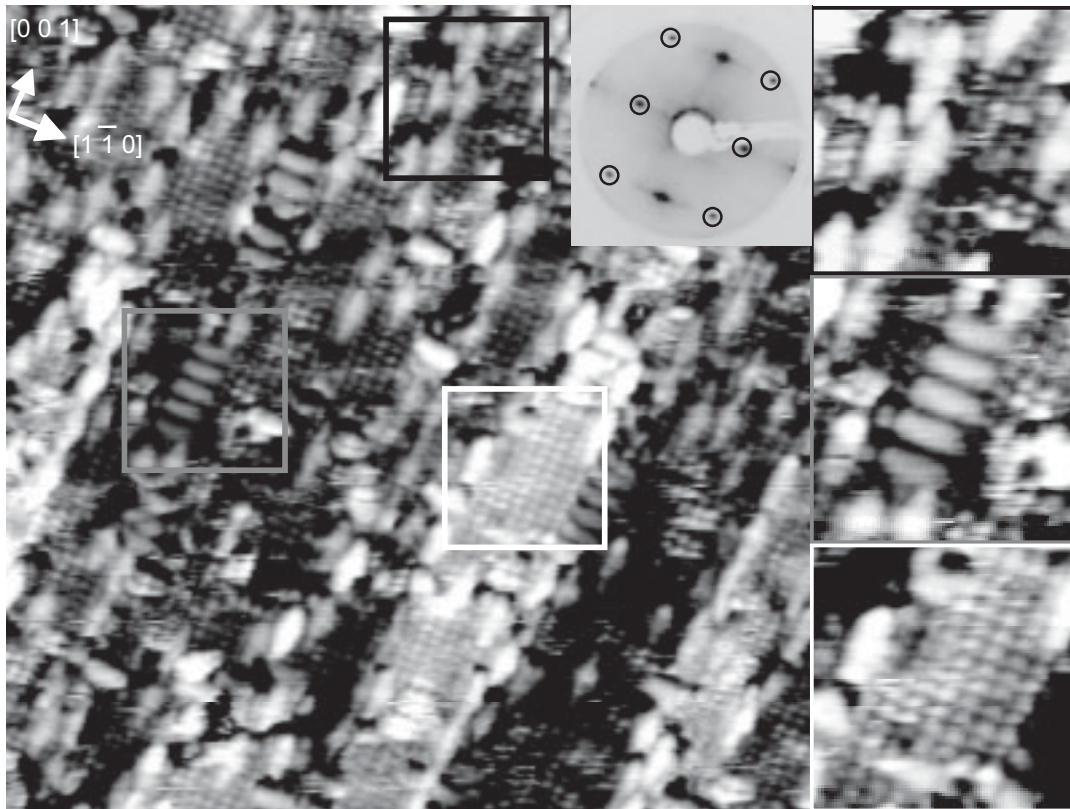
Figure 10: Nominal coverage of 0.5 ML of pentacene on the p(2x1)O reconstructed sample (U_{bias} = –1.0 V, I = 0.21 nA, 25 x 25 nm^2). Inset: LEED at 48.0 eV. Right: zoom-in of black square: pentacene on p(2x1)O; grey square: pentacene on clean Cu and white square: p(2x1)O reconstruction.

Due to the modified corrugation of the surface covered with the added CuO rows the molecules cannot move as close together in the $[1\bar{1}0]$-direction as it would be necessary for considerable interaction between neighbouring molecules. Lee et al. showed that the onset of attractive interaction between two molecules in the vacuum is at distances around 0.7 nm along the short molecular axis[86]. We assume that the molecules adsorb always at the same position with respect to the p(2x1)O substrate due to the high surface corrugation along the $[1\bar{1}0]$-direction. Thus, the spacing must be a multiple of the lattice constant of the p(2x1)O structure along this direction, which is 0.51 nm. Because of the size of the pentacene molecules, which are probably still lying flat, the distance between two neighbouring molecules must be at least two times this spacing i.e. 1.02 nm. This is also visible by the three pentacene molecules in the black square in Figure 10. There are two molecules separated by a third molecule which is shifted upward – along the [0 0 1]-direction – due to the missing space in-between the two molecules. This spacing of two p(2x1)O lattice vectors, is large compared to the spacing of the pentacene on the clean Cu(110) which is 0.72 nm. Thus, no ordering of the molecules along the $[1\bar{1}0]$-direction occurs on the p(2x1)O islands due to the weak interaction between the neighbouring molecules. Sometimes several molecules (up to five) form rows along the [0 0 1]-direction because of the lower degree of surface corrugation along this direction. Molecules can rather freely approach each other along this direction, which seems to provide sufficient condensation energy for the formation of linear chains in spite of the limited contact area along this molecular axis.
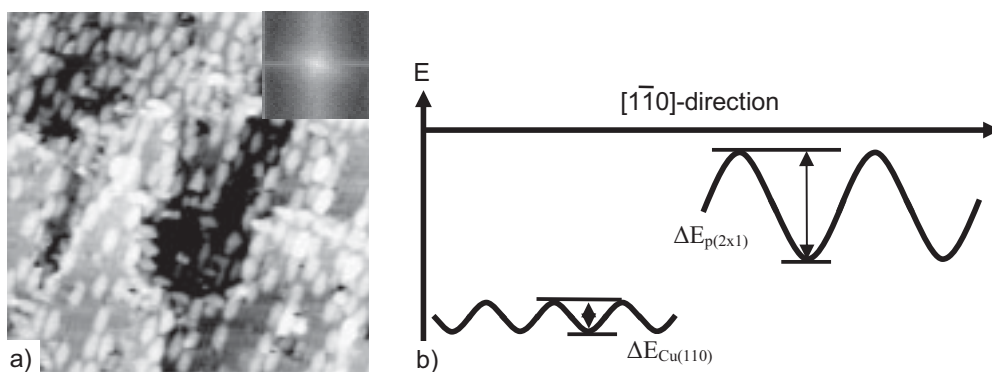
Figure 11: a) 0.5 ML of pentacene on the p(2x1)O reconstructed sample (U_{bias} = −0.7 V, I = 0.25 nA, 25 x 25 nm^2). b) sketch of the adsorption energies and diffusion energies (ΔE) for pentacene on p(2x1)O and pentacene on clean Cu(110).

Figure 11a shows another STM image with a slightly higher local coverage, although it has been taken on the same sample as the one shown in Figure 10, but on a different spot. Due to the comparably small diffusion and a small gradient in the pentacene concentration, the two areas on the sample show different coverages. For the sample with the slightly higher coverage no long-range ordering could be found as well, which is visible by the FFT in the inset of Figure 11a. It has to be pointed out that no molecular resolution could be achieved for

higher coverages. We relate this to the increasing interaction between the STM tip and the weakly bound molecules which lead to frequent tip changes as well as to clustering of the molecules also for coverages below 1 ML.

The molecules adsorbed on the p(2x1)O surface exhibit no mobility in the STM image, although the molecular coverage is well below 1 ML and there is still some free space in both STM images shown in Figure 10 (cf. the p(2x1)O reconstruction is visible in the white square) and Figure 11a. This is in contrast to the adsorption of pentacene on the clean metal, where the molecules show a rather high diffusivity along the $[1\overline{1}0]$-direction for coverages below 0.6 ML (cf. chapter 4.3, Figure 1a and b). However, the preferential adsorption of pentacene molecules on the metal substrate after their deposition suggests that there is considerable diffusivity on the oxide islands to allow for the molecules to find the preferred adsorption sites on the metal. In contrast, it has been shown that other molecules like porphyrins on insulator layers, like NaCl, exhibit a comparably high diffusivity as long as the NaCl layer is not completely covered with molecules[23]. Thus, we can conclude that the interaction of the molecules with the CuO is stronger than the interaction of molecules with ultrathin insulator films. In fact, LCAO (Linear Combination of Atomic Orbitals) semi-empirical calculations showed that there is no band gap near the Fermi energy for the CuO added-row reconstruction[87]. Thus, the p(2x1)O surface does not behave like a semiconductor (the band gap of bulk CuO is 1.2 eV[88]), but like a metal.

Having a closer look on the different diffusion barriers for pentacene on Cu(110) and p(2x1)O we can draw a qualitative energy diagram showing the adsorption energies as well as the diffusion barriers (Figure 11b). This diagram shows the diffusion barrier of pentacene on Cu(110) ($\Delta E_{Cu(110)}$) and of pentacene on the p(2x1)O surface ($\Delta E_{p(2x1)}$) for the $[1\overline{1}0]$-direction. The lattice constant for the p(2x1)O reconstruction is twice the Cu lattice constant in the $[1\overline{1}0]$-direction and thus the curve for the p(2x1)O surface also has twice the wave length of the Cu(110) curve. The higher adsorption energy for pentacene on Cu(110) is indicated by the lower energy of this curve (the adsorption energy is always negative). The diffusion barrier for pentacene on Cu(110) ($\Delta E_{Cu(110)}$) has been calculated in chapter 4.3 and is 150 meV. $\Delta E_{p(2x1)}$ has not been calculated, yet, but we assume that it is considerably larger than $\Delta E_{Cu(110)}$ due to the higher surface corrugation and due to the absence of mobility for molecules on this surface at room temperature. This is indicated by the bigger amplitude of the corresponding curve in Figure 11b. Further calculations for the adsorption energy as well as the diffusion barrier for pentacene on p(2x1)O are in progress.

XPS data on the p(2x1)O sample show that the O1s binding energy is 529.8 eV (cf. Figure 12a), which is comparable to the binding energy of the O1s peak in CuO (529.7 eV) reported in literature[89]. After adsorption of 0.5 ML of pentacene on the p(2x1)O substrate the binding energy of the O1s peak is the same, only the intensity decreased slightly which is associated to the attenuation of emitted O1s photoelectrons by the molecular layer. The binding energy of the pentacene C1s on the clean Cu(110) substrate (cf. Figure 12b) is 284.8 eV, which agrees well with the binding energy reported for benzene (284.7 eV)[41]. For

0.5 ML of pentacene on the p(2x1)O surface the binding energy of the C1s peak is shifted by 0.2 eV to lower binding energies. We assume that this shift can be related to different screening effects due to the electronically different environment of the pentacene on the bare Cu(110) surface compared to the oxygen covered Cu(110) surface. A more detailed discussion about screening effects in XPS is provided in chapter 5.3.3.
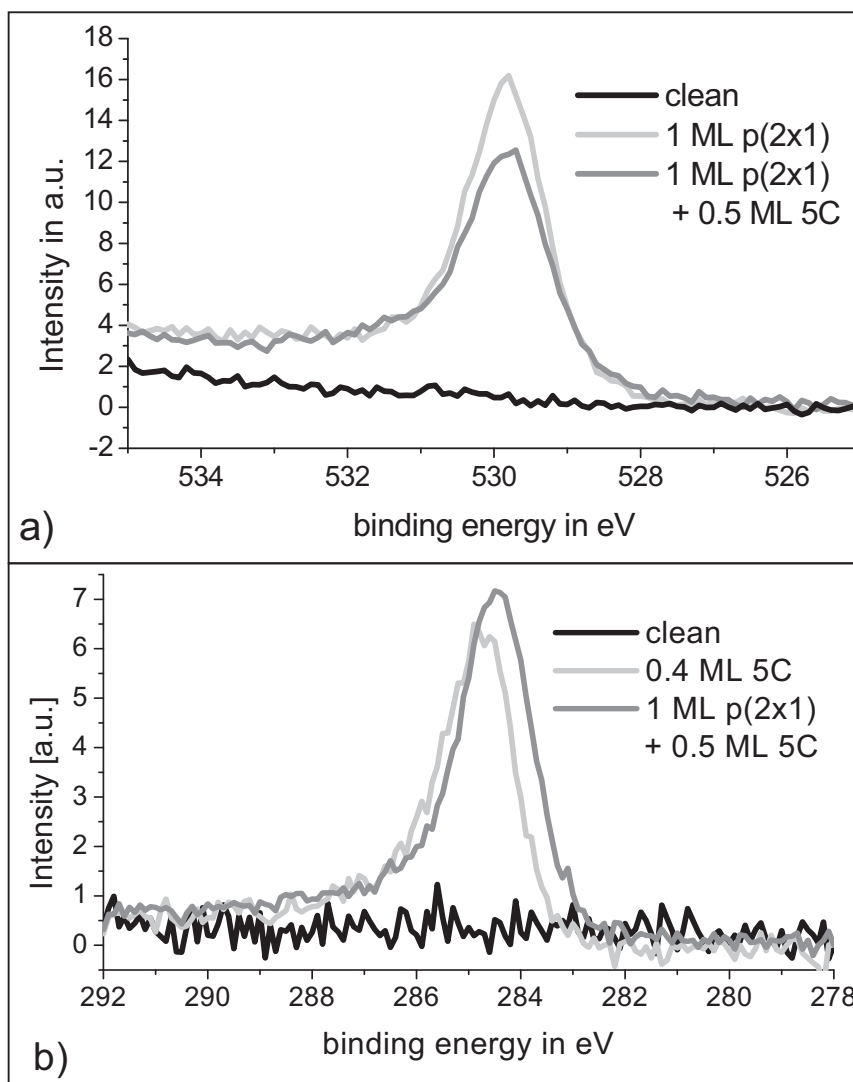

Figure 12: XPS data of Cu(110) covered with pentacene, p(2x1)O and p(2x1)O + pentacene a) O1s peak; b) C1s peak.

4.5 Oxygen induced condensation and phase transformation of pentacene on Cu(110)

The fascinating observation of two different mobile phases, which depend on the coverage and which are driven by small differences in the intermolecular interaction (cf. chapter 4.3) leads to a new approach for further studies on the self-assembly and on intermolecular as well as molecular/substrate interactions: It is well known that oxygen forms a highly ordered added-row reconstruction on the Cu(110) surface[84,90,91], as already described in the previous chapter. Furthermore, it has been reported that the mobility of Cu ad-atoms and O-atoms is sufficiently high – also at room temperature – for the self-assembly and the formation of the CuO added-row reconstruction, driven by an energy gain of 0.54 eV[92]. As a consequence, we combined the observation of mobile pentacene molecules on the Cu(110) surface with the p(2x1)O reconstruction by exposure of a sample partly covered with pentacene to oxygen.

4.5.1 Oxygen induced condensation of pentacene molecules

Figure 13 shows STM images of a sample covered with 0.4 ML of pentacene before (a) and after oxygen exposure (b). The oxygen exposure has been performed in the STM chamber at an oxygen partial pressure of $5*10^{-10}$ mbar. Figure 13a shows the (n x 3)-mobile phase as described in detail in chapter 4.3. After the adsorption of oxygen the pentacene molecules are not mobile anymore and can be resolved in the STM (cf. Figure 13b). Additionally, the p(2x1)O reconstruction is well visible between the pentacene molecules. It seems that the pentacene molecules tend to form rows running along the [0 0 1]-direction and are not randomly distributed on the surface. This is also visible in the LEED pattern in the inset of Figure 13b, which shows the p(2x1)O reconstruction spots as reported in chapter 4.4 and exhibits additional spots, which can be attributed to the pentacene rows as explained in the next subsection.

Figure 13c shows an STM image, which has been taken during a leakage in the STM chamber, which led to a base pressure of $6 \cdot 10^{-10}$ mbar, compared to $3 \cdot 10^{-10}$ mbar without leakage[i]. Besides the rows of mobile molecules twelve molecules are condensed in the lower part of the STM image. Between these molecules a small bright spot is visible. We attribute this either to an O-atom or to a CuO molecule adsorbed on the surface. On each side of this bright spot six pentacene molecules are immobilized. Hence, we can conclude that the adsorption of oxygen does not only hinder the molecular diffusion in the directly involved

---

[i] We compared the STM images taken with a leakage in the STM chamber to the ones which have been taken by oxygen exposure and which are mostly shown in this chapter and can state that both show the same behaviour. Thus, we conclude that the small adsorbate visible in this STM image is a CuO molecule or an O atom.

diffusion channel where the oxide is adsorbed but it also affects the diffusion of the molecules in neighbouring diffusion channels. Thus, a single oxygen atom adsorbed on the Cu(110) surface has a strong influence on the adsorption of neighbouring pentacene molecules. Organic electronic devices are often not produced under ultra high vacuum conditions as used here but under high vacuum in the range of 10^{-8} mbar or even by wet chemistry processing. Thus, we assume that "defects" like the oxygen atom shown here play a crucial role in the self-assembly of the organic semiconducting molecules and therewith in the device performance.
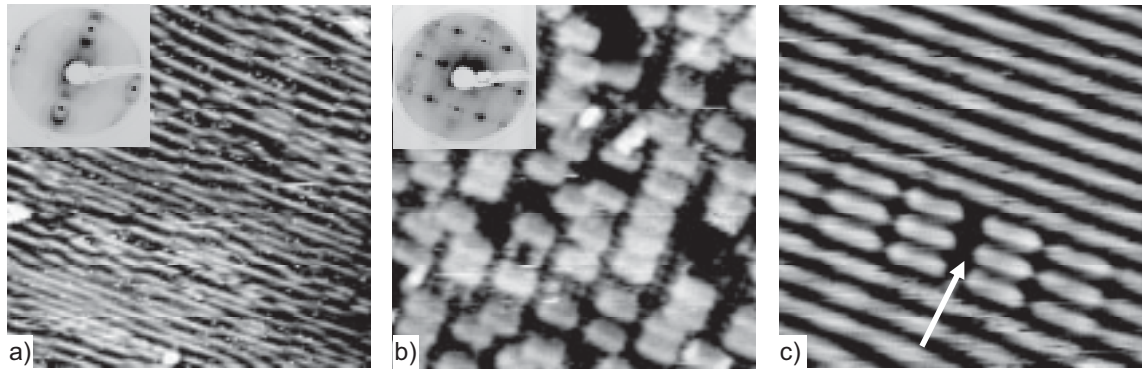
Figure 13: a) 0.4 ML of pentacene, (n x 3)-phase; inset: LEED pattern taken at 48.0 eV (U_{bias} = −1.6 V, I = 0.08 nA, 25 x 25 nm^2). b) 0.4 ML of pentacene after exposure to oxygen, the p(2x1)O reconstruction beside the pentacene molecules is visible, inset: LEED pattern taken at 68.7 eV, (U_{bias} = +0.3 V, I = 0.07 nA, 12.5 x 12.5 nm^2). c) single oxygen atom or CuO molecule between the pentacene molecules is highlighted by the white arrow; this STM image has been taken with a leakage in the STM chamber[i] (U_{bias} = −0.2 V, I = 0.4 nA, 8 x 8 nm^2).

Liem et al. explain the added-row oxygen reconstruction on the Cu(110) surface by the following mechanism[92]. (i) An O_2 molecule is adsorbed on the Cu(110) surface and dissociates into two oxygen atoms. (ii) These oxygen atoms diffuse on the surface until they find a Cu ad-atom. The diffusion barrier for the oxygen atoms along the $[1\overline{1}0]$-channels is approximately half the diffusion barrier perpendicular to the channels, which is 300 meV. (iii) Cu ad-atoms from steps diffuse on the surface until they hit an oxygen atom. (iv) The Cu and oxygen atom bind together by forming a charge transfer complex. We assume that in presence of the pentacene molecules the procedure of the CuO formation remains the same, only the diffusion is most likely reduced by the additional pentacene molecules, which also diffuse on the surface. Coincidentally, the diffusion barriers of pentacene molecules and oxygen adsorbates along the $[1\overline{1}0]$-channels are the same[25,92]. It has also been shown that short CuO chains can hop between neighbouring [0 0 1]-rows at room temperature[83,93,94]. We assume that this hopping phenomenon is strongly reduced in the presence of the pentacene molecules by a site-blocking mechanism. In conclusion, the condensation of the pentacene molecules is a multi-step/multi-component process and the complete understanding of this mechanism

would need additional variable-temperature STM measurements as well as detailed theoretical calculations.

4.5.2 *Oxygen induced reconstruction of pentacene on Cu(110)*

Figure 14 shows the time dependent evolution of the condensation and phase transformation for a sample covered with 0.6 ML of pentacene during oxygen exposure. It has been observed that the adsorption of oxygen during scanning was reduced due to shadowing effects of the tip. Therefore, the position of the STM tip has been changed after each STM image in Figure 14 to provide a fresh surface area.
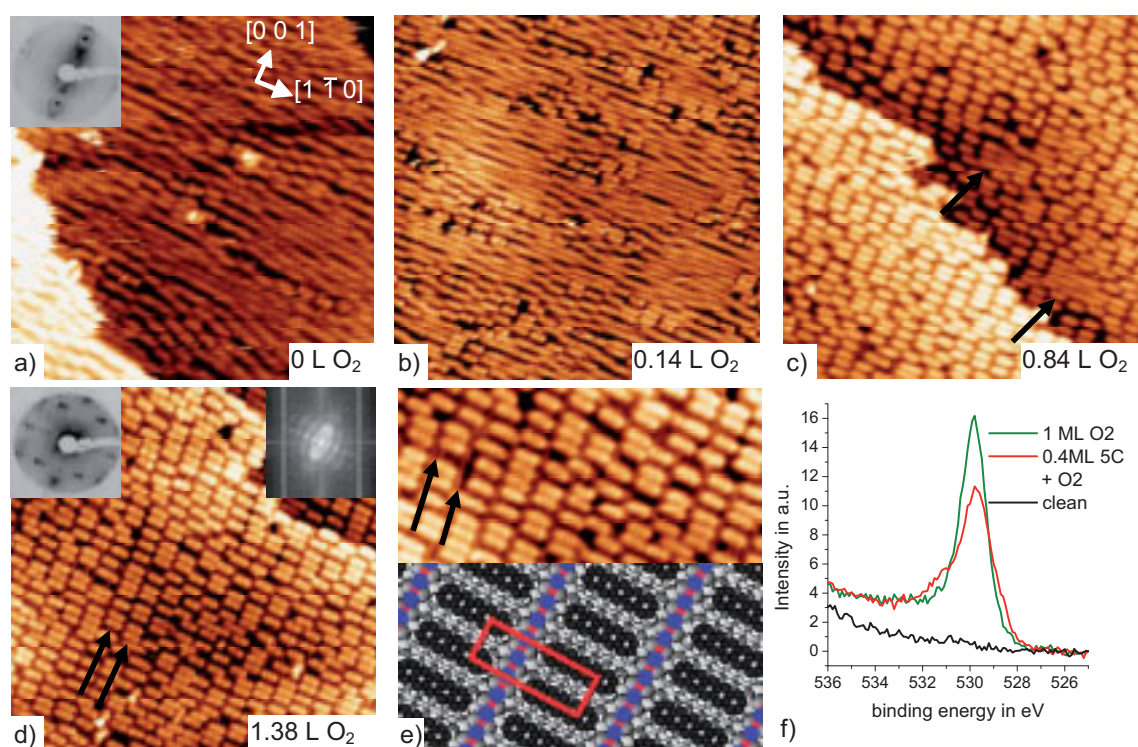
Figure 14: 0.6 ML pentacene on Cu(110) during oxygen exposure a) 0 L O_2, b) 0 .14 L O_2, c) 0.84 L O_2, d) 1.38 L O_2; inset in a) and d) top left: LEED pattern: 63 eV, d) top right: FFT of the STM image; e) bottom: adsorption scheme with additional Cu-atoms marked in red and oxygen atoms marked blue, top zoom of d) (a)-c) U_{bias} = −1.2 V, I = 0.08 nA, d) U_{bias} = +1.2 V, I = 0.07 nA, a)-d) 30 x 30 nm^2, e) top: 20 x 10 nm^2). f) XPS O1s peak of 1 ML of p(2x1)O, 0.4 ML of pentacene after oxygen exposure and on clean surface.

The image in Figure 14a was taken before the oxygen exposure started and the mobile (n x 2)-structure was observed. After exposure to a small amount of oxygen the molecules appear immobilized at some sites (Figure 14b). The comparison of Figure 14b and Figure 13c

shows that the initial immobilization does not always result in an ordered arrangement of the neighbouring molecules as shown in Figure 13c, but in most cases the molecules, which condense due to the adsorption of oxygen atoms, show a considerable disorder. Condensation nuclei usually contain between three to six pentacene molecules. In most cases it was not possible to resolve the oxygen adsorbates and the molecules with the same STM settings and tip conditions and therefore only the condensed molecules resulting form the oxygen adsorption but not the oxygen itself is visible in the STM images (cf. Figure 14b and c).

After exposure to 0.84 L oxygen (L = 1 torr·μs ≈ 1,33·10^{-6} mbar·s) nearly all molecules are condensed and only few mobile molecules, marked with black arrows in Figure 14c, are visible. After nucleation, the areas where the molecules are first condensed are growing laterally until they converge with neighbouring condensed areas. After exposure to 1.38 L oxygen no molecular mobility is visible anymore (cf. Figure 14d). Figure 14e top shows a zoom of the image in Figure 14d, and some positions where the adsorbed CuO is visible are marked with arrows.

Astonishingly, in Figure 14d the molecules are not only immobilized by the additional oxygen but they are also well ordered in rows running along the [0 0 1]-direction. Two of the longest rows are marked with black arrows in Figure 14d. The LEED pattern in Figure 14d top left shows an (8 x 2) diffraction pattern, which has never been observed without oxygen exposure of the sample but could be reproducibly prepared by exposure of the partly covered pentacene surfaces to oxygen. Thus, we can conclude that the spacing between neighbouring Cu-atoms along the [1 $\overline{1}$ 0]-direction is eight Cu-atoms, i.e. one lattice constant more than for the (7 x 2)-structure, which is observed on the clean Cu(110) (cf. chapter 4.3, Figure 1). This leads to the proposed adsorption model, which is shown in Figure 14e bottom. The rows of the pentacene molecules which are running along the [0 0 1]-direction are separated by one CuO row resulting in a spacing of eight Cu-atoms. The red rectangle indicates the (8 x 2) unit cell, which has been derived from the LEED images. We assume that the oxygen forms the same added-row reconstruction as on clean Cu(110) samples without molecular adsorbates. The hypothesis that oxygen adsorbs as CuO is verified by the XPS data on the O1s peak, which shows that the oxygen binding energy for the O/pentacene/Cu(110) system is the same as for the p(2x1)O reconstruction (cf. Figure 14f). The added-row oxygen reconstruction is further confirmed by STM images of samples with low pentacene coverage: small one monolayer deep vacancy islands have been found (cf. Figure 15, top) similar to the one shown in Figure 8b in chapter 4.4. This vacancy island results from the supply of Cu ad-atoms from the flat terraces due to the reduced diffusion at high oxygen coverage.

In Figure 14d and at the top of Figure 14e it is visible that the spacing of the molecules in the [0 0 1]-direction is not always the minimum spacing of two Cu-atoms as observed for 1 ML of pentacene without oxygen (cf. chapter 4.3) but there are also molecules which are separated by three or more Cu lattice spacings. This can be also seen in the LEED image in Figure 14d: the spots at ½ of the substrate reciprocal lattice vector in the [0 0 1]-direction are smeared out, which indicates a weak long-range ordering in this direction. The left arrow in

Figure 14e points to some CuO molecules adsorbed in-between the pentacene molecules along this direction. Although the LEED image shows a well ordered adsorbate structure the long-range ordering is slightly lower in the locally resolved FFT taken on Figure 14d and shown in the inset top right. We conclude that the quality of the self-assembly strongly depends on the pentacene coverage as well as on the kinetics, which is determined by the mobility of the different components of this system.

After complete immobilisation of the pentacene molecules the structure as observed by STM and LEED did not change with increasing oxygen exposure. The XPS data of the O1s peak shows a saturation of the peak intensity after complete immobilization of the pentacene molecules. This can be attributed to the strongly reduced sticking coefficient of oxygen when the Cu surface is completely filled with adsorbates.

Our findings on the oxygen induced reconstruction and the adsorption structure shown in Figure 14e leads to the conclusion that the self-assembly for this system strongly depends on several factors: The self-assembly is determined by the pentacene coverage. The theoretical amount of pentacene, which is necessary to form the (8 x 2)-structure is 0.78 ML, where 1 ML is the coverage needed for the (6 1, -1 4)-structure as shown in chapter 4.3. However, a coverage of 0.6 to 0.8 ML of pentacene on the clean Cu(110) already strongly reduces the mobility of the molecules and leads to the formation of the (7 x 2)-structure as reported in chapter 4.3. The reduced mobility of the molecules at these coverages reduces the long-range ordering and leads to less ordered adsorption structures, after oxygen exposure. This observation leads to the second important factor for this system, which is the diffusion. The here reported system is a three component system: pentacene, oxygen and Cu. All three components need a sufficiently high mobility to form the well ordered (8 x 2)-phase. Of course, the diffusion of all three components will be strongly reduced with increasing coverage due to site blocking effects. We assume that annealing during the oxygen exposure would facilitate the self-assembly due to the higher diffusion at elevated temperatures.
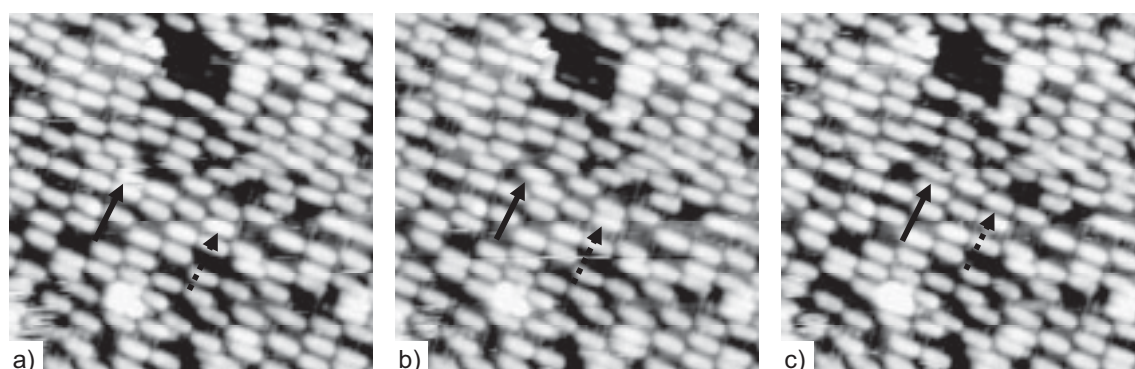
Figure 15: 0.3 ML of pentacene on Cu(110), STM images of the same area; the black arrows indicate mobile molecules (U$_{bias}$ = −1.2 V, I = 0.1 nA, 20 x 20 nm^2).

In Figure 13 and Figure 14 it is visible that the oxygen exposure can pin the mobility of the pentacene molecules. For small pentacene coverages as shown in Figure 13b the CuO reconstruction is clearly visible in-between the molecules. The adsorption of CuO leads to a reduction of the mobility, which provides a good tool for a more detailed investigation of the intermolecular interaction. In Figure 15 three STM images taken consecutively on the same sample spot are shown. The oxygen exposure has been stopped slightly before all mobility was frozen. Thus, the remaining mobility can give an additional insight in the formation of this (8 x 2)-structure and in the intermolecular interactions. The black arrows in Figure 15 highlight molecules which are not immobilized. The molecule highlighted by the black solid arrow in Figure 15 shows a comparably high diffusivity, which manifests itself in its fuzzy appearance. In Figure 15a and c this molecule hopped away during imaging resulting in two "broken" molecules.

Furthermore, also mobility along the [0 0 1]-direction was observed, highlighted by the dashed arrow. The hopping of molecules along the [0 0 1]-direction is a very important observation because a good long-range ordering can only be expected if the mobility in both crystallographic directions is sufficient. The repulsive interaction along the [0 0 1]-direction, already proposed in chapter 4.3 can be confirmed by the molecules highlighted by the dashed arrow in Figure 15. First the centred molecule of the three molecules hops one Cu-atom in the direction of the arrow resulting in two densely packed molecules (cf. Figure 15b). Then the upper molecule hops away due to the repulsive interaction of these two nearest molecules (cf. Figure 15c). The fact that the final position as imaged in Figure 15c has been stable for more than one hour after the last jump, leads to the assumption that these molecules are in their equilibrium position. The series of STM images in Figure 15 has been taken with a time interval of approximately ten minutes.

4.6   Summary and outlook

The detailed study of the pentacene/Cu(110) interface led to several new findings. The interaction of the organic molecules with the substrate strongly influences the Shockley surface state of the Cu(110) surface. Instead of examining the molecular orbitals, like it is usually done for molecular/substrate interfaces, we investigated the influence of the molecular adsorbate on the substrate surface. For these studies the surface state is a very suitable probe because it is localized on the surface and strongly decays in the bulk. In the here reported case it has been shown that a complex interplay of several interfacial phenomena like charge injection, mixing and hybridization of electronic states, Pauli repulsion and polarization of the organic adsorbate in the surface dipolar field leads to a shift of the surface state away from the Fermi energy. Furthermore, we are the first to observe that the adsorbate structure determines the changes in the surface state. While the occupation of the surface state for 0.8 ML of pentacene is the same as for the clean Cu(110) it increased slightly after adsorption of 1 ML

pentacene. This increase is not isotropic but results in an increased anisotropy of the surface state. We relate this increase of the anisotropy to the increasing intermolecular interaction which arise from the denser packing along the $[1\bar{1}0]$-direction.

Furthermore, we investigated the growth behaviour of pentacene on the Cu(110) surface in more detail. Five different adsorption structures have been shown depending on the coverage and on the relative position of the molecules. The two different mobile structures, which have been observed for coverages below 0.6 ML, are of particular interest because most molecular systems only show one mobile phase before condensation. Although many studies of the growth of pentacene on Cu(110) have been performed till now, we have been able to refine the phase behaviour of pentacene for coverages between 0.2 and 1 ML on this substrate: Three different condensed and two mobile phases have been identified.

After determining this complex multiphase behaviour we additionally investigated the growth of pentacene on the oxidized p(2x1)O Cu(110) surface. The observation that pentacene preferentially adsorbs on the bare metal led to the conclusion that the interaction between the molecules and the oxidized surface is weaker than the interaction of the molecules with the clean metal surface. However, the pentacene molecules exhibit a much lower mobility on the p(2x1)O. This reduced mobility, which also results in no long-range ordering, has been explained by the different surface corrugation in chapter 4.4 (cf. Figure 11b). While there is a low surface corrugation along the $[1\bar{1}0]$-direction of the Cu(110) surface, which results in diffusing molecules in these grooves, the surface corrugation along this direction is much higher for the p(2x1)O surface due to the CuO rows running perpendicular to this direction. This different surface corrugation also results in a different orientation of the molecules. While on the clean metal the molecules are oriented with their long axis parallel to the $[1\bar{1}0]$-direction they are rotated by 90° on the p(2x1)O surface resulting in an orientation with the long axis parallel to the [0 0 1]-direction. Calculation on the adsorption energy and the diffusion barrier depending on the molecular orientation on the p(2x1)O surface are in progress and will hopefully lead to a deeper insight into the adsorbate/substrate interaction.

Additionally, it has been shown that the molecular mobility on clean Cu(110) can be strongly reduced by oxygen exposure due to the formation of CuO rows on the surface, which serve as pinning centres for the pentacene molecules. The increase of the long-range ordering by the oxygen exposure, which may lead to long molecular chains, each chain separated by one CuO row is especially interesting. Further theoretical studies of the influence of the adsorption of oxygen on the mobility of the pentacene molecules and the self-assembly are in progress. Experiments on the structure of pentacene rows separated by CuO chains should be continued to study the influence of adsorbates on the surface states. It has been shown that for coverages of 1 ML the occupation of the surface state is asymmetrically changed due to increased intermolecular interaction. By separating the pentacene molecules with the CuO chains this intermolecular interactions can be strongly reduced and the influence of a single molecular row on the surface state could be studied. The measurement of the surface state is

especially suited for this system, since the surface state is quenched upon chemisorption of oxygen on Cu(110)[95].

In conclusion, several new aspects of the well known pentacene/Cu(110) system have been investigated. This was only possible by using complementary measurement techniques like STM, LEED, XPS and angle-resolved UPS. Further insight into this system would be gained by extending the measurement methods to techniques which measure the unoccupied molecular orbitals, like IPES or STS.

A further investigation of the two different mobile phases by temperature dependent STM measurements would allow for the study of the freezing of the mobile pentacene molecules on Cu(110). With these studies an Arrhenius plot could be determined and it would be possible to experimentally confirm the barrier of diffusion which has been calculated. Coverage dependent measurements at variable temperature then could lead to further insight on the intermolecular interaction for the mobile phase. It is expected that the condensation of the molecules takes place at higher temperatures for higher coverages due to increasing intermolecular interactions.

We have been the first group to show a shift of the surface state to higher binding energies upon adsorption of a molecular monolayer. It would be interesting to extend this project to other molecular/substrate systems. The investigation, by ARPES, of the (8 x 2)-phase which has been prepared by oxygen exposure to a sample covered with 0.6 ML of pentacene, has been already mentioned above. Another interesting system would be the adsorption of pentacene on Ag(110). It is believed that the interaction between the silver surface and the molecules should be smaller due to the less reactive character of the silver compared to copper substrates. It has been shown that PTCDA strongly chemisorbs on Ag(111) resulting in a shift of the surface state by approximately 600 meV[96]. It would be interesting to investigate the interactions of the pentacene with the Ag surface to get a deeper insight into the influence of organic adsorbates on metal Shockley surface states. Another approach would be to investigate different adsorbates like pentacene-quinone or PTCDA on the Cu(110) surface.

5 Interaction of OEPs with metals and ultrathin NaCl layers

5.1 Introduction: Molecules on insulator surfaces

In view of applications of organic molecules as single molecular electronic devices for a new generation of computers it is necessary to assemble them in a very controlled way. While single molecular positioning, e.g. with the tip of a scanning tunnelling microscope is time consuming, self-assembly provides a concept that is promising towards the integration of molecules or molecular layers for functional data storage devices. Several different concepts for data storage in single molecules have been proposed. Either the information can be stored in the molecular conformation and/or adsorption position[17,18,97], or it can be stored electronically either in the charge state[7] or in the electronic spin[98]. If a single molecule or atom is to be used as charge storage device the electronic interaction between the adsorbate and its environment has to be reduced so that sufficient decoupling for maintaining a stable charge state is achieved.

In semiconductor technology, one approach to realize electronic decoupling between the active semiconducting layer and the contacting interface is the use of insulator substrates, e.g. the gate oxide, instead of metals. However, for surface science studies, the use of bulk insulators significantly limits the number of analysis methods. Their insulating character prohibits STM in most cases and techniques like XPS, UPS and LEED become difficult due to charging of the substrate. With the invention of the atomic force microscope[99] and its further development to achieve atomic resolution[100] this obstacle could be overcome and since then several experiments on the molecular self-assembly mainly on alkali halide single-crystals and Al_2O_3 have been carried out. The review article by Bennewitz and references therein give a detailed overview on the studies of adsorbates on wide band gap insulators[101].

The self-assembly of organic molecules on bulk insulators is strongly determined by the weak interaction between organic molecules and the insulator surface. On insulator substrates in general, molecular aggregation is driven to a higher degree by the intermolecular interaction than by the interaction of the adsorbates with the substrate. An example is provided by the similar adsorption structure of C_{60} on NaCl and KBr, mostly determined by the van der Waals radius of the molecules[102]. Often the molecules are mobile on insulators for low coverages[103] and only low temperature or pre-patterned surfaces pin the molecules[104,105]. For example, it has been shown that PTCDA preferably grows in nanometre sized monolayer deep vacancy islands on a KBr(001) surface[105]. The same behaviour has been observed for chloro-[subphthalocyaninato] boron-(III) (SubPc) where the enhanced interaction of the molecular dipole with the charged corners of monolayer deep vacancy islands in KBr lead to an immobilization of the SubPc molecules[104]. On flat, not pre-patterned insulator substrates the organic molecules usually do not grow in a layer by layer mode, but in an island growth mode. For example, a nominal coverage of only 0.3 ML of PTCDA already results in islands

with a height of 20-30 molecular layers[106]. Only few systems are known where monolayer thick islands of organic molecules can be grown without a considerable amount of bulk-like crystallites; one example is the growth of PTCDA on NaCl where the three-dimensional growth starts at coverages of 0.85 ML[107].

Instead of using bulk insulators as reported in the previous paragraph, organic molecules can also be adsorbed on ultrathin insulator films. Such systems can be characterized with all surface analysis techniques including STM. It has been shown that electron tunnelling through several monolayers of insulators is possible because the charge density of the electronic states of the metal extends into the vacuum[108]. The high variety of metal substrates and insulator ad-layers lead to many different systems like CaF_1/CaF_2 on Si (111)[109], Al_2O_3 mostly on Al containing substrates like $Ni_xAl(111)$[110,111] and NiAl(110)[112], NiO on Ni[113] and Ag[114], NaCl on various metal substrates with different crystallographic orientation (cf. Ref.[108] and references therein) and MgO on Ag(001)[108,115] and other metal surfaces. The evolution of the electronic behaviour of ultrathin insulator layers was demonstrated for MgO on Ag(001). Here, STS showed that an interface state detected for the first and second monolayer of MgO exists and the third layer already represented a band gap corresponding to that of a MgO single-crystal surface[108].

There are two main approaches for the preparation of ultrathin insulator films on metal substrates: Oxides like MgO, NiO or CoO are either prepared by oxidizing the metal substrate in an oxygen atmosphere at high temperatures or by evaporating the metal precursor in an oxygen stream. Although it is possible to e.g. directly evaporate MgO by electron beam evaporation[116] this direct evaporation is practically not applied for the growth of ultrathin oxide films due to the ease of oxidation of the metal precursor in the UHV in an oxygen background pressure. In contrast, alkali halides and earth alkali halides like CaF/CaF_2 are directly thermally evaporated[23,74]. Mass-spectrometric studies showed that NaCl mainly evaporates as di-ionic cluster (one sodium ion and one chlorine ion). The concentration of di-ionic clusters decreases with increasing evaporation temperature but it is higher than 85% for temperatures below 850 K[117]. The temperatures used for the evaporation of NaCl in the here described experiments are well below 850 K, ranging from 650 to 700 K.

Several studies of the growth and the electronic properties of organic molecules on ultrathin alkali-halide layers have been reported. Organic molecules generally show a high mobility on the ultrathin insulators. The molecules can be immobilized by cooling the substrate to low temperature[118] or by complete filling of a monolayer[23,73] and thus they can be imaged with the STM. So far, only for CuOEP on NaCl/Pd(111) pinning of the molecules has been achieved on the NaCl layer at room temperature also at small molecular coverages[119]. A small difference in the layering of iron phthalocyanines (FePc) on NaCl/Cu(111)[73] compared to the layering of CuOEP on NaCl/Cu(111)[23] can be found in literature. A hierarchical layer formation of the CuOEP on NaCl/Cu(111) has been observed, i.e. first the molecules are adsorbed on the bare metal, after complete filling of the metal area, which leads to a freezing of the molecular mobility, the molecules are adsorbed on the first layer of NaCl. Here again

the molecules are very mobile until the first NaCl layer is completely covered with the molecules and after this the molecules can also be found on the second layer of NaCl[23]. In contrast, the adsorption of FePc on NaCl/Cu(111) deviated from the hierarchical layer formation. After filling both, the free metal area and the first NaCl layer, FePc starts to form a second layer on top of the FePc molecules on the metal whereas no molecules were observed on the second monolayer of NaCl[73]. Thus, small differences in the intermolecular interaction energies of the FePc and CuOEP as well as in the interaction of the molecules with the NaCl/Cu(111) surface lead to different growth modes of the planar molecules on ultrathin insulator layers.

The adsorption of atoms or molecules on ultrathin insulators can lead to new insights into the modified electronic structure. Most prominently, decoupling of the electronic states of the adsorbate and the substrate occurs. Thereby, it is possible to directly image the electronic states of organic molecules and to compare them with DFT calculations[31,118,120]. It was also demonstrated that the charge state of an individual gold atom on an NaCl layer can be changed in a controlled way by voltage pulses applied via the STM tip[118,121]. For Ag atoms on NaCl it is even possible to control and image three different charge states (Ag^0, Ag^{+1}, Ag^{-1})[122]. It has been demonstrated that the charged Ag^{+1} and Ag^{-1} have different stabilities depending on the ionization potential and the electron affinity of the Ag atom, respectively and depending on the interaction of the charged particles with the underlying NaCl layer. While the Ag^{-1} is unstable for some adsorption sites the positively charged Ag^{+1} is stabilized by its position at bridge sites between two Cl anions and the comparably low ionization potential of silver[122].

Furthermore, ultrathin insulator substrates have been used in order to observe fluorescence and phosphorescence spectra by exciting organic molecules with tunnelling electrons in STM[112,123]. Especially for Zn(II)-etioporphyrin on Al_2O_3/NiAl(110) it was shown that the fluorescence strongly depends on the molecular conformations and on the electronic states of the molecules. A LUMO state near the Fermi energy seems to be necessary for the light emission, while molecules without this special LUMO state did not show any light emission in the range of 500 to 1000 nm wavelength[112].

The aim of this study is the investigation of the electronic interactions of the CuOEP with the Cu(111) metal and with the ultrathin insulator layers. Thereby, we want to discover the driving force of the hierarchical ordering of CuOEP on Cu(111)/NaCl[23]. We assume that the electronic interaction of the CuOEP molecules with the substrate decreases with increasing NaCl thickness. This would be seen in the molecular electronic states of the CuOEP molecules: a strong electronic interaction should lead to organic electronic states, which deviate from the gas phase electronic states in their position as well as in their full width half maximum. For smaller electronic interactions the orbitals should be similar to the gas phase electronic states. Organic molecular electronic states are usually investigated by UPS, NEXAFS and IPES. All these analysis techniques are very suitable for these measurements, but they require homogenous surfaces, because they average across big surface areas

($500\ \mu m^2$ – $2\ mm^2$). Due to the island growth of NaCl on Cu(111) the first step towards the detection of electronic states in dependence of the insulator thickness was to find a suitable system of alkali halides on metal surfaces, which shows a layer by layer, or at least a Stransky-Krastanov growth.

5.2   Optimized growth conditions for large alkali halide islands

The goal of this study of ultrathin insulator films on different metal substrates is the creation of homogenously covered surfaces, in order to provide the necessary basis for the study of molecules on ultrathin insulators with averaging techniques like UPS, XPS and NEXAFS. In contrast to organic molecules on metals, which usually show a Stransky-Krastanov (layer plus island) growth on metal surfaces, most insulators tend to grow in the Volmer-Weber (island) growth mode on metal surfaces. The island size and distribution can be controlled by the annealing temperature and the growth rate. A known exception to the Volmer-Weber growth is the growth of CaF_2 on Si(111) surfaces which shows a Stransky-Krastanov growth mode[124]. For this system a wetting layer of Si-Ca-F leads to growth of CaF_2 in Stransky-Krastanov growth mode. However, in this case, the first layer – the Si-Ca-F – shows semiconducting and not insulating behaviour.

Table 2: lattice misfit[ii] of several alkali halide/metal systems.

Insulator/metal	Lattice misfit 45° orientation	Lattice misfit 0° orientation
NaCl/Ag	2.30 %	-27.70 %
NaCl/Cu	-9.38 %	36.02 %
LiCl/Cu	-0.39 %	-29.67 %
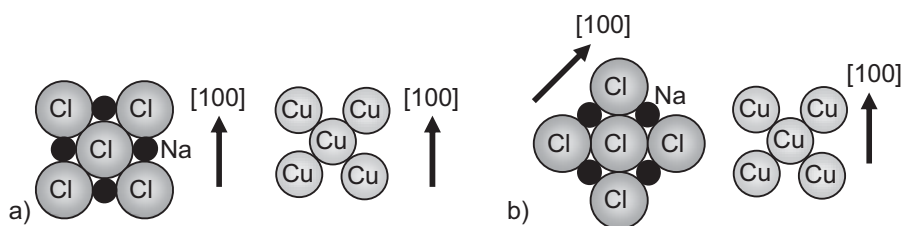
Figure 16: relative orientation of NaCl on Cu(001) a) 0° orientation, b) 45° orientation.

Several parameters determine the growth mode of epitaxial systems: (i) the surface tension of the adsorbate and the substrate, (ii) the adsorbate/adsorbate and the adsorbate/substrate interaction, (iii) the lattice misfit, (iv) the substrate temperature and (v) the

---

[ii] The lattice misfit has been calculated by: (n·a(substrate)–m·a(film))/a(film); a: lattice constant; n and m: integers; positive sign indicates a smaller adsorbate lattice compared to the substrate lattice[29].

adsorbate flux. Parameters (i)-(iii) determine the thermodynamics of the growth while parameters (iv) and (v) determine the growth kinetics. An increasing lattice misfit is less favourable for Frank van der Merwe growth due to induced stress in the adsorbate layer. Table 2 shows the lattice misfit of several alkali halide/metal systems. The lattice misfit has been calculated for the alkali halide [1 0 0]-direction parallel to the [1 0 0]-direction of the substrate, or rotated by 45°. The two different orientations are demonstrated in Figure 16. The lattice misfit for alkali halides on the trigonal (111) surfaces along one of the [1 $\overline{1}$ 0]-direction is the same as for the 45° rotation on the (001). Thus, depending on the orientation of the alkali halide overlayer with respect to the substrate orientation the lattice misfit can be minimized. For example, it has been shown that NaCl on Ag(111) shows two different rotational orientations: one parallel to the [1 $\overline{1}$ 0]-direction and one 45° rotated with respect to this orientation[125]. Table 2 shows that the smallest lattice misfit is given for a 45° rotation of the LiCl on the Cu(001). Thus it is expected that this system leads to a homogenous growth. In the following we will focus on the growth of LiCl on Cu(001) as well as on the growth of NaCl on Cu(111), Ag(111), Cu(001) and Cu(311).

Table 3: Temperature dependent lattice constants for Ag, Cu and NaCl and values for the smallest lattice misfit of NaCl on Ag and Cu[ii]; values for the thermal expansion of NaCl from[126], for Cu and Ag from[127].

	a (NaCl)	a (Ag)	a (Cu)	Lattice misfit Ag in %	Lattice misfit on Cu in %
300 K	5.640 Å	4.085 Å	3.615 Å	-2.37	-9.35
400 K	5.664 Å	4.093 Å	3.621 Å	-2.15	-9.59
500 K	5.688 Å	4.101 Å	3.627 Å	-1.92	-9.82
600 K	5.714 Å	4.109 Å	3.633 Å	-1.67	-10.08
700 K	5.744 Å	4.117 Å	3.639 Å	-1.34	-10.41

Evaporation on substrates kept at elevated temperatures usually leads to larger grains of the adsorbate due to increased adsorbate diffusion. However, the lattice constants depend on the temperature. As the thermal expansion of insulators is different to the one of the metals, the temperature dependent lattice misfits for NaCl on Ag and Cu have been calculated for 45° orientation (cf. Figure 16b) and are summarized in Table 3. The evaporation temperature of NaCl in our experiments is between 650 and 700 K. Thus, annealing to higher substrate temperatures seems to be inappropriate, accordingly only temperatures of maximum 500 K have been used during NaCl growth. The lattice misfit for the system of NaCl on Ag(111) decreases with increasing temperature due to the higher thermal expansion of the insulator. This decrease may additionally favour the growth of large islands at elevated temperature.

In general, it is not straightforward to compare the lattice misfit or the different lattice parameters of the metal substrates with alkali halide lattice parameters. As the metallic bond leads to very strict distances between neighbouring atoms, the ionic bond can stand tension or compression forces better due to the longer ranging attractive Coulomb interaction between the two differently charged building blocks of the insulator. Additionally, the lattice constant

of a single insulator layer may be considerably different than the one of the bulk insulator. This leads to the often observed carpet-like growth[128] where the insulator is slightly compressed at the bottom of the step and slightly extended on top of the step. As a consequence changes in the NaCl lattice constant for ultrathin layers of up to 6% have been observed earlier[125]. These big changes in the lattice constants lead to stress in the adsorbate layer when the second and third layer are grown on top and may lead to a higher defect density and/or to Stransky-Krastanov growth.

It is still discussed whether the first monolayer of NaCl on single metal crystals is a single layer of NaCl or if the dipoles of the NaCl are oriented perpendicular to the surface resulting in a double layer. Actually, for NaCl on Cu(111)[129] and Ge(001)[130] it is assumed that the first layer is a double layer, while it is reported that the first layer of NaCl on Al(111) and Al(001) is a single layer[128]. Due to the different DOS of NaCl compared to the metal substrate this question is difficult to solve in STM, which does not show a real height image but strongly depends on the DOS above the adsorbate and the substrate surface. Despite this discussion we call the lowest layer observed in STM a monolayer and the next layer on top of it the second layer keeping in mind that the first layer may be a double layer.

5.2.1   *LiCl on a surface with square lattice: Cu(001)*

Table 2 shows that the smallest lattice misfit for alkali halides and Cu or Ag single crystals exists for LiCl on Cu. For this system, the lattice misfit is only 0.39% for the growth of the LiCl islands with the [1 0 0]-direction parallel to the Cu [1 $\bar{1}$ 0]-direction. It has been reported that LiCl shows a Frank van der Merwe (layer by layer) growth on Cu(001)[131]. These studies have been performed with reflection high-energy electron diffraction (RHEED) with LiCl grown on Cu(001) at room temperature and at 450 K. To the best of our knowledge the growth of LiCl films on Cu(001) has not been investigated with STM, yet. Consequently, we have performed an STM and LEED study of this system. For this study LiCl has been deposited on the Cu(001) samples kept at room temperature.

Figure 17a shows the STM image of a sample covered with 0.4 ML LiCl. Two different orientations of the LiCl islands can be observed. Most of the islands grow with their [1 0 0]-direction in a 45° orientation with respect to the [1 0 0]-direction of the substrate, while a few grow in a 0° orientation. This is in contrast to earlier reports, which claim that LiCl deposited onto Cu(001) kept at room temperature only grows with the [1 0 0]-direction parallel to the [1 $\bar{1}$ 0]-direction of the substrate[131,132]. Additionally, also for the comparably small coverage of 0.4 ML on some islands a second layer starts to grow, which is also in contrast to previous reports on the growth of LiCl on Cu(001), which shows a layer by layer growth[131,132]. Figure 17b shows a zoom-in in a region where two islands with different orientation coalesce, the blue arrow in Figure 17a highlights the zoom-in region. The different

orientations of the two domains are clearly visible by the atomic resolution of both islands. We assume that similarly to NaCl also for LiCl only the chloride ions can be imaged in STM[133].
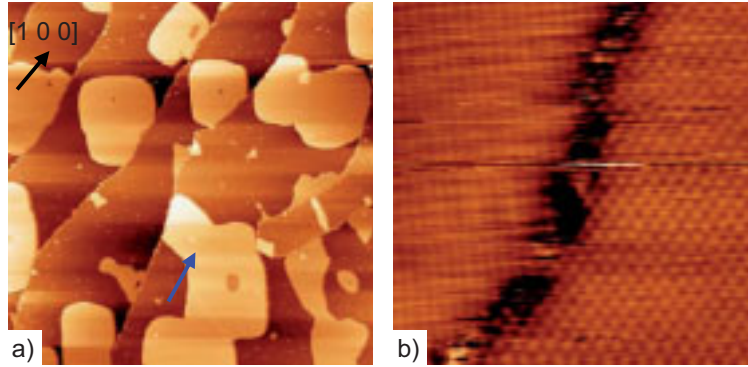
Figure 17: 0.4 ML of LiCl on Cu(001), a) overview; b) zoom-in of a) marked with a blue arrow (U_{bias} = -3.0 V, I = 0.05 nA, a) 500 x 500 nm², b) 10 x 10 nm²).
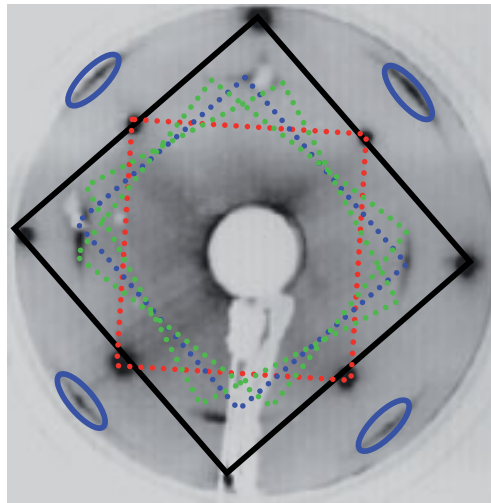
Figure 18: LEED pattern taken at 57.4 eV on the sample shown in Figure 19; The black square indicates the Cu(001) lattice; the red square indicates the LiCl lattice rotated by 45° with respect to the Cu(001) lattice; the blue square indicates the LiCl lattice with 0° rotation; the green squares indicate the small rotational freedom of the 0° island; the blue ellipses show the smearing out of the second order spots of the 0° island.

Figure 18 shows a detailed analysis of the LEED pattern taken for 0.5 ML of LiCl on Cu(001). The black square indicates the reciprocal lattice of the Cu(001) substrate. The red square highlights the spots, which can be associated to the 45° islands. The second order spots of this lattice are overlapping with the first order spots of the clean substrate. The blue square indicates the 0° islands. The spots for the 0° islands are slightly smeared out, indicating a

small rotational freedom of approximately ±10°, which is indicated by the two green rectangles. The second order spots for this domain are marked with blue ellipses. It is clearly visible that the peaks for the 45° islands are sharper and more intense than the one for the 0° islands. The different spot intensities indicate the preferred adsorption of LiCl in the 45° orientation, which is the orientation with the smallest lattice misfit. This observation is in-line with the STM images, which show more islands with the [1 0 0]-direction rotated by 45° with respect to the [1 0 0]-direction of the Cu(001).

There are several differences in the growth of LiCl and NaCl on metal surfaces; the growth of NaCl on different metal surfaces is shown in detail in the next chapters. The most prominent difference is that LiCl islands only grow on top of the terraces and the carpet-like growth over steps as observed for NaCl is not visible in Figure 17a. This can have two reasons: (i) The diffusion barrier of LiCl over the Cu(001) steps at room temperature is too high and consequently no LiCl can diffuse over the steps and start the carpet-like growth. It seems that LiCl islands start to grow at step edges which serve as nucleation sites and the islands then extend over the terraces until they meet another step edge, where the lateral growth stops. (ii) The different interaction between the LiCl and the Cu(001) surface compared to the interaction between NaCl and metal surfaces may lead to less favourable adsorption at steps resulting in island growth on terraces. NaCl prefers to overgrow steps because the induced stress in the NaCl layer by the lattice misfit can be reduced by this carpet-like growth. Due to the smaller lattice misfit of LiCl/Cu(001) the stress in the LiCl adsorbate layer may be smaller, which may result in a less favourable growth over steps.

In Figure 19 STM images of another sample with 0.5 ML LiCl are shown. The sample in Figure 19b has been recorded at the same position as Figure 19a after a zoom-in and zoom-out series, which has been performed on the bottom left part of Figure 19a. Two islands in each image are highlighted with black contours. The black and white arrows in both images highlight big changes in the shape of the LiCl islands. While a complete island has disappeared below the black solid arrow, a new island has grown next to the white arrow. The size of the islands on the right and left side of the black solid arrow has increased. As the zoom-in has been performed on the bottom left corner we assume that the change in the LiCl island close to the white arrow in the top part of this image cannot be related to a tip induced change. The black dotted arrow highlights a second layer of LiCl, which also changed its shape. The grey arrow highlights a vacancy island which moved upward in the second image. This can be clearly seen by the small second layer below the grey arrow highlighted by a black circle, which is farer away from the vacancy island in Figure 19b, compared to the distance in Figure 19a.

We assume that the observed changes in the shape and size of the LiCl islands are due to small differences in the thermodynamics of the differently oriented islands, which leads to a rearrangement of LiCl to form the thermodynamically more stable adsorption geometry. This reorientation may take place by a rearrangement of small LiCl clusters from an island with one orientation to an island with the other orientation, which leads to a growth of one island

while a neighbouring island is shrinking. The big changes of the islands shapes have only been found for areas where two islands with different orientation converge. The adsorption energy for one LiCl dimer has been calculated to 0.43 eV[131], which is quite low and may lead to motion of small clusters. The driving force of this reorientation is presumably not an Ostwald ripening process because in Figure 19 the bigger islands disappear and smaller islands are growing, (cf. black and white arrow in Figure 19a and b). Furthermore, we have taken a movie on the sample one day after preparation. Two of these images which have been taken with a time interval of 45 min are shown in Figure 20 and no changes could be observed in these two images. In conclusion, this study shows that the rearrangement of the LiCl islands is not induced by the STM tip but a slow relaxation of the islands took place.
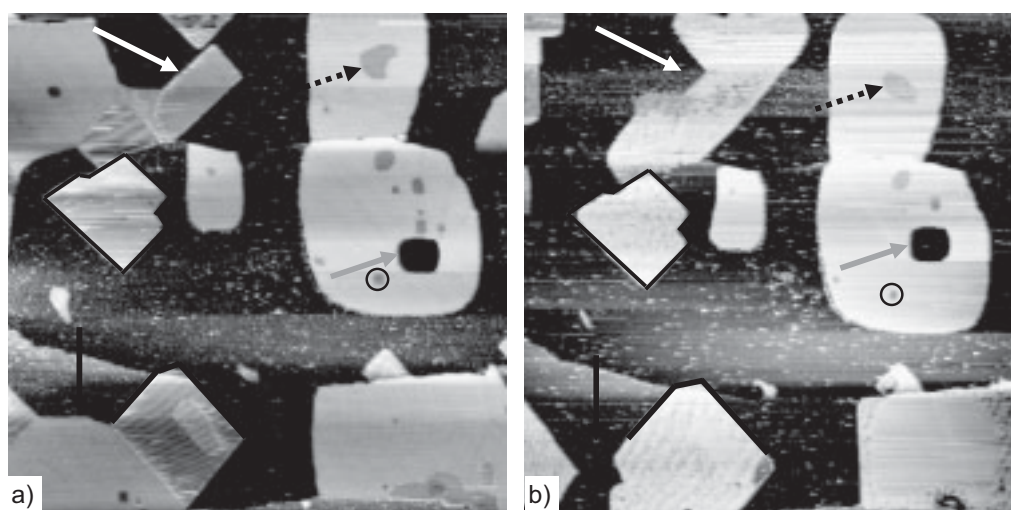
Figure 19: 0.5 ML of LiCl on Cu(001) evaporated at room temperature, a) and b) show the same area, but with a delay time of 2 h 20 min (U$_{bias}$ = –1.2 V, I = 0.04 nA, 350 x 350 nm^2).

Even though we can most likely exclude that the changes shown in Figure 19 are induced by the tip, we nevertheless found that the tip/sample interactions are not negligible. After the acquisition of four or five images the resolution decreased, as visible in Figure 20: the LiCl islands are sharper in Figure 20a than in Figure 20b. By gentle bias changes of the tip, its imaging capabilities could be improved again for a short time. Another indication for the significant tip/LiCl interaction in this case is the appearance of the second layer. In the STM images the second LiCl layer mostly appears darker than the first layer. This is in contrast to NaCl on metal surface where the second layer usually appears as a protrusion. We assume that this cannot be related to the different electronic structure of LiCl compared to the one of NaCl but may be related to some LiCl adsorbed on the tip. Consequently, the tunnelling electrons have to tunnel through three layers (one on the tip and two on the surface) instead of two. Due to these difficulties in imaging the LiCl islands and due to the deviation from the layer by layer growth of LiCl on Cu(001) we have decided to concentrate on the well established system of NaCl on metal surfaces.
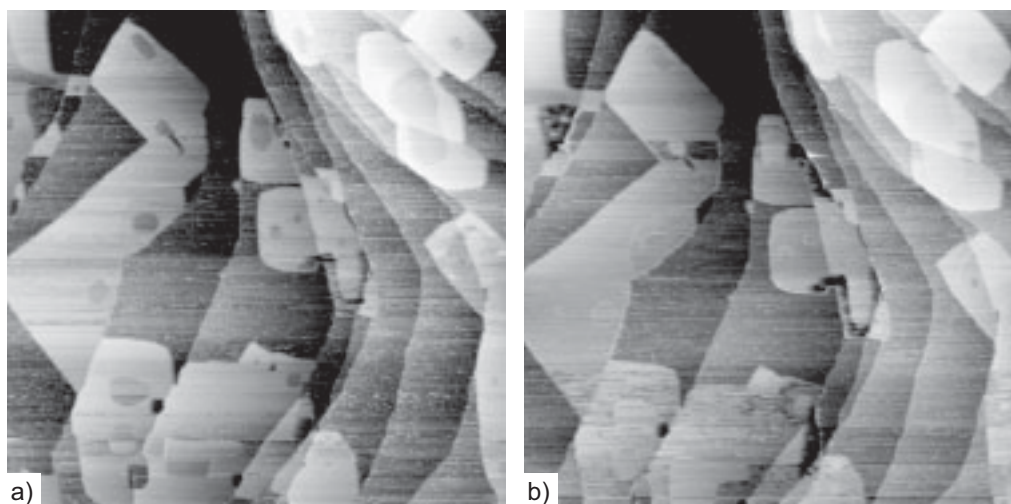
Figure 20: 0.5 ML of LiCl on Cu(001), evaporated at room temperature, image taken the next day; a) and b) show the same area, but with a delay time of 45 min (U_{bias} = –1.2 V, I = 0.04 nA, 400 x 400 nm²).

### 5.2.2   NaCl on surfaces with trigonal lattice: Ag(111) and Cu(111)

For the study of the NaCl growth on the two trigonal surfaces of Ag(111) and Cu(111), NaCl has been evaporated at different substrate temperatures varying from room temperature to 470 K. Table 4 shows, the island sizes of the first monolayer as well as the coverage of NaCl on the metal, and coverage of second and third monolayer with respect to the first monolayer for different growth temperatures and nominal NaCl coverage on Ag(111). For the deposition at room temperature the island size is smaller and the coverage of the second layer of NaCl is higher than at elevated temperatures. This is as expected and can be explained by the reduced diffusion of the NaCl monomers after evaporation due to the reduced substrate temperature. With increasing nominal coverage the island size increases and also the coverage of the second and third layer increases. The two experiments which have been performed at the same annealing temperature of 390 K and which have approximately the same coverage (0.39 ML and 0.42 ML) show a variation of the island size of the first layer as well as of the coverage of the second layer. A detailed study of all these parameters is in progress. However, some additional points about the growth of NaCl on the Ag(111) and Cu(111) substrates will be discussed in this chapter.

Table 4: Coverage and annealing dependent size distribution of NaCl islands on Ag(111).

NaCl coverage in ML[iii]	Annealing temperature in K	Island size of first layer in μm^2	Total area covered with NaCl	Coverage 2nd layer w.r.t. 1st layer in %	Coverage 3rd layer w.r.t. 1st layer in %
0.41	300	0.071±0.016	33%	15±13	0
0.39	390	0.13±0.04	38%	< 5	0
0.42	390	0.24±0.08	34%	10±7	0
1.3	430	0.52±0.23	74%	60±17	12

Figure 21 shows two STM images of NaCl grown on Cu(111). The black arrows in Figure 21a point to small "vacancy trenches" in the first monolayer of NaCl. We assume that already during the evaporation of NaCl these areas remain unfilled due to imperfect epitaxial growth, which is driven by the lattice misfit. These trenches compensate for the stress in the adsorbate layer due to the lattice misfit and thus have been more often observed for NaCl on Cu(111) than on Ag(111), which coincides well with the bigger lattice misfit (cf. Table 2).
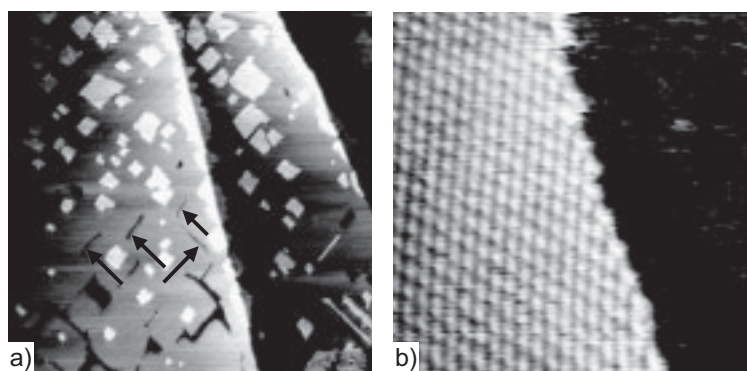

Figure 21: NaCl on Cu(111), deposition at room temperature (U_{bias} = –2.6 V, I = 0.05 nA, 250 x 250 nm^2). b) atomic resolution (U_{bias} = –2.2 V, I = 0.22 nA, 10 x 10 nm^2).

Additionally, the carpet-like growth, as reported earlier[134], can be seen in Figure 21a. The growth of the first NaCl layer as well as of additional layers starts at steps and kinks. Consequently, nearly the whole step in the centre of the STM image is covered with a second NaCl layer. Figure 21b shows an atomically resolved STM image of 1 ML of NaCl on Cu(111) (left side) and the clean Cu(111) on the right side. The lattice does not appear as cubic but as a distorted lattice due to the piezo-creep and -drift at room temperature. Note that only the chlorine ions can be imaged in STM because both the conduction and the valence band of NaCl consist mainly of chlorine states[133].

[iii] The coverage has been calculated directly from the STM images and shows a small discrepancy compared to the coverage calculated by the QCMB frequency change and by XPS measurements.
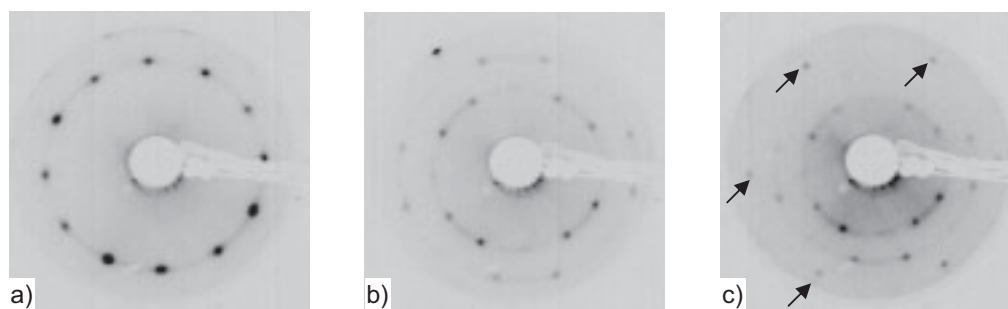
Figure 22: LEED pattern of NaCl on Cu(111) taken at a) 34.2 eV, b) 56.3 eV, c) 62.8 eV, black arrows in c) mark the substrate spots.

The LEED patterns for NaCl on Cu(111) in Figure 22 show twelve spots surrounding the central (0,0) spot, which demonstrate the three different orientations of the four-fold NaCl(001) adsorbate layer on the three-fold Cu(111) substrate. The relative intensity of the spots differs depending on the sample position. The faint circle on which the diffraction spots are lying, indicates that the crystallographic directions of the NaCl islands are not exactly aligned with the substrate crystallographic directions. In Figure 22c also the substrate spots are visible; four of them are marked with black arrows. Detailed discussion of the LEED patterns for NaCl on Cu(111) and Ag(111) can be found in reference[125].

There are two main differences in the growth of NaCl on Cu(111) and Ag(111). The first difference concerns the relative orientation of the NaCl islands with respect to the crystallographic orientation of the metal substrate. NaCl on Cu(111) (cf. Figure 22) grows with the NaCl $[1\,0\,0]$-direction parallel to one of the three equivalent $[1\,\bar{1}\,0]$-directions of the Cu(111) substrate. In contrast, NaCl on Ag(111) shows two different orientations: one parallel to the main directions of the substrate and the other one rotated by 45°[125].

The second difference is the island size on the two different metal substrates. Figure 23 shows two STM images of a) NaCl on Cu(111) and b) NaCl on Ag(111). The first has been prepared by deposition of NaCl while the sample was kept at room temperature whereas the latter has been evaporated on the Ag(111) sample held at 400 K. Figure 23a shows only one island on the right side extending over the whole scan range, with a considerable amount of second layer of NaCl, while several smaller islands are visible in Figure 23b. Due to the limitation of the scanning range which is in most cases smaller than the NaCl islands on Cu(111) it was not possible to measure the island size of NaCl on Cu(111).

This trend of larger NaCl islands on Cu(111) compared to Ag(111) has been observed for all experiments carried out on Ag(111) and Cu(111). As the lattice misfit of NaCl on Ag(111) is smaller than the one for NaCl/Cu(111) (cf. Table 2) one would intuitively expect bigger islands on Ag(111) due to lower stress in the adsorbate layer. This is however not confirmed by the results shown in Figure 23. In the case of NaCl on Ag(111) and Cu(111) the interaction between NaCl and the different metal substrates, also leading to different diffusion barriers, results in the different islands sizes.
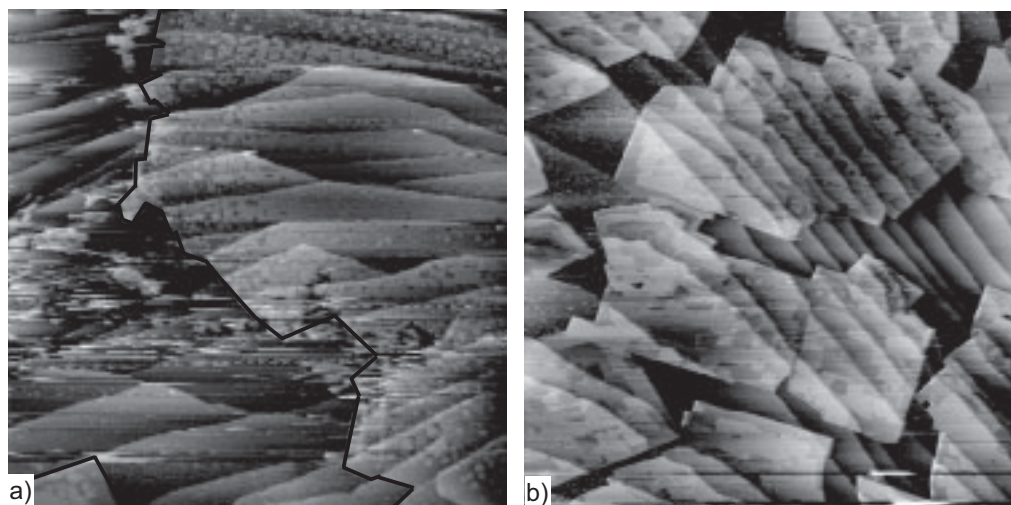
Figure 23: a) NaCl on Cu(111) grown at room temperature, the NaCl islands are highlighted by a black line ($U_{bias} = -2.1$ V, I = 0.05 nA, 1.5 x 1.5 μm^2). b) NaCl on Ag(111) grown at 400 K ($U_{bias} = -3.0$ V, I = 0.10 nA, 1.5 x 1.5 μm^2).

In Figure 23a on the left side a big part of the Cu(111) surface is not covered by NaCl (the black lines in this image highlight the border of the NaCl islands). In contrast, less free metal areas are visible for NaCl on Ag(111) (cf. Figure 23b) and the distance between neighbouring NaCl islands on Ag(111) is smaller than on Cu(111). This may be a hint that the mean free path of NaCl on Cu(111) is larger than on Ag(111). In conclusion, these results on Cu(111) and Ag(111) show that the growth of NaCl is mainly determined by intrinsic properties of the particular system, which cannot be influenced during the growth, i.e. by elevated substrate temperature or different evaporation rates. A deeper insight into this topic would be gained by the use of other noble metal surfaces like the Au(100) or Au(111) surface as well as by the insertion of surfactant layers which can change the surface properties and consequently the adsorbate/substrate interactions.

After the observation of bigger islands on Cu(111) we decided to use the Cu(001) surface as a substrate. In Figure 22 it has been shown that three different rotational domains of NaCl on the trigonal surface exist. Thus, a next step towards homogenous surfaces is the choice of a substrate with a four-fold symmetry, which may lead to a more homogenous growth.

5.2.3   NaCl on a surface with squared lattice: Cu(001)

Figure 24a shows an overview of a Cu(001) sample partly covered with NaCl; on the left side of the black line an extended NaCl island is visible while the right area in the STM image shows the clean Cu(001). For NaCl on Cu(001) islands with a diameter of several micrometers could be obtained and therefore they are bigger than the ones on Cu(111) and

Ag(111). However, the increased island size often resulted in an increased coverage of a second, third and fourth NaCl layer, as can be seen in Figure 24a. In the vicinity of the big NaCl islands also huge areas of bare metal are visible (cf. Figure 24b). The free metal areas can also be up to several μm^2.
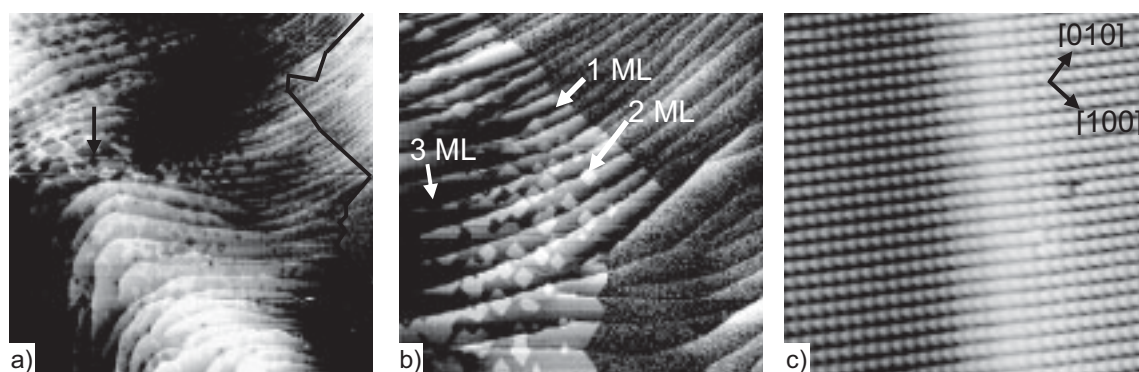
Figure 24: NaCl on Cu(001), substrate temperature during growth: 450 K. a) the border between the NaCl island and the clean Cu is marked by the black line; the two arrows indicate a fourth layer of NaCl, ($U_{bias} = -2.0$ V, $I = 0.06$ nA, 2 x 2 μm^2). b) the first, second and third monolayer are indicated by the white arrows ($U_{bias} = -2.0$ V, $I = 0.06$ nA, 1 x 1 μm^2). c) atomic resolution ($U_{bias} = -1.2$ V, $I = 0.07$ nA, 10 x 10 nm^2).

Figure 24b is a zoom-in of the right side of Figure 24a with the NaCl island on the left side and bare metal on the right side. Up to three NaCl layers can be observed, although only half of the surface shown in this STM image is covered with NaCl. The third layer appears darker than the second and the first layer due to the increasing insulating properties with increasing NaCl thickness. Depending on the tip conditions, sometimes the second layer appears as a depression while for other tip conditions even the third layer can appear as a protrusion. Hence, the apparent height of the NaCl islands strongly depends on the tunnelling parameters as well as on the STM tip. The fourth layer of NaCl always appears as a depression (cf. black arrows in Figure 24a). Notably, no trenches are visible for NaCl on Cu(001) in contrast to NaCl on Cu(111) as shown in Figure 21a.

The observation of micrometer sized NaCl islands and micrometer sized free metal areas can shed some new light on the diffusion of di-ionic NaCl clusters on the Cu(001) surface: (i) The mean free path of NaCl on Cu(001) at 450 K is at least several microns. (ii) The diffusion easily proceeds over step edges of the metal substrate. However, there are still some other important questions like the diffusion of NaCl on the NaCl islands and hopping from NaCl to the metal area and in the reverse direction. Due to the high coverage of the NaCl island with a second (~85%), third (~40%) and fourth (~3%) layer we assume that the diffusion over the NaCl-Cu step is rather high at 450 K. Otherwise the free metal area would be filled for lower nominal coverages as the one shown in Figure 24.

For NaCl on Cu(001) all islands exhibit the same orientation with respect to the Cu(001) substrate. The arrows in Figure 24c indicate the crystallographic orientation of the NaCl islands which is well visible in the atomically resolved STM image. The Cu(001) crystal has the same orientation as the NaCl layer. Thus, we can conclude that the NaCl islands grow with a 0° rotation on the Cu(001) as already reported earlier[132], although the lattice misfit is bigger in this direction (cf. Table 2). Kiguchi et al. stated that alkali halide/metal systems with a big lattice misfit only grow in the 0° orientation, even if the lattice misfit for this direction is bigger than for the 45° orientation, while alkali halide/metal systems with a small lattice misfit can also grow in a 45° orientation[132]. As a consequence for NaCl on Ag(001) both orientations, 0° and 45°, have been observed[125,135], due to the small lattice misfit for the 45° growth of NaCl on Ag(001), which is only 2.4%, in contrast to NaCl on Cu(001), where only 0° orientation has been observed.

In conclusion, the NaCl island size increased by more than 100% on the Cu(001) compared to Ag(111) and seemed to increase slightly on Cu(001) compared to Cu(111), although it is difficult to quantify the island size for these two systems because most of the islands are bigger than the maximum scan range, which can not exceed 2 μm. Islands with a diameter of several square micrometers in size seem to be possible. But with the increasing island size also the amount of second, third and fourth layer of NaCl increases. The fact that still big parts of the metal are not covered with NaCl indicates a considerable diffusion of NaCl on Cu(001). Although it is possible to measure UPS and XPS locally by means of a focused photon spot in the size of 1 μm^2, this approach does not seem to be appropriate for our system due to the following reasons: (i) A difficult aligning of the sample would be necessary. (ii) A focused photon spot in the size of 1 μm^2 requires high photon fluxes, which may lead to beam damage of the samples. (iii) The measurements would still average over a different number of NaCl layers and thus measurements depending on the NaCl thickness would not be possible. At this point it seems to be more convenient to search for another system, which may lead to a homogenously covered surface. Thus, in a next step we further reduced the substrate symmetry to a two fold symmetry, which is given by a stepped Cu(311) surface.

5.2.4   NaCl on a stepped surface: Cu(311)

Repp et al. showed that NaCl exhibits a Stransky-Krastanov growth on the stepped Cu(311) surface[136], i.e. the growth of the first monolayer is completed before a second monolayer starts to grow. This different growth was explained by the Smoluchowski effect[137] of the stepped surface, which leads to a charge modulation of the surface and as a consequence to a higher interaction with the polar NaCl ad-layer. The further growth deviates from the layer by layer growth mechanism i.e. the third layer starts to grow before the second layer is completed[136].
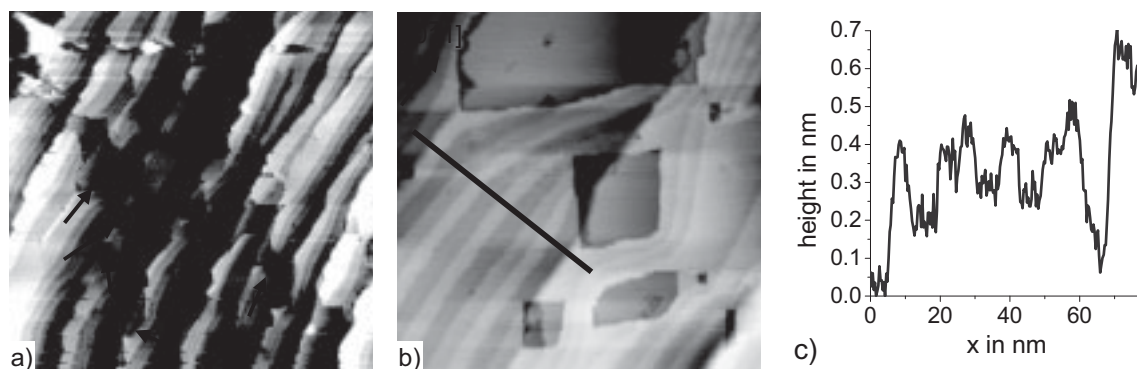
Figure 25: 0.8 ML of NaCl on Cu(311), substrate temperature during growth: 470 K a) overview, black arrows highlight bare metal areas ($U_{bias} = +1.3$ V, $I = 0.06$ nA, 450 x 450 nm^2). b) zoom-in, ($U_{bias} = +1.3$V, $I = 0.06$ nA, 130 x 130 nm^2). c) line profile as indicated in b).

Figure 25 shows a Cu(311) surface covered with 0.8 ML of NaCl. In Figure 25a some areas which are not covered with NaCl, are marked with black arrows. Beside these small vacancy islands in the NaCl layer the surface is homogenously covered with 1 ML of NaCl and no islands which could be attributed to a second layer of NaCl are visible. The areas covered by NaCl exhibit stripes, which are parallel to the intrinsic steps of the Cu(311) single-crystal (in Figure 25b top left, the crystallographic direction of the intrinsic steps is marked). Close to the bare metal patches these stripes deviate from this crystallographic direction and often tend to grow around the free metal areas (cf. Figure 25b). Figure 25c shows the line profile perpendicular to these stripes as indicated by the black line in Figure 25b. The step height between the stripes is (1.4 ± 0.2) Å and the average spacing is (5.5 ± 0.5) nm. These values have been averaged from different STM images taken with different coverage of NaCl to reduce a possible tip influence on these values.

These stripes are not visible on the clean Cu(311) surface without NaCl. We assume that an adsorbate induced reconstruction of the Cu(311) surface leads to these stripes, as shown in Figure 26. Due to Smoluchowski smoothing effect the chlorine ions are adsorbed on top of the outermost Cu-atoms, while the sodium ions are on top of the second row of Cu-atoms[136]. One additional Cu-atom placed on top of the Cu rows as indicated with the arrow in Figure 26 results in a height change of 1.43 Å, which is close to the step height of (1.4 ± 0.2) Å of the stripes determined from the STM images. This surface reconstruction leads to variable Cl-Cl distances, which can compensate the stress in the NaCl layer induced by the extension of the Cl-Cl distance on the Cu(311) compared to the Cl-Cl distance in bulk NaCl. The average spacing of the stripes is (5.50 ± 0.52) nm, which relates to approximately 13 outermost Cu-atoms. In Figure 26 reconstructions with only three to four Cu-atoms are shown for better visibility. We also assume that this surface reconstruction is overgrown by the NaCl layer as it is the case for the carpet-like growth, i.e. there is no abrupt change in the NaCl height from one reconstruction to the other but the small intrinsic steps are smoothly overgrown.

The proposed reconstruction needs a considerable mass transport of Cu-atoms between the reconstruction areas, i.e. perpendicular to the intrinsic Cu(311) steps. We assume that this is only possible at elevated temperatures – the NaCl layers shown here have been deposited on the samples held at 470 K.
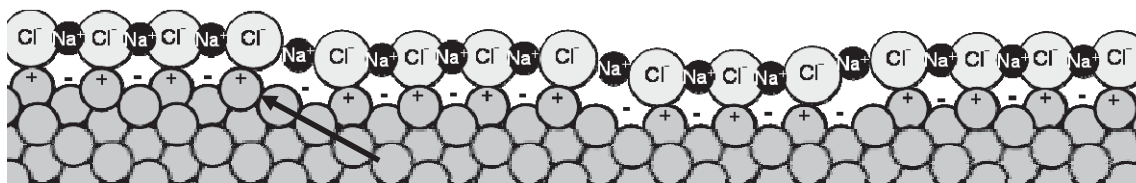
Figure 26: Growth model of NaCl on Cu(311); the charge modulation of the Cu(311) is indicated and the different height of the NaCl resulting from the proposed surface reconstruction can be seen; adopted from Ref.[136].

The LEED patterns shown in Figure 27 indicate the cubic growth mode which was expected for the NaCl(001) ad-layer. In contrast, the LEED pattern of the clean Cu(311) shows a rectangular lattice which results from the (311) orientation of the surface (cf. Figure 27a). For a better comparison of the clean and NaCl covered surfaces the same substrate spots are marked with circles in Figure 27a and Figure 27c. It was not possible to determine any features which can be clearly related to the proposed reconstruction. Nevertheless, in Figure 27b there are some faint stripes close to the NaCl spots indicated with black arrows, which may be a hint for the reconstruction. These stripes may reflect the different sizes of the reconstruction length, which shows an average spacing of 13 Cu-atoms but the biggest length of the stripes which we observed relates to 16 Cu-atoms spacing and the smallest to 11 Cu-atoms spacing.
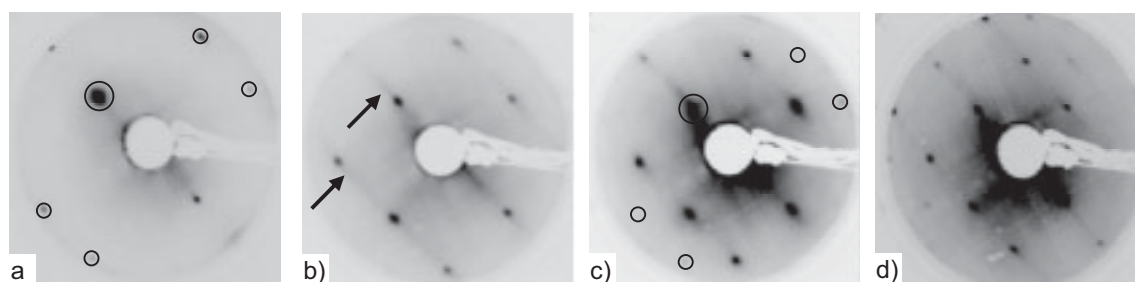
Figure 27: LEED pattern of a) clean Cu(311), some of the substrate spots are marked with black circles, and b)-d) NaCl on Cu(311). Black arrow in b) mark faint diffraction stripes (cf. discussion in the text). c) same substrate spots as in a) are marked with black circles; a) 61.0 eV, b) 47.9 eV, c) 60.8 eV, d) 80.4 eV.

In conclusion, the Stransky-Krastanov growth observed for NaCl on Cu(311), which deviates from the growth modes of NaCl on trigonal and square surfaces can be explained by the Smoluchowski smoothing effect of the highly corrugated (311)-surface and is assisted by

a special surface reconstruction as described above. This surface reconstruction may arise from minimizing epitaxial strain by introducing a surface corrugation through ad-atom diffusion. Localized dipoles arise on the stepped surface due to the strong corrugation as illustrated in Figure 26. Such the outermost Cu-rows are positively charged. This results in a very well ordered adsorption of the NaCl with the chlorine ions on top of the positively charged Cu-atoms and the sodium ions on top of the negatively charged Cu-atoms (cf. Figure 26). For other stepped surfaces like the Cu(211) a nano-patterning after adsorption of NaCl on the substrate has been reported, resulting in NaCl covered (311)-facets and NaCl free (533)-facets[138].

5.2.5 *Comparison of the growth of LiCl and NaCl on different surfaces*

In conclusion, the detailed study of the growth of NaCl on different single-crystal metal surfaces resulted in NaCl islands with a size of several micrometers on Cu(111) and Cu(001). For the trigonal Cu(111) and Ag(111) surfaces we can draw the following conclusions: (i) The 3-fold symmetry of the substrates leads to at least three different rotational equivalent adsorption orientations for the four-fold NaCl(001) islands. This results in different rotational-domains, which reduces the probability of a homogenously covered surface. (ii) The presumably small interaction of NaCl with Cu(111) and Ag(111) substrates reduces the probability of a Stransky-Krastanov or Frank van der Merwe growth and leads to a Volmer-Weber growth. (iii) The 50% bigger islands size on Cu(111) compared to Ag(111) may be a hint for the higher diffusion of NaCl on this surface. (iv) The bigger island size on Cu(111) indicates that the growth of NaCl is mostly determined by intrinsic properties like the interaction of the adsorbate and the substrate. Factors like substrate temperature, which determines the diffusion, evaporation rate and lattice misfit, seem to play a less important role.

Additionally, the growth of LiCl on Cu(001) has been investigated and it exhibits some remarkable differences compared to the growth of NaCl on metal surfaces. First of all, it could be shown that LiCl does not reveal a carpet-like growth but the growth is stopped at step edges. Secondly, LiCl shows a surprisingly high diffusivity after deposition on Cu(001), which leads to a change in the shape of the LiCl islands. As the last point, we have demonstrated that LiCl does not grow in a layer by layer mode on Cu(001) as suggested in earlier publications[131,132].

By choosing a substrate with a square lattice like the Cu(001) the problem concerning the different rotational domains observed for NaCl on trigonal substrates can be eliminated. Additionally, the growth of NaCl on the Cu(001) surface leads to approximately 30% bigger NaCl islands compared to NaCl/Cu(111), but still more than 30% of the metal surface is not covered by NaCl. Thus, we can conclude that NaCl on Cu(001) also exhibits a Volmer-Weber growth mode, although the islands are slightly bigger than on surfaces with trigonal lattices.

This growth study of NaCl on Cu(111), Ag(111) and Cu(001) provides an insight in the diffusion processes, which strongly determine the layer formation and growth. As the islands on Ag(111) are closer together than on Cu(111) and Cu(001), we assume that the diffusion of the NaCl on the Ag substrate is smaller than on the Cu substrates. Another factor which strongly determines the growth of the NaCl islands is the hopping or diffusion of NaCl clusters from the metal to the NaCl islands and back to the metal. From our STM observations we conclude that this diffusion is also possible at room temperature for NaCl on Cu(111) and Cu(001).

The next step towards homogenously covered surfaces with NaCl layers was the choice of a substrate which shows a charge corrugation of the surface. This charge corrugation may lead to an attractive interaction between the NaCl dipoles and the substrate. Such a substrate is provided by the stepped Cu(311) surface. Due to the Smoluchowski smoothing effect the rows of the Cu(311) surface show a charge corrugation. This leads to a stronger interaction of the NaCl dipoles with the surface and – as shown in the previous chapter – leads to a Stransky-Krastanov growth of NaCl on Cu(311). In consequence it is possible to produce a NaCl coverage of more than 80% without a second layer of NaCl. Hence, it is possible to investigate the electronic interactions of organic molecules with the Cu(311) and NaCl/Cu(311) substrates with averaging techniques like UPS, XPS and NEXAFS.

5.3 Electronic interactions of OEPs with NaCl and metal surfaces

Two different systems and various analytical techniques have been chosen to investigate the electronic interactions of OEPs with NaCl and metal surfaces. In a first study the electronic states of CuOEP on Ag(111) have been investigated with locally resolved scanning tunnelling spectroscopy. A second study comprises UPS and XPS measurements of CuOEP on NaCl and on Cu(311).

5.3.1 *Electronic states of CuOEP on Ag(111): STS*

The STS experiments have been performed as described in chapter 3.2. The goal of the scanning tunnelling spectroscopy measurements was to resolve the occupied and unoccupied electronic states of CuOEP on metal surfaces as well as on ultrathin insulator surfaces. We used NaCl islands on Ag(111) surfaces for the STS experiments because this allows for the direct comparison of CuOEP/NaCl/metal and CuOEP/metal on the same sample.

We observed that CuOEP molecules remain mobile on the Ag(111) surface as well as on NaCl islands when the molecules are deposited on the sample kept at 77 K. In agreement with Ramoino et al.[23] we observed the subsequent filling of metal, first and second NaCl layer

terraces also for the low temperature sample preparation. Specifically, diffusion of the molecules across steps from the NaCl ad-layer to the bare metal resulted in CuOEP molecules being only adsorbed on the bare metal and not on the NaCl islands after cooling the sample to 5 K in the LT-STM. Hence, our spectroscopy measurements reported here, have been performed on CuOEP on Ag(111). The cooling of the sample to 5 K led to the formation of CuOEP islands aside free areas of metal. This situation allows for direct control measurements on the well-known surface state of the bare metal in order to assure a smooth electronic structure of the tip. For higher CuOEP coverage the molecules adsorb also on NaCl[23]. However, in this case the metal areas of the sample are fully covered with CuOEP, which makes it more difficult to obtain reliable STS measurements. Therefore, we concentrated our STS measurements only on CuOEP directly adsorbed on the metal.

Figure 28 shows the I-U-spectra recorded at different positions of CuOEP molecules on Ag(111). The spectra have been measured on CuOEP within an ordered CuOEP array highlighted by the arrow in the inset of Figure 28a. Several spectra have been acquired on top of the Cu central atoms (dark centre of the molecules, as visible in the inset of Figure 28a) and on top of the octa-ethyl subunits (bright areas of the molecules). Before and after recording each spectrum on the molecules a spectrum of the clean Ag was taken (black line) in order to exclude tip changes during the spectroscopy measurements. The observed peak positions in the spectra measured on the same molecular subunit are very reproducible, only the overall intensity varies for different spectra possibly due to small deviations in the tip position. Figure 28a represents the I/V curve and Figure 28b shows the differential tunnelling spectra (dI/dV).
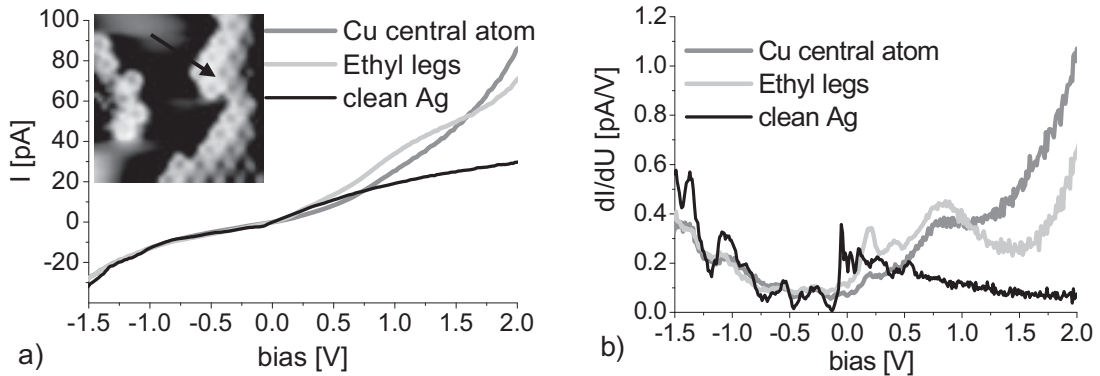
Figure 28: STS spectra of CuOEP on Ag(111), negative bias indicate occupied states of the sample; spectra taken at 5 K a) I/V curve; inset: STM image (U_{bias} = –1.0 V, I = 13 pA, 13 x 13 nm^2). b) differential conductance spectra; set-point values: U_{bias} = –1.0 V, I = 13 pA.

STS measurements on the bare Ag(111) area (Figure 28b) show the surface state at approximately 60 meV, in agreement with literature values[139]. At negative bias, the dI/dV curve taken on the clean Ag(111) displays several peaks, which could be associated to a featured density of states of the tip. These features are also present in the spectra taken on top

of the CuOEP molecules, although the intensity here is smaller. As no additional peaks which can be related to the HOMO of the molecules are visible at biases between the Fermi energy and -2.2 eV, I will concentrate on the unoccupied states of the molecules (i.e. positive bias), where the spectra of the clean metal is featureless.

Both spectra recorded on different sub-units of the CuOEP show one broad pronounced peak in the unoccupied states at 0.85 eV. Two additional peaks near the Fermi energy at 0.4 eV and 0.2 eV have been observed in the spectra taken on the ethyl legs. The peak at 0.4 eV is not observed on top of the central Cu-atom of the molecule. The peak at 0.2 eV is also visible for the central Cu-atom, but less pronounced than on the ethyl legs.

The exact interpretation of the two peaks near the Fermi energy observed with STS remains difficult and complementary techniques like NEXAFS or IPES together with ab-initio calculations would be helpful to relate these peaks to molecular electronic states. Assuming that these peaks are not due to the interaction of the tip with the molecules, we will discuss several different options of the origin of these electronic states.

These peaks can e.g., be interpreted as LUMOs deriving from a charge transfer from the molecule to the sample leading to partly unoccupied states. This interpretation of the charge transfer from the molecule to the metal is supported by a work function decrease as shown in the thesis of L. Ramoino[125]. Work function decreases can be related to several effects: (i) The electron cloud of the metal spreading into the vacuum leads to a surface dipole (pointing toward the surface). Adsorbates on the surface push these electrons back in the direction of the metal, which leads to a reduction of the surface dipole and therewith to a reduction of the work function. (ii) A small dipole arising from the orientation of the ethyl legs[140] also leads to a reduction of the work function. (iii) A charge transfer between the molecule and the sample can lead to an additional decrease of the work function. Although it is difficult to relate a work function to a charge transfer without additional data, the significant decrease of the work function by about 1.1 eV[125] is in line with the interpretation of a charge transfer from the molecules to the surface. Another interpretation of these peaks close to the Fermi energy is the hybridization of the metal electronic states with the molecular orbitals leading to metal induced gap states (MIGS).

Nevertheless, the STS spectra of CuOEP on Ag(111) together with the work function shift[125] indicate that the molecules are not weakly physisorbed. The surface state of the Ag(111) is not observed in spectra taken above the molecules. For simple physisorbed molecules like PTCDA on Au(111) STS measurements show that the surface state is still observed upon adsorption of the molecules and is slightly shifted towards the Fermi energy[141]. We have performed additional ARPES measurements on partly and fully CuOEP covered Cu(111), which also showed that the surface state is completely quenched after adsorption of a full monolayer of CuOEP on the Cu(111) (cf. Figure 29). Although it is difficult to compare the interaction of the molecular adsorbates with different metal surfaces, we can conclude that the interaction between the CuOEP and the Ag(111) as well as between CuOEP and Cu(111)

is stronger than in the case of physisorption and that the molecules are most likely chemisorbed on both surfaces.
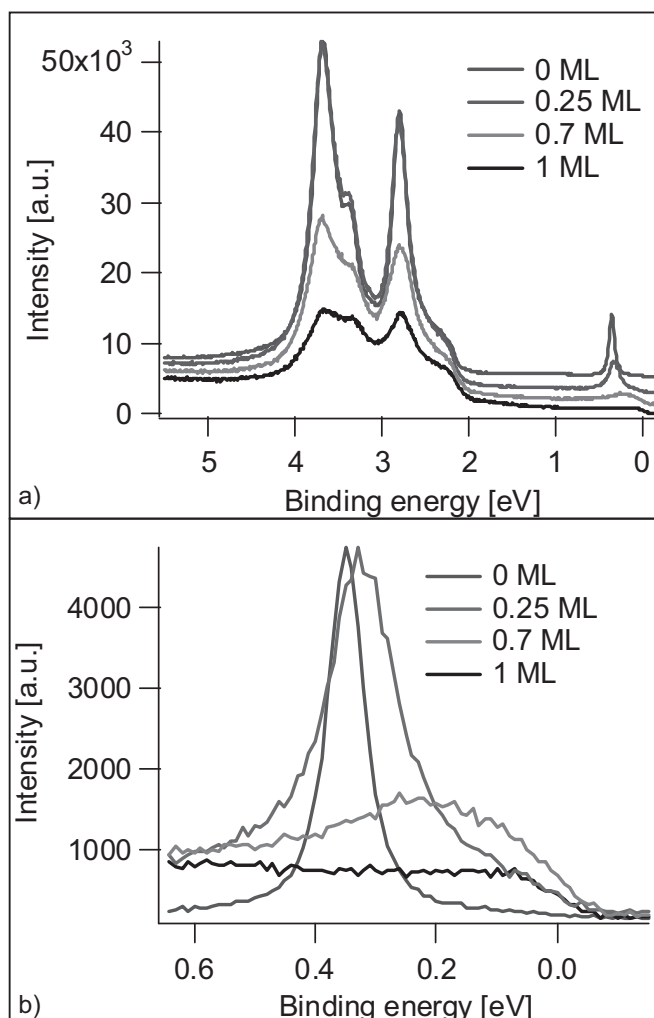

Figure 29: ARPES data of CuOEP on Cu(111); a) overview showing the Cu3d bands; b) details of the surface states.

5.3.2   *Electronic states of OEPs on NaCl and Cu(311): UPS*

After the successful preparation of an almost homogenous monolayer of NaCl on the Cu(311) surface with less than 20% bare metal area (cf. Figure 25), UPS measurements have been performed on the clean and NaCl covered Cu(311) sample covered with CuOEP. For these studies a nominal NaCl coverage of 1.2 ML has been chosen to assure that most of the Cu(311) surface is covered with NaCl. Accordingly, STM measurements show more than 90% coverage of the first layer and approximately 20% coverage of the second layer. The

UPS spectra of the samples covered with CuOEP and NaCl are summarized in Figure 30. Figure 30a shows a broad binding energy region where the NaCl valence band between 6 and 8 eV can be identified (cf. dash-dotted line). The peak positions of the NaCl valence band are the same as shown in earlier publications but the relative peak intensities vary in different publications[142,143]. The spectrum displayed by the black, solid line was measured on the clean Cu(311) and clearly shows the Cu3d band between 2 and 4 eV. Additionally, the spectra of a thin (dotted line) and a thick (4 ML) layer of CuOEP (grey, solid line) are shown in Figure 30a. The intensity of the Cu3d band is much smaller for the 0.8 ML covered sample and it is completely quenched for the sample covered with 4 ML of CuOEP.

The intensity of the NaCl valence band after adsorption of CuOEP on NaCl/Cu(311) (cf. dash-dotted line in Figure 30a) is approximately the same as for the NaCl/Cu(311) spectrum (dashed line). The smaller decrease of the intensity of the valence band compared to the Cu3d band can be related to the larger mean free path of the electrons with smaller kinetic energies (cf. Figure 4b, page 10). The increased intensity of the valence band peak at higher binding energies can be explained by the additional electronic states of CuOEP at 7 eV (cf. dotted and grey, solid line in Figure 30a) i.e. the peak at 8 eV in the case of NaCl + CuOEP consists of two peaks: the valence band of NaCl and the electronic states of CuOEP. DFT calculations on the molecular orbitals for CuOEP show a HOMO-4 state at -6.8 eV[119].

Figure 30b shows the Cu3d region: For better comparison of peak position the spectra of 1.2 ML NaCl, 1.2 ML NaCl + 1 ML CuOEP and 4 ML CuOEP have been multiplied by five. The spectrum for 0.8 ML of CuOEP and the one for 1.2 ML of NaCl are qualitatively similar to the spectrum taken on the clean Cu(311) sample, mainly the peak intensities are strongly reduced. This strong decrease of the Cu3d band can be explained by the comparably small mean free path. The spectra for molecules on NaCl and the thick layer of CuOEP on the Cu(311) surface do not show the Cu3d peaks, due to the small mean free path of the emitted electrons. Instead the spectrum for 4 ML of CuOEP shows a peak at 1.9 eV, which can be assigned to the HOMO of CuOEP; DFT calculations show a binding energy of -1.5 eV for the HOMO[119]. The peak at 3 eV of the thick CuOEP layer is assigned to the HOMO-1 state of the molecules, which is slightly higher than the calculated binding energy of -2.6 eV[119].

The spectra taken for 4 ML of CuOEP and for 1 ML of CuOEP on NaCl have essentially the same shape but the latter is shifted by approximately 0.8 eV to higher binding energies. The shift of the spectra for the molecules on NaCl and the thick molecular layer is most likely related to the different electronic environment of the molecules. The insulating NaCl with its strongly localized electrons, compared to metal substrates, leads to a smaller screening of the photohole in the CuOEP valence band and thus to higher binding energies (cf. equation 7, page 11). The effect of screening on the binding energy is also present for the core level binding energies and will be discussed in more detail in the next chapter.
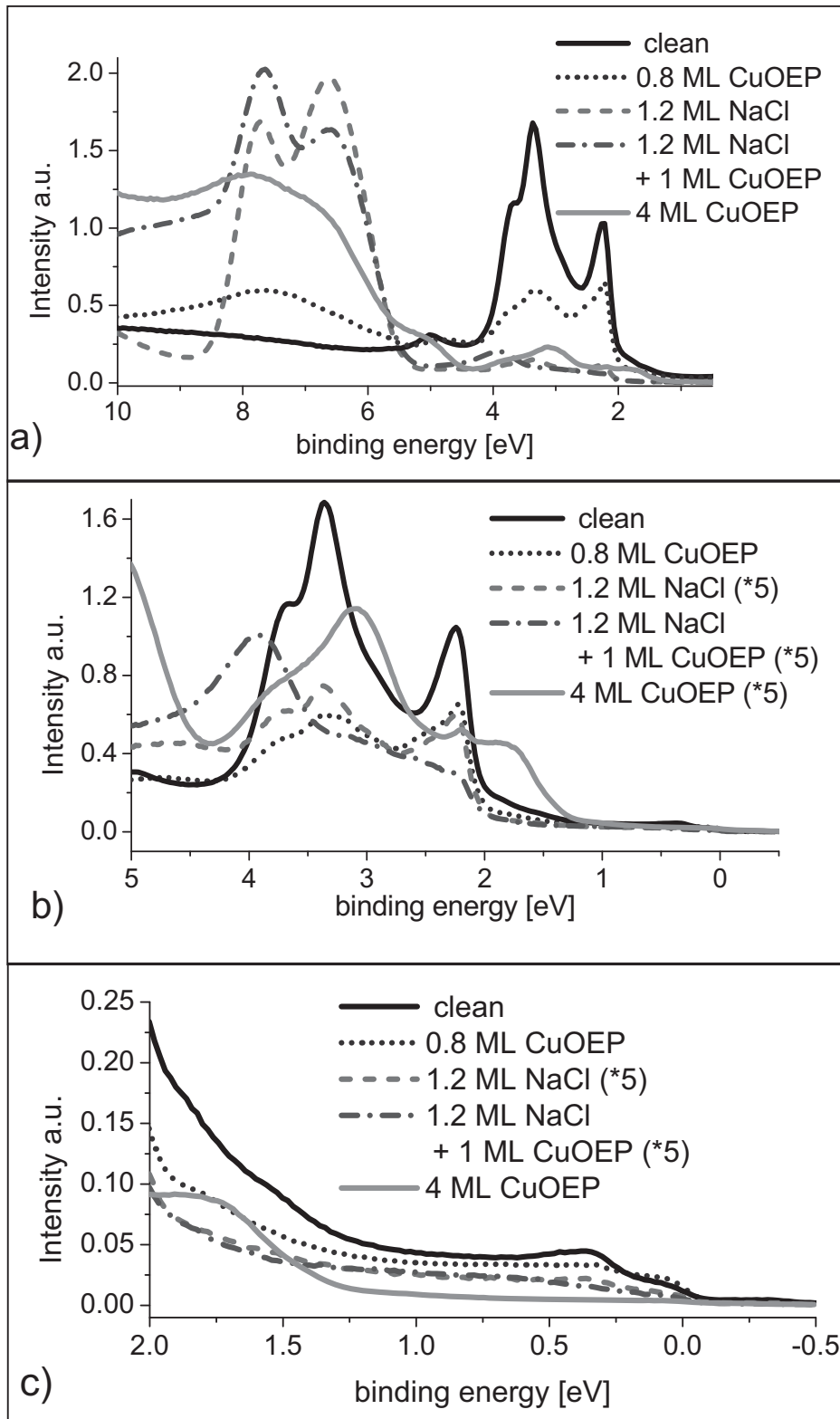
Figure 30: UPS data of clean Cu(311) and Cu(311) covered with NaCl, CuOEP, and NaCl + CuOEP; a) overview. b) zoom-in in the Cu3d region; the spectra for 1.2 ML NaCl, 1.2 ML NaCl + 1 ML CuOEP, and 4 ML of CuOEP have been multiplied by five. c) zoom-in in the near Fermi energy region; the spectra for 1.2 ML NaCl and 1.2 ML NaCl + 1 ML CuOEP have been multiplied by five.

In Figure 30c the detailed spectra near the Fermi energy is shown. In the spectra for the thin CuOEP layer on Cu(311) and for CuOEP/NaCl/Cu(311) no features are visible, which can be related to the CuOEP molecules. The only feature visible is the HOMO of the thick molecular layer at approximately 1.9 eV. We assume that the HOMO of the thin CuOEP layer is slightly shifted to higher binding energies and as a consequence it is overlapping with the Cu3d states of the substrate. Thus, we conclude from the UPS measurements that the HOMO of CuOEP on the bare metal as well as on NaCl is close to the Cu3d band and consequently cannot be resolved for sub-monolayer to monolayer coverages on copper surfaces. Furthermore, for the spectra measured with angle-resolved UPS for CuOEP on Cu(111) no HOMO is visible between the Cu3d peaks and the Fermi energy (cf. Figure 29, page 72).
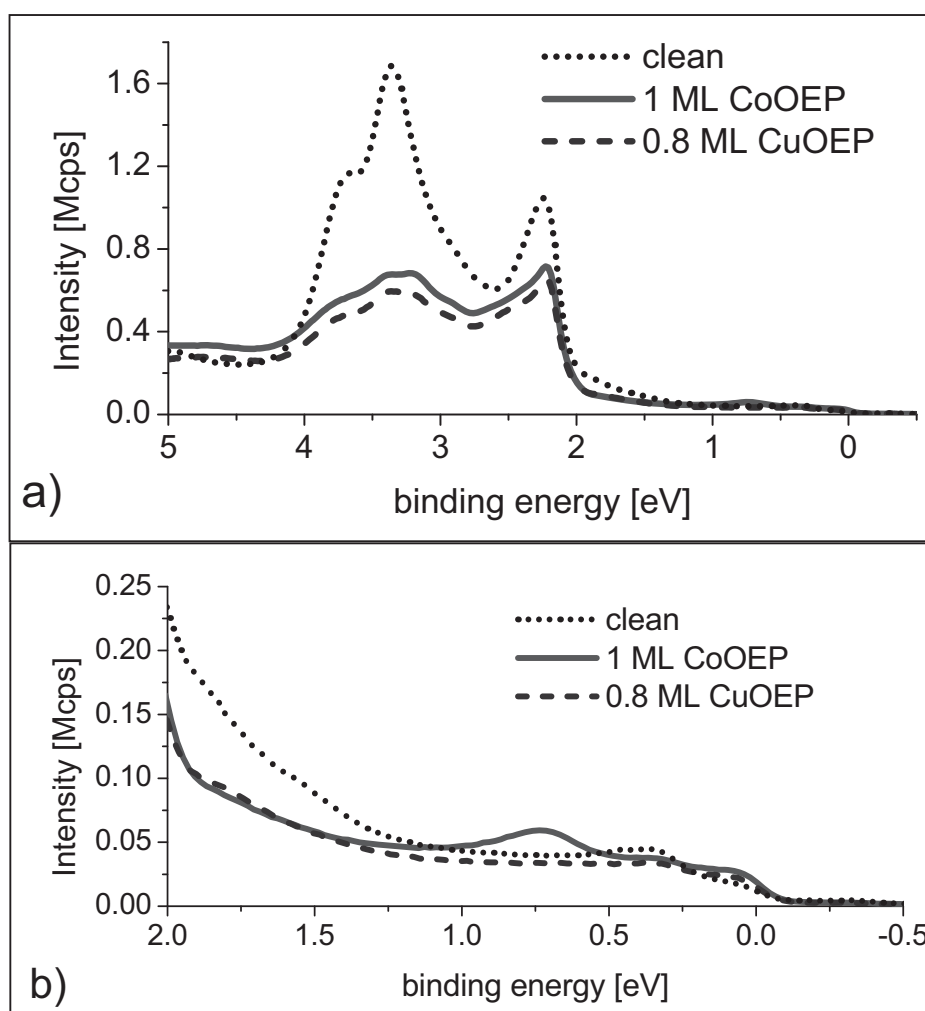
Figure 31: UPS data of clean Cu(311) and Cu(311) covered with CoOEP or CuOEP; a) overview, b) zoom-in in the near Fermi energy region.

After the observation that the HOMO of CuOEP is not measurable for monolayer coverage on Cu(311) due to overlapping with the Cu3d peak, another octa-ethyl porphyrine with Co as central atom was chosen for further UPS studies. It is well known that Co-containing phthalocyanines show a HOMO near the Fermi energy, which derives from the partly filled Co d_{z^2} state[144]. Furthermore, this Co state leads to different appearances of the central atom for Co-phthalocyanines compared to Cu-phthalocyanines in STM measurements[145]. As the electronic state of Co in the phthalocyanine molecules is the same as in the octa-ethyl porphyrins we assume that the CoOEP should also show a HOMO near the Fermi energy. Figure 31 shows the UPS data on CoOEP compared to those of CuOEP on Cu(311). The change of the Cu3d band is the same for both organic molecules only the overall intensity varies slightly (cf. Figure 31a). The valence band spectrum in Figure 31b shows a broad peak around 0.75 eV for the CoOEP, which is absent in the spectrum taken on CuOEP. Thus, for the continuation of these studies on the influence of the NaCl layer thickness on the OEP molecular orbitals, the system of CoOEP/NaCl/Cu(311) seems to be a very appropriate system, due its HOMO at 0.8 eV. However, the question of the influence of screening still has to be solved for a comparison of the results of CoOEP on Cu(311) with CoOEP on NaCl/Cu(311).

5.3.3   XPS of CuOEP on NaCl and Cu(311)

This chapter will focus on some interesting observations in the XPS data taken on the same system as shown in the previous chapter, i.e. NaCl/Cu(311) covered with CuOEP. Figure 32 shows the C1s and the N1s peaks measured on Cu(311) samples covered with different amounts of CuOEP and with NaCl + CuOEP. For a better comparability the spectra of the thick CuOEP layer have been divided by four. As can be seen from the spectrum taken on the NaCl sample without molecules there are some carbon impurities leading to a broad peak around 288 eV. This broad peak is also visible for the CuOEP on the NaCl but is absent for the CuOEP on the metal sample. Obviously, there are large shifts in the binding energy for both, the N1s and the C1s peak, of CuOEP on the clean metal compared to CuOEP on NaCl. The exact binding energies are listed in Table 5.

In Figure 32b, which shows the N1s XPS region, for all spectra except the thick CuOEP layer a broad peak at a binding energy of 402 eV is visible, which is a Cu Auger peak. Despite this Auger peak, the N1s peaks are well visible at binding energies between 398 and 400 eV. For the N1s peak the binding energy shift of CuOEP/NaCl compared to the thin layer of CuOEP/Cu(311) is slightly bigger than the shift for C1s. For the N1s binding energy of the thick CuOEP layer compared to the monolayer a small shift of 0.24 eV is observed.
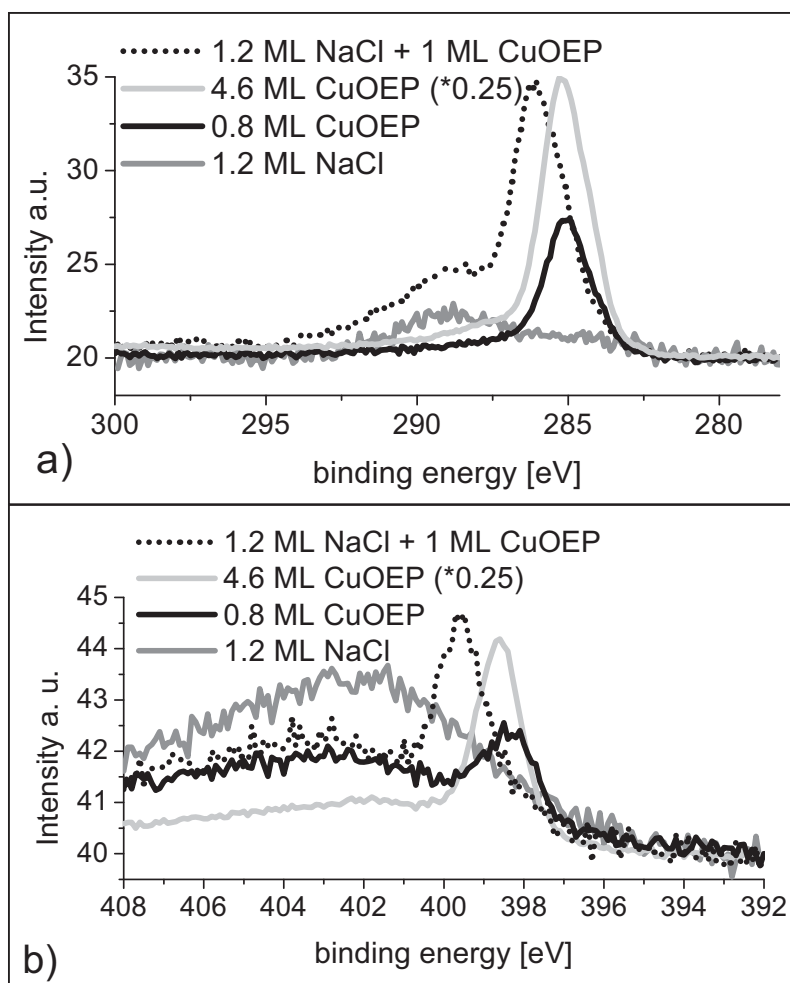
Figure 32: XPS data of Cu(311) covered with NaCl, NaCl + CuOEP and CuOEP; a) C1s peak; b) N1s peak; the spectra for 4 ML of CuOEP has been multiplied by 0.25.

Table 5: XPS binding energies for NaCl, CuOEP and NaCl + CuOEP on Cu(311); [a] literature values from[146]; [b] literature values from[147].

	C1s	N1s	Cl2p	Na1s	Cu2p
1.2 ML NaCl	-	-	200.08 eV	1073.22 eV	932.58 eV
0.8 ML CuOEP	285.07 eV	398.38 eV	-	-	932.63 eV
4.6 ML CuOEP	285.18 eV	398.62 eV	-	-	932.60 eV
1.2 ML NaCl+ 1 ML CuOEP	286.11 eV	399.60 eV	199.91 eV	1073.10 eV	932.61 eV
Literature values	unknown[iv]	398.2 eV[b]	198.4 eV[a]	1071.5-1072.5 eV[a]	932.7 eV[a]

In the following, the binding energy shifts observed for the C1s and the N1s should be discussed in more detail. As can be seen in Table 5 the binding energy of the Cu2p substrate peak is always the same independent of the adsorption of organic molecules or NaCl and is

---

[iv] The C1s contains several different chemical species, which could not be resolved in the XPS peak and consequently cannot be compared to literature values.

comparable to the literature value, which are also given in Table 5. Thus, we can conclude that the shift is not related to changes in the XPS set-up, like a change in the work function of the analyser. As already discussed in chapter 3.1.2 in equation 7 (page 11) several different parameters influence the effective binding energy: (i) the chemical shift, (ii) the Madelung term and (iii) external as well as (iv) internal relaxation of the photohole.

The fact that the binding energy of the C1s peak for the thick molecular layer and the thin layer on Cu(311) are approximately the same leads to the assumption that no chemical reaction between the CuOEP and the Cu(311) took place. In consequence, the shifts of the binding energy for the C1s and the N1s peak do not result from a chemical reaction and the term of ΔE_{chem} as shown in equation 7 can be neglected.

The Madelung term ΔE_{mad} is only relevant for the Cl2p and Na1s peak position because of the polar character of the NaCl. When looking for literature values of the Na1s peak for NaCl already a discrepancy of 1 eV has been found[146] (cf. Table 5). The main problem of determining the exact binding energies of bulk NaCl is charging, which occurs during the photoemission process. Due to the insulating character of bulk NaCl this charging has to be compensated by a constant electron flux from an electron flood-gun. Our experiments have been performed without a flood-gun and although tunnelling through the NaCl layer is possible, as seen in the STM images, a small charging of the surface may occur. Generally, it is always easier to compare relative peak shifts and relative intensities measured with the same set-up and similar samples than to quantitatively compare them with literature values.

The last factor to be discussed is the influence of the relaxation energies $\Delta E_{r,int}$ and $\Delta E_{r,ext}$ on the shift of the binding energies. The internal relaxation of the excited system usually takes place by filling the photoelectron hole with an electron from a higher orbital. This relaxation should be comparable for all systems discussed here because it is directly related to the carbon or nitrogen atom which emitted the photoelectron. A bigger difference is expected in the external relaxation factor $\Delta E_{r,ext}$ for the molecule on top of the NaCl layer and on the Cu surface. While the photoholes of the molecules, which are directly adsorbed on the metal surface, are well screened by the high polarizability of the metal, the photoholes on top of the NaCl, which has a considerable smaller polarizability, are less well screened. Thus, we conclude that the big shifts in the binding energies of the C1s and the N1s mostly result from different screening effects. This different screening is also slightly visible for the N1s peak in the thick CuOEP layer. Here a shift of 0.25 eV could be observed due to the reduced polarizability of the CuOEPs compared to the metal substrate.

5.4 Summary and outlook

In summary, we have shown that by adjusting the insulator/substrate system it is possible to grow homogenous layers of NaCl on metal surfaces. In the here reported case the most homogenous insulator layers could be obtained for NaCl on the stepped Cu(311) surface, which exhibits a charge corrugation due to Smoluchowski smoothing effect and thus enhances the interaction of the insulator with the metal substrate. It could be shown that more than 80% of the Cu(311) surface is covered with NaCl before the second layer starts to grow. Homogenous layers of insulators are necessary to investigate the electronic interactions of organic molecules with insulator and metal substrates in dependence of the NaCl layer thickness with averaging techniques like XPS, UPS and NEXAFS.

Furthermore, we investigated the electronic states of CuOEP on Ag(111) with LT-STS. A new feature in the unoccupied states near the Fermi energy has been observed and the intensity of this feature strongly depends on the exact position of the tip with respect to the molecule. This feature is more pronounced when the spectra are taken above of the octa-ethyl substituents compared to the position above of the Cu-centre of the molecules, which indicates that the density of states is not homogenously distributed over the CuOEP molecule. This observation of a new electronic state near the Fermi energy gives rise to several questions. (i) Is this state also visible on other metal surfaces like Cu(111) or Au(111)? The molecular/substrate interaction is expected to change and influence this state. (ii) Does this state derive from a partial charge transfer from the HOMO to the metal surface? (iii) Is this electronic state also present for CuOEP on NaCl? To solve these questions additional measurements like STS on CuOEP/Cu(111), CuOEP/Au(111) and CuOEP/NaCl/Ag(111) are necessary. Further analysis techniques, like inverse photoemission and NEXAFS, combined with theoretical calculations may help to gain a deeper insight into the nature of these near Fermi level states.

UPS and XPS measurements of the OEPs have been performed on Cu(311) and NaCl/Cu(311) because for this system it was possible to grow a homogenous NaCl layer. The photoemission measurements revealed another difficulty in determining the electronic states of the CuOEP on the ultrathin insulator as well as on the metal substrate. The gap between the HOMO of the CuOEP molecule and the Fermi energy is larger than 2 eV; consequently the HOMO is overlapping with the Cu3d band, which starts at approximately 2 eV below the Fermi energy. Due to the significant contribution of the metal states for small molecular coverages it was not possible to subtract the Cu3d band from the measured spectra of 0.8 ML of CuOEP on Cu(311). Thus, to further investigate the electronic interaction of organic molecules with metals and ultrathin insulators, a molecule/insulator/substrate system has to be found where either the HOMO of the molecules is closer to the Fermi energy or where the substrate band is further away from the Fermi energy. A possible system for which the HOMO of the molecules is closer to the Fermi energy is CoOEP, where the HOMO derives

from the partly filled Co d_{z^2}-state[145] and thus is only 0.8 eV below E_F (cf. Figure 31b). Another possibility would be to use a silver substrate where the d-band starts at approximately 4 eV below the Fermi energy. Though, for this system an insulator which is growing in a Stransky-Krastanov or Frank van der Merwe mode would be necessary to get homogenous surfaces. To date, only the growth of NaCl on Ag(1 1 19) has been investigated and it is reported that the surface is only completely covered at thicknesses larger than 4 ML[148].

Nevertheless, it was possible to determine the occupied molecular states of a thick layer of CuOEP on Cu(311) and for 1 ML of CuOEP on NaCl. It was found that the states are shifted by approximately 0.8 eV for adsorption on the NaCl. This shift has been related to screening effects as also shown for the XPS peak shifts in chapter 5.3.3. These screening effects, which are always present when creating a photohole, complicate the comparison of UPS data of molecules on metals and molecules on ultrathin insulators. Either the shift due to the screening effect can be calculated or additional STS measurements should be performed to determine the HOMO and LUMO position of the molecules depending on the insulator layer thickness. By comparing STS measurements with UPS, IPES and NEXAFS experiments it may be even possible to quantify this screening which would be very helpful in context of other systems because we assume that screening is not only valid for molecules on insulators but also for the comparison of monolayers and multilayers of adsorbates, as also seen by the shift of the N1s peak for a monolayer compared to a multilayer of CuOEP.

6 Concluding remarks

The electronic interaction of semiconducting organic molecules with metals, oxidized metals and insulator surfaces has been studied. By the combination of complementary surface sensitive analysis techniques, it has been possible to study the relationship of structural and electronic properties. For example, the direct imaging of adsorbates via STM combined with measurements of the substrate electronic states by ARPES led to a very unique observation for the pentacene/Cu(110) system: An increase of the anisotropy of the surface state which has been attributed to an increase of the packing density along one distinct direction.

The goal of this study has been the investigation and tuning of the electronic interactions of organic semiconductors with various substrates. In a first step, a highly interacting system – pentacene/Cu(110) – has been investigated. It could be shown that the specific molecular/substrate and intermolecular interactions lead to a complex phase behaviour as well as to a change of the Shockley surface state of the Cu(110) surface. Such strongly interacting interfaces can be found in devices like field-effect transistors at the drain and source contacts and strongly influence the charge injection of such devices. This strong adsorbate/substrate interaction could be reduced by oxidation of the Cu(110) surface. The interaction of pentacene with the oxidized Cu(110) is strong enough to immobilize the molecules and results in a flat adsorption geometry of the pentacene molecules but it is weaker than the interaction between the molecules and the clean Cu(110). By exposure of oxygen to a partly pentacene covered Cu(110) surface the intermolecular interactions can be reduced by adsorption of CuO rows in-between the pentacene molecules, while the molecule/substrate interactions remain unchanged. The consequent decoupling of neighbouring molecules may provide an interesting case in the context of single molecular electronics.

A further step to reduce the adsorbate/substrate interactions is the adsorption of organic molecules on ultrathin insulator films. Understanding the mechanisms leading to the well ordered structures observed here may lead to gate/semiconductor interfaces with less defects and consequently to a better performance of the electronic device. For this study the growth of alkali halide thin films has been improved to provide homogenous insulating layers, i.e. samples mostly covered with 1 ML of NaCl while limiting the coverage of second layer islands. Such homogeneous samples are a prerequisite to study electronic adsorbate/adsorbent interactions with non-local techniques like UPS and NEXAFS and to compare the results to local studies like STM and STS. The UPS data on CuOEP on 1 ML of NaCl and of a thick layer of CuOEP on Cu(311) show the same shape while the whole spectrum is observed to be shifted by approximately 0.8 eV to higher binding energies for CuOEP on NaCl. This rigid shift of the electronic states of the CuOEP is related to the different screening of the photohole by the chemically different environment. Such screening effects may also play a role in the electron transport in electronic devices.

6 CONCLUDING REMARKS

In conclusion, we have been able to specifically modify the organic semiconductor/substrate interface for the study of model systems which differ in their electronic interaction strength. A comparative study of these systems with local and non-local probes including surface conductivity measurements seems to be possible and can lead to a better understanding of such interface also in the context of device performance.

Bibliography

[1] H. Hoppe, N.S. Sariciftci, *Organic solar cells: An overview*, J. Mater. Res. **19**, 1924 (2004).

[2] C.W. Tang, S.A. VanSlyke, *Organic electroluminescent diodes*, Appl. Phys. Lett. **51**, 913 (1987).

[3] R. McNeill, R. Siudak, J.H. Wardlaw, D.E. Weiss, *Electronic conduction in polymers*, Aust. J. Chem., **16**, 1056 -1103 (1963).

[4] D.A. Muller, T. Sorsch, S. Moccio, F.H. Baumann, K. Evans-Lutterodt, G. Timp, *The electronic structure at the atomic scale of ultrathin gate oxides*, Nature **399**, 758 (1999).

[5] M. Schulz, *The end of the road for silicon?*, Nature **399**,729 (1999).

[6] http://download.intel.com/technology/architecture-silicon/32nm/IEDM_2008_32nm_paper.pdf (April 2009).

[7] B. Yu, M. Meyyappan, *Nanotechnology: Role in emerging nanoelectronics*, Solid-State Electronics **50**, 536 (2006).

[8] G.H. Gelinck, H.E.A. Huitema, E. van Veenendaal, E. Cantatore, L. Schrijnemakers, J.B.P.H. Van der Putten, T.C.T. Geuns, M. Beenhakkers, J.B. Giesbers, B.-H. Huisman, E.J. Meijer, E.M. Benito, F.J. Touwslager, A.W. Marsman, B.J.E. van Rens, D.M. de Leeuw, *Flexible active-matrix displays and shift registers based on solution-processed organic transistors*, Nature Materials **3**, 106 (2004).

[9] C. Di, G. Yu, Y. Liu, D. Zhu, *High-performance organic field-effect transistors: molecular design, device fabrication and physical properties*, J. Phys. Chem. B **111**, 14083 (2007).

[10] M. Kitamura, Y. Arakawa, *Pentacene-based organic field-effect transistors*, J. Phys.: Condens. Matter **20**, 1 (2008).

[11] S.Y. Yang, K. Shin C.E. Park, *The effect of gate-dielectric surface energy on pentacene morphology and organic field-effect transistor characteristics*, Adv. Funct. Mater. **15**, 1806 (2005).

[12] C. Di, G. Yu, Y. Liu, X. Xu, D. Wei, Y. Song, Y. Sun, Y. Wang, D. Zhu, J. Liu, D. Wu, *High-performance low-cost organic field-effect transistors with chemically modified bottom electrodes*, J. Am. Chem. Soc, **128**, 16418 (2006).

[13] S. Lee, B. Koo, J. Sin, E. Lee, H. Park, *Effects of hydroxyl groups in polymeric dielectrics on organic transistor performance*, Appl. Phys. Lett. **88**, 162109 (2006).

[14] http://www.zyvex.com/nanotech/feynman.html (April 2009).

[15] G. Binnig, H. Rohrer, *Scanning tunneling microscopy*, Helvetica Physica Acta **55**, 762 (1982).

[16] I.-W. Lyo, P. Avouris, *Field-induced nanometer – to atomic – scale manipulation of silicon with the STM*, Science **253**, 173 (1991).

[17] D.M. Eigler, C.P. Lutz, W.E. Rudge, *An atomic switch realized with the scanning tunnelling microscope*, Science **352**, 600 (1991).

BIBLIOGRAPHY

[18] A.J. Heinrich, C.P. Lutz, J.A. Gupta, D.M. Eigler, *Molecule cascades*, Science **298**, 1381 (2002).

[19] J.-M. Lehn, *Supramolecular Chemistry-Scope and Perspectives Molecules, Supermolecules, and Molecular Devices (Nobel Lecture)*, Angew. Chem. Int. Ed. Engl. **27**, 89 (1988).

[20] G.M. Whitesides, J.P. Mathias, C.T. Seto, *Molecular self-assembly and nanochemistry: a chemical strategy for the synthesis of nanostructures*, Science **254**, 1312 (1991).

[21] J.D. Halley, D.A. Winkler, *Consistent concepts of self-organization and self-assembly*, Complexity **14**, 10 (2008).

[22] K. John M. Bär, *Alternative mechanisms of structuring biomembranes: self-assembly vs. self-organization*, Phys. Rev. Lett. **95**, 198101 (2005).

[23] L. Ramoino, M. von Arx, S. Schintke, A. Baratoff, H.-J. Güntherrodt, T.A. Jung, *Layer-selective epitaxial self-assembly of porphyrins on ultrathin insulators*, Chem. Phys. Lett. **417**, 22 (2006).

[24] A. Scheybal, K. Müller, R. Bertschinger, M. Wahl, A. Bendounan, P. Aebi, T. A. Jung, *Modification of the Cu(110) Shockley surface state by an adsorbed pentacene monolayer*, Phys. Rev. B 79, 115406 (2009).

[25] K. Müller, A. Kara, T.K. Kim, R. Bertschinger, A. Scheybal, J. Osterwalder, T. A. Jung, *Multimorphism in molecular monolayers: pentacene on Cu(110)*, Phys. Rev. B **79**, 245421 (2009).

[26] K. Müller, A. Kara, J. Osterwalder, T.A. Jung, *Pentacene adsorption on partly and fully oxygen covered Cu(110) surface*, manuscript in preparation.

[27] http://www.siliconfareast.com/epitaxy.htm (April 2009).

[28] http://en.wikipedia.org/wiki/Thin_film (April 2009).

[29] Lecture notes: Physics of thin films, PES 449 / PHYS549, http://www.uccs.edu/~tchriste/courses/PHYS549/549lectures/index.html (April 2009).

[30] http://www.britannica.com/EBchecked/topic/421892/nucleation (April 2009).

[31] J. Repp, G. Meyer, S.M. Stojkovic, A. Gourdon, C. Joachim, *Molecules on insulating films: scanning-tunneling microscopy imaging of individual molecular orbitals*, Phys. Rev. Lett. **94**, 026803 (2005).

[32] B. Hulsken, R. Van Hameren, J.W. Gerritsen, T. Khoury, P. Thordarson, M.J. Crossley, A.E. Rowan, R.J.M. Nolte, J.A.A.W. Elemans, S. Speller, *Real-time single-molecule imaging of oxidation catalysis at a liquid-solid interface*, Nature Nanotechnology **2**, 285 (2007)

[33] S.-W. Hla, L. Bartels, G. Meyer, K.-H. Rieder, *Inducing All Steps of a Chemical Reaction with the Scanning Tunneling Microscope Tip: Towards Single Molecule Engineering*, Phys. Rev. Lett. **85**, 2777 (2000).

[34] C.J. Chen, *Introduction to Scanning tunnelling microscopy*, second edition, Oxford University Press, New York, 2008.

[35] D.A. Bonnell, *Scanning Tunneling Microscopy and Spectroscopy*, VCH, 1993.

[36] R. Berndt, *Rastertunnelspektropskopie am Beispiel von Oberflächenzuständen*, 29. Ferienkurs des Instituts für Festkörperphysik, 1998.

[37] S. Hüfner, *Photoelectron Spectroscopy principles and applications*, Springer-Verlag Berlin Heidelberg, 2003

[38] H. Hertz, *Über einen Einfluss des ultravioletten Lichtes auf die elektrische Entladung*, Ann. Physik **267**, 983 (1887).

[39] A. Einstein, *Über einen die Erzeugung und Verwandlung des Lichtes betreffenden heuristischen Gesichtspunkt*, Ann. Physik **322**, 132 (1905).

[40] M. Henzler, W. Göpel, *Oberflächenphysik des Festkörpers*, Teubner Stuttgart, 1994.

[41] U. Gelius, P.F. Heden, J. Hedman, B.J. Lindberg, R. Manne, R. Nordberg, C. Nordling, K. Siegbahn, *Molecular Spectroscopy by Means of ESCA*, Phys. Scr. *2*, 70 (1970).

[42] P. Hofmann, *Lecture Notes on Surface Science*, University of Århus, 2005.

[43] www.mateck.de (May 2009).

[44] I. Horcas, R. Fernandez, J.M. Gomez-Rodriguez, J. Colchero, J. Gomez-Herrero, A.M. Baro, *WSXM: A software for scanning probe microscopy and a tool for nanotechnology*, Rev. Sci. Instrum. **78**, 013705 (2007).

[45] http://www.taica.co.jp/gel-english/alpha/index.html (February 2009).

[46] http://apps.isiknowledge.com/ search for "*pentacene*" performed on 5th of April 2009.

[47] M. Ahles, R. Schmechel, H. von Seggern, *n-type organic field-effect transistor based on interface-doped pentacene*, Appl. Phys. Lett. **85**, 4499 (2004).

[48] P. Parisse, S. Picozzi, M. Passacantando, L. Ottviano, *Experiments and theory on pentacene in the thin film phase: structural, electronic, transport properties, and gas response to oxygen, nitrogen, and ambient air*, Thin Solid Films, **515**, 8316 (2007).

[49] G.E. Thayer, J.T. Sadowski, F. Meyer zu Heringdorf, T. Sakurai, R.M. Tromp, *Role of surface electronic structure in thin film molecular ordering*, Phys. Rev. Lett. **95**, 256106 (2005).

[50] S. Lukas, G. Witte, Ch. Wöll, *Novel mechanism for molecular self-assembly on metal substrates: Unidirectional rows of pentacene on Cu(110) produced by a substrate-mediated repulsion*, Phys. Rev. Lett. **88**, 028301 (2002).

[51] S. Söhnchen, S. Lukas, G. Witte, *Epitaxial growth of pentacene films on Cu(110)*, J. Chem. Phys. **121**, 525 (2004).

[52] Q. Chen, A.J. Macdowall, N.V. Richardson, *Ordered structures of tetracene and pentacene on Cu(110) surfaces*, Langmuir **19**, 10164 (2003).

[53] L. Gavioli, M. Ranetti, D. Pasca, M. Padovani, M. Sancrotti, M.G. Betti, *Quasi-1D pentacene structures assembled on the vicinal Cu(119) surface*, Surf. Sci. **566-568**, 624 (2004)

[54] L. Casakux, M.F. Danisman, B. Nickel, G. Bracco, T. Toccoli, S. Ianotta, G. Scoles, *Hyperthermal molecular beam deposition of highly ordered organic thin films*, Phys. Rev. B **90**, 206101 (2003).

BIBLIOGRAPHY

55 C.B. France, P.G. Schroeder, J.C. Forsythe, B.A. Parkinson, *Scanning tunneling microscopy study of the coverage-dependent structures of pentacene on Au(111)*, Langmuir **19**, 1274 (2003).

56 O. McDonald, A.A. Cafolla, D. Carty, G. Sheerin, G. Hughes, *Photoemission, NEXAFS and STM studies of pentacene thin films on Au(100)*, Surf. Sci. **600**, 3217 (2006).

57 G. Bavdek, A. Cossaro, D. Cvetko, C. Africh, C. Blasetti, F. Esch, A. Morgante, L. Floreano, *Pentacene Nanorails on Au(110)*, Langmuir, **24**, 767 (2008).

58 A. Ferretti, C. Baldacchini, A. Calzolari, R. Di Felice, A. Ruini, E. Molinari, M.G. Betti, *Mixing of electronic states in pentacene adsorption on copper*, Phys. Rev. Lett. **99,** 046802 (2007).

59 P.G. Schroeder, C.B. France, J.B. Park, B.A. Parkinson, *Energy level alignment and two-dimensional structure of pentacene on Au(111) surfaces*, J. Appl. Phys. **91**, 3010 (2002).

60 G. Horowitz, *Organic field-effect transistors*, Adv. Mater., **10**, 365 (1998).

61 B. Crone, A. Dodabalapur, Y.-Y- Lin, R.W. Filas, Z. Bao, A. LaDuca, R. Sarpeshkar, H.E. Katz, W. Li, *Large-scale complementary integrated circuits based on organic transistors*, Nature, **403**, 521 (2000).

62 M. Daraktchiev, A. von Mühlenen, F. Nüesch, M. Schaer, M. Brinkmann, M-N. Bussac, L. Zuppiroli, *Ultrathin organic transistors on oxide surfaces*, New J. Phys., **7**, 133 (2005).

63 C. Goldmann, D.J. Gundlach, B. Batlogg, *Evidence of water-related discrete trap state formation in pentacene single-crystal field-effect transistors*, Appl. Phys. Lett., **88**, 063501 (2006).

64 K.P. Pernstich, D. Oberhoff, C. Goldmann, B. Batalogg, *Modeling the water related trap state created in pentacene transistors*, Appl. Phys. Lett., **89**, 213509 (2006).

65 A. Vollmer, O.D. Jurchescu, I. Arfaoui, I. Salzmann, T.T.M. Palstra, P. Rudolf, J. Niemax, J. Pflaum, J.P. Rabe, N. Koch, *The effect of oxygen exposure on pentacene electronic structure*, Eur. Phys J. E **17**, 339 (2005).

66 Y. Hu, G. Dong, Y. Hu, L. Wang, Y. Qiu, *Oxygen effect on the electrical characteristics of pentacene transistors*, J. Phys. D: Appl. Phys., **39**, 4553 (2006).

67 L. Tsetseris, S.T. Pantelides, *Intercalation of oxygen and water molecules in pentacene crystals: First-principles calculations*, Phys. Rev. B, **75**, 153202 (2007).

68 W.L. Kalb, K. Mattenberger, B. Batlogg, *Oxygen-related traps in pentacene thin films: Energetic position and implications for transistor performance*, Phys. Rev. B **78**, 035334 (2008).

69 K.S. Teng, P.R. Dunstan, S.P. Wilks, R.H. Williams, *STM/STS investigation of the interaction of Si with atomic scale vacancies on cleaved GaAs*, Appl. Surf. Sci. **235**, 313 (2004).

70 H.W.M. Salemink, O. Albrektsen, P. Koenraad, *Tunneling spectroscopy across GaAs/Al$_x$Ga$_{1-x}$As interfaces at nanometer resolution*, Phys. Rev. B **45**, 6946 (1992).

71 N. Koch, *Energy levels at interfaces between metals and conjugated organic molecules*, J. Phys.: Condens. Matter 20, 184008 (2008).

[72] S. De Feyter and F.C. De Schryver, *Two-dimensional supramolecular self-assembly probed by scanning tunneling microscopy*, Chem. Soc. Rev. **32**, 139 (2003).

[73] A. Scarfato, S.-H. Chang, S. Kuck, J. Brede, G. Hoffmann, R. Wiesendanger, *Scanning tunneling microscope study of iron(II) phthalocyanine growth on metals and insulating surfaces*, Surf. Sci. **602**, 677 (2008).

[74] H. Rauscher, T.A. Jung, J.-L. Lin, A. Kirakosian, F.J. Himpsel, U. Rohr, K. Müllen, *One-dimensional confinement of organic molecules via selective adsorption on CaF$_1$ versus CaF$_2$*, Chem. Phys. Lett. **303**, 363 (1999).

[75] F. Cicoira, J.A. Miwa, M. Melucci, G. Barbarella, F. Rosei, *Ordered assembly of α-Quinquethiophene on a copper oxide nanotemplate*, Small **2**, 1366 (2006).

[76] M. Oehzelt, L. Grill, S. Berkebile, G. Goller, F.P. Netzer, M.G. Ramsey, *The molecular orientation of para-Sexiphenyl on Cu(110) and Cu(110) p(2×1)O*, ChemPhysChem **8**, 1707 (2007).

[77] R. Otero, Y. Naitoh, F. Rosei, P. Jiang, P. Thostrup, A. Gourdon, E. Lægsgaard, I. Stensgaard, C. Joachim, F. Besenbacher, *One-dimensional assembly and selective orientation of Lander molecules on an O-Cu template*, Angew. Chem.. Int. Ed. **43**, 2092 (2004).

[78] M. Koini, T. Haber, O. Werzer, S. Berkebile, G. Koller, M. Oehzelt, M.G. Ramsey, R. Resel, *Epitaxial order of pentacene on Cu(110)–(2 × 1)O: One dimensional alignment induced by surface corrugation*, thin solid films **517**, 483 (2008).

[79] L.D. Sun, M. Hohage, R. Denk, P. Zeppenfeld, *Oxygen adsorption on Cu(110) at low temperature*, Phys. Rev. B **76**, 245412 (2007).

[80] K. Kern, H. Niehus, A. Schatz, P. Zeppenfeld, J. Goerge, G. Comsa, *Long-range spatial self-organization in the adsorbate-induced restructuring of surfaces: Cu{100}-(2×1)O*, Phys Rev Lett. **67**, 855 (1991).

[81] M. Karimi, T. Tomkowski, G.Vidali, O. Biham, *Diffusion of Cu on Cu surfaces*, Phys, Rev. B **52**, 5364 (1995).

[82] H. Yildirim, A. Kara, S. Durukanoglu, T.S. Rahman, *Calculated pre-exponential factors and energetics for adatom hopping on terraces and steps of Cu(1 0 0) and Cu(1 1 0)*, Surf. Sci. **600**, 484 (2006).

[83] N. Hartmann, R.J. Madix, *Growth and ordering of Cu-O islands during oxygen adsorption on Cu(110) at 470 K*, Surf. Sci. **488**, 107 (2001).

[84] Y. Kuk, F.M. Chua, P.J. Silverman, J.A. Meyer, *O chemisorption on Cu(110) by scanning tunneling microscopy*, Phys. Rev. B **41**, 12393 (1990).

[85] F. Cicoira, J.A. Miwa, D.F. Perpichka, F.Rosei, *Molecular assembly of Rubrene on a metal/metal oxide nanotemplate*, J. Phys Chem. A **111**, 12674 (2007).

[86] K. Lee, J. Yu, *Ab initio study of pentacene on Au(0 0 1) surface*, Surf. Sci. **589**, 8 (2005).

[87] P. Cortona, C. Sapet, *Electronic structure of the Cu(1 1 0)-p(2×1)O surface by the semi-empirical LCAO method*, Surf. Sci. **566-568**, 1102 (2004).

[88] Y.K. Jeong, G.M. Choi, *Nonstoichiometry and electrical conduction of CuO*, J. Phys. Chem. Solids **57**, 81 (1996).

BIBLIOGRAPHY

89   A. Galtayries, J. Grimblot, J.-P. Bonnelle, *Interaction of SO_2 with different polycrystalline Cu, Cu_2O and CuO surfaces*, Surf. Interface Anal. **24**, 345-354 (1996).

90   D.J. Coulman, J. Wintterlin, R.J. Behm, G. Ertl, *Novel mechanism for the formation of chemisorption phases: The (2x1)O-Cu(110) "added-row" reconstruction*, Phys. Rev. Lett. **64**, 1761 (1990).

91   F. Jensen, F. Besenbacher, E. Læsgaard, I. Stensgaard, *Surface reconstruction of Cu(110) induced by oxygen chemisorption*, Phys. Rev. B **41**, 10322 (1990).

92   S.Y. Liem, G. Kresse, J.H.R. Clarke, *First principles calculation of oxygen adsorption and reconstruction of Cu(110) surface*, Surf. Sci. **415**, 194 (1998).

93   F. Besenbacher, F. Jensen, E. Læsgaard, K. Mortensen, I. Stensgaard, *Visualization of the dynamics in surface reconstructions*, J. Vac. Tech. B **9**, 874 (1991).

94   J. Witterlin, R, Schuster, D.J. Coulman, G. Ertl, *Atomic motion and mass transport in the oxygen induced reconstructions of Cu(110)*, J. Vac. Tech. B **9**, 902 (1991).

95   R. Courths, S. Hüfner, P. Kemkes, G. Wiesen, *Electronic structures investigation of Cu(110), Ag(110) and Ni(110) surfaces covered with chemisorbed oxygen up to half a monolayer*, Surf. Sci. **376**, 43 (1997).

96   C. H. Schwalb, S. Sachs, M. Marks, A. Schöll, F. Reinert, E. Umbach, U. Höfer, *Electron lifetime in a Shockley-type metal-organic interface state*, Phys. Rev. Lett. **101**, 146801 (2008).

97   N. Wintjes, D. Bonifazi, F.Y. Cheng, A. Kiebele, M. Stöhr, T.A. Jung, H. Spillmann, F. Diederich, *A supramolecular multiposition rotary device*, Angew. Chem. Int. Ed. **46**, 4089 (2007).

98   W.J.M. Naber, S. Faez, W.G. van der Wiel, *Organic spintronics*, J. Phys. D: Appl. Phys. **40**, R205 (2007).

99   G. Binnig, C. Quate, C. Gerber, *Atomic force microscope*, Phys. Rev. Lett. **56**, 930.

100   F.J. Giessibl, *Atomic resolution of the Silicon (111)-(7x7) surface by atomic force microscopy*, Science **267**, 68 (1995).

101   R. Bennewitz, *Structured surfaces of wide band gap insulators as templates for overgrowth of adsorbates*, J. Phys.: Condens. Matter **18**, R417 (2006).

102   S. Burke, J.M. Mativetsky, S. Fostner, P. Grütter, *C_{60} on alkali halides: Epitaxy and morphology studied by noncontact AFM*, Phys. Rev. B **76**, 035419 (2007).

103   L. Nony, R. Bennewitz, O. Pfeiffer, E. Gnecco, A. Baratoff, E. Meyer, T. Eguchi, A. Gourdon, C. Joachim, *Cu-TBPP and PTCDA molecules on insulating surfaces studied by ultra-high-vacuum non-contact AFM*, Nanotechnology **15**, S91 (2004).

104   L. Nony, E. Gnecco, A. Baratoff, A. Alkauskas, R. Bennewitz, O. Preiffer, S. Maier, A. Wetzel, E. Meyer, Ch. Gerber, *Observation of individual molecules trapped on a nanostructured insulator*, Nano Letters **4**, 2185 (2004).

105   J.M. Mativetsky, S.A. Burke, S. Fostner, P. Grütter, *Templated growth of 3,4,9,10-perylenetetracarboxylic dianhydride molecules on a nanostrcutred insulator*, Nanotechnology **18**, 105303 (2007).

[106] T. Kunstmann, A. Schlarb, M. Fendrich, Th. Wagner, R. Möller, T. Hoffmann, *Dynamic force microscopy study of 3,4,9,10-perylenetetracarboxylic dianhydride on KBr*, Phys. Rev. B **71**, 121403 (2005).

[107] S.A. Burke, W. Ji, J.M. Mativetsky, J.M. Topple, S. Fostner, H.-J. Gao, H. Guo, P. Grütter, *Strain induced dewetting of a molcular system: bimodal growth of PTCDA on NaCl*, Phys. Rev. Lett. **100**, 186104 (2008).

[108] S. Schintke, W.-D. Schneider, *Insulators at the ultrathin limit: electronic structure studied by scanning tunnelling microscopy and spectroscopy*, J. Phys.: Condens. Matter **16**, R49 (2004).

[109] J. Viernov, D.Y. Tetrovykh, T.K. Men, A. Kirakosian, J.-L. Lin, F.J. Himpsel, *Linear arrays of CaF$_2$ nanostructures on Si*, Appl. Phys. Lett. **74**, 2125 (1999).

[110] T. Maroutian, S. Degen, C. Becker, K. Wandelt, R. Berndt, *Superstructures and coincidences of a thin oxide film on a metallic substrate: A STM study*, Phys. Rev. B **68**, 155414 (2003).

[111] R. Franchy, J. Masuch, P. Gassmann, *The oxidation of the NiAl(111) surface*, Appl. Surf. Sci. **93**, 317 (1996).

[112] X.H. Qiu, G.V. Nazin, W. Ho, *Vibrationally resolved fluroescence excited with submolecular precision*, Science **299**, 542 (2003).

[113] M. Bäumer, D. Kappus, H. Kuhlenbeck, H.-J. FrEund, G. Wilhelmi, A. Brodde, H. Neddermeyer, *The structure of thin NiO(100) films grown on Ni(100) as determined by low-energy-electron diffraction and scanning tunneling microscopy*, Surf. Sci. **253**, 116 (1991).

[114] T. Bertrams, H. Neddermeyer, *Growth of NiO(100) layers on Ag(100): characterization by scanning tunnelling microscopy*, J. Vac. Sci. Technol. B **14**, 1141 (1996).

[115] S. Schintke, S. Messerli, L. Libioulle, M. Pivetta, R. Patthey, M. Stengel, A. de Vita, W.-D. Schneider, *Insulator at the ultrathin limit: MgO on Ag(001)*, Phys. Rev. Lett. **87**, 276801 (2001).

[116] A. Chowdhury, J. Kumar, *Morphology, surface topography and optical studies on electron beam evaporated MgO thin films*, Bull. Mater. Sci., **29**, 513 (2006).

[117] M.F. Butman, A.A. Smirnov, L.S. Kudin, Z.A. Munir, *Mass-spectrometric study of the temperature variation in the dimer-to-monomer ration in the free-surface vaporization fluxes from alkali halide single crystals*, J. Mater. Synthesis Process. **8**, 93 (2000).

[118] J. Repp, G. Meyer, *Scanning tunnelling microscopy of adsorbates on insulating films. From the imaging of individual molecular orbitals to the manipulation of the charge state*, Appl. Phys. A **85**, 399 (2006).

[119] L. Ramoino, S. Schintke, A. Alkauskas, M. von Arx, A. Baratoff, H.-J. Güntherodt, *Molecular adsorption geometry and tunneling voltage-dependent imaging of ethyl side groups: copper octaethylporphyrin adsorbed on metals and ultrathin insulators*, manuscript in preparation.

[120] P. Liljeroth, J. Repp, G. Meyer, *Current-induced hydrogen tautomerization and conductance switching of naphthalocyanine molecules*, Science **317**, 1203 (2007).

BIBLIOGRAPHY

[121] J. Repp, G. Meyer, F.E. Olsson, M. Persson, *Controlling the charge state of individual gold adatoms*, Science **305**, 493 (2004).

[122] F.E. Olsson, S. Paavilainen, M. Persson, J. Repp, G. Meyer, *Multiple charge states of Ag atoms on ultrathin NaCl films*, Phys. Rev. Lett. **98**, 176803 (2007).

[123] E. Ćavar, M.-C. Blüm, M. Pivetta, F. Patthey, M. Chergui, W.-D. Schneider, *Fluorescence and phosphorescence from individual C_{60} molecules excited by local electron tunneling*, Phys. Rev. Lett. **95**, 196102 (2005).

[124] F.J. Himpsel, U.O. Karlsson, J.F. Morar, D. Rieger, J.A. Yarmoff, *Determination of interface states for CaF_2/Si(111) from near-edge x-ray-absorption measurements*, Phys. Rev. Lett. **56**, 1497 (1986).

[125] L. Ramoino, Thesis, *Adsorption and self-organization of CuOEP on heterogeneous surfaces: tuning the molecule-substrate interaction*, University of Basel, 2005.

[126] Z. Fang, *Temperature dependence of interatomic separation for alkali halides*, Phys. Stat. Sol. (b), **241**, 2886 (2004).

[127] http://www.engineeringtoolbox.com/linear-expansion-coefficients-d_95.html (March 2009)

[128] W. Hebenstreit, J. Reinger, Z. Horozova, M. Schmid, R. Podloucky, P. Varga, A*tomic resolution by STM on ultra-thin films of alkali halides: experiment and local density calculations*, Surf. Sci. **424**, L321 (1999).

[129] J. Repp, G. Meyer, K.H. Rieder, *Snell's law for surface electrons: refraction of an electron gas imaged in real space*, Phys. Rev. Lett. **92**, 036803 (2004).

[130] K. Glöckler, M. Sokolowski, A. Soukopp, E. Umbach, *Initial growth of insulating overlayers of NaCl on Ge(100) observed by scanning tunneling microscopy with atomic resolution*, Phys. Rev. B **54**, 7705 (1996).

[131] M. Kiguchi, K. Saiki, T. Sasaki, *Heteroepitaxial growth of LiCl on Cu(001)*, Phys. Rev. B **63**, 205418 (2001).

[132] M. Kiguchi, S. Entani, K. Saiki, H. Inoue, A. Koma, *Two types of epitaxial orientations for growth of alkali halide on fcc metal substrates*, Phys. Rev. B **66**, 15424 (2002).

[133] P.K. de Boer, R.A. de Groot, *The origin of the conduction band in table salt*, Am. J. Phys. **67**, 443 (1999).

[134] J. Repp, Thesis, *Rastertunnelmikroskopie und -spektroskopie an Adsorbaten auf Metall und Isolatoroberflächen*, Freie Universität Berlin (2002).

[135] M. Pivetta, F. Patthey, M. Stengel, A. Baldereschi, W.-D. Schneider, *Local work function Moiré pattern on ultrathin ionic films: NaCl on Ag(100)*, Phys. Rev. B**72**, 115404 (2005).

[136] J. Repp, S. Fölsch, G. Meyer, K.-H. Rieder, *Ionic films on vicinal metal surfaces: enhanced binding due to charge modulation*, Phys. Rev. Lett. **86**, 252 (2001).

[137] R. Smoluchowski, *Anisotropy of the electronic work function of metals*, Phys. Rev. **60**, 661 (1941).

[138] S. Fölsch, A. Helms, A. Riemann, J. Repp, G. Meyer, K.H. Rieder, *Nanoscale surface patterning by adsorbate-induced faceting and selective growth: NaCl on Cu(211)*, Surf. Sci. **497**, 113 (2002).

90

[139] J. Kliewer, R. Berndt, E.B. Chulkov, W.M. Silikin, P.M. Echenique, S. Crampin, *Dimensionality effects in the lifetime of surface states*, Science **288**, 1399 (2000).

[140] A. Alkauskas, L. Ramoino, S. Schintke, M. von Arx, A. Baratoff, H.-J. Gntherodt, T.A. Jung, *Energy level alignment at metal−octaethylporphyrin interfaces*, J. Phys. Chem. B **109**, 23558 (2005).

[141] N. Nicoara, E. Román, J.M. Gómez-Rivas, J.A. Martín-Gago, J. Méndez, *Scanning tunneling and photoemission spectroscopies at the PTCDA/Au(1 1 1) interface*, Org. Electron. **7**, 287 (2006).

[142] H. Morgner, *Analysis of MIES and UPS data of LiF and NaCl*, Surf. Sci. **420**, 95 (1999).

[143] C. Tegenkamp, H. Pfnür, *Correlation of electronic and local structure of 4-hydroxy-thiopehnol on NaCl (100) and Ag(100)*, J. Chem. Phys. **118**, 7578 (2003).

[144] A. Rosa, E.J. Baerends, *Metal-macrocycle interaction in phthalocyanines: density functional calculations of ground and excited states*, Inorg. Chem. **33**, 584 (1994).

[145] X. Lu, K.W. Hipps, X.D. Wang, U. Mazur, *Scanning tunneling microscopy of metal phthalocyanines: d^7 and d^9 cases*, J. Am. Chem. Soc. **118**, 7197 (1996).

[146] J.F. Moulder, W.F. Stickle, P.E. Sobol, K.D. Bomben, *Handbook of X-ray photoelectron spectroscopy*, Perkin-Elmer Corporation (1992).

[147] D.H. Karweik, N. Winograd, *Nitrogen charge distributions in free-base porphyrins, metalloporphyrins, and their reduced analogues observed by x-ray photoelectron spectroscopy*, Inorganic Chemistry **15**, 2336 (1976).

[148] J. Kramer, C. Tegenkamp, H. Pfnür; *The growth of NaCl on flat and stepped silver surfaces*, J. Phys.: Condens. Matter **15**, 6473 (2003).

Acknowledgements

List of publications

Publications:

J. Wloka, **K. Müller**, P. Schmuki: *Pore Morphology and Self-Organization Effects during Etching of n-Type GaP (100) in Bromide Solutions*; Electrochemical and Solid State Letters 8, B72-B75 (2005).

K. Müller, J. Wloka, P. Schmuki: *Novel Pore Shape and Self-Organization Effects in n-GaP(111)*; Solid State Electrochemistry 13, 807 (2009).

A. Scheybal, **K. Müller**, R. Bertschinger, M. Wahl, A. Bendounan, P. Aebi, T.A. Jung: *Modification of the Cu(110) Shockley Surface State by an Adsorbed Pentacene Monolayer*; Phys. Rev. B **79**, 115406 (2009).

K. Müller, A. Kara, T.K. Kim, R. Bertschinger, A. Scheybal, J. Osterwalder, T.A. Jung: *Multimorphism in molecular monolayers: pentacene on Cu(110)*; Phys. Rev. B **79**, 245421 (2009).

J. Lobo-Checa, M. Matena, **K. Müller**, J.H. Dil, F. Meier, L.H. Gade, T.A. Jung, M. Stöhr: *Surface state confinement imposed by a supramolecular porous network: Band formation from coupled quantum wells*; Science, **325**, 300 (2009).

K. Müller, A. Kara, J. Osterwalder, T.A. Jung: *Pentacene adsorption on partly and fully oxygen covered Cu(110) surface*; manuscript in preparation

K. Müller, A. Kara, J. Osterwalder, T.A. Jung: *Oxygen induced condensation and phase transformation of pentacene on Cu(110)*; manuscript in preparation

A. Kara, **K. Müller**, T. Brugger, T. Greber, T.A. Jung: *Chemisorption of Pentacene on Cu(110): DFT and experimental investigations*; manuscript in preparation.

Conference Presentations:

K. Müller, A. Scheybal, R. Bertschinger, M. Wahl, A. Bendounan, P. Aebi, T.A. Jung; Modification of the Cu(110) Shockley Surface State by an Adsorbed Pentacene Monolayer; talk at International Conference of Nanoscience and Technology 2007, July 2007, Stockholm Sweden.

K. Müller, A. Scheybal, , R. Bertschinger, A. Bendounan, T.K. Kim, M. Wahl, P. Aebi, T. A. Jung; Molecular Self-Assembly and Electronic Coupling of Pentacene on Cu(110); invited talk at SLS Symposia on Low Dimension Systems, July 1st 2008, Villigen, Switzerland.

K. Müller, A. Kara, A. Scheybal, R. Bertschinger, T.K. Kim, J. Osterwalder, T. A. Jung; Coverage Dependent Phase Behavior of Pentacene Monolayers on Cu(110); talk at International Conference of Nanoscience and Technology 2008, July 2008 Keystone Colorado, USA.

K. Müller, A. Kara, R. Bertschinger, A. Scheybal, J. Osterwalder, T.A. Jung: Oxygen induced condensation and phase transformation of pentacene on Cu(110); talk at 17th ISSC 30th March – 2nd April 2009, Reading UK.

K. Müller, R. Bertschinger, A. Scheybal and T.A. Jung, Multiphase adsorption and layering of pentacene on Cu(110); poster at SPG Annual meeting 2006, February 13th – 14th, Lausanne, Switzerland.

K. Müller, R. Bertschinger, A. Scheybal and T.A. Jung; Control of the self-organization of a pentacene ad-layer by post deposition of oxygen; poster at SAOG 23rd Annual Meeting 2007, January 26th, Fribourg, Switzerland.

K. Müller, R. Bertschinger, A. Scheybal and T.A. Jung; Control of the self-organization of a pentacene ad-layer by post deposition of oxygen; poster at SPG Annual meeting 2007, February 20th – 21st, Zurich, Switzerland.

K. Müller, A. Scheybal, R. Bertschinger and T.A. Jung Modification of the Cu(110) Shockley surface state by an adsorbed pentacene monolayer; poster at SPG Annual meeting 2007, February 20th – 21st, Zurich, Switzerland.

Curriculum vitae

Name: Kathrin Müller
Birth: 04.06.1980, Ansbach, Germany
Nationality: German

Education:
1990-2000:   Platen-Gymnasium Ansbach, Germany
June 2000:   Abitur
2000-2005:   Studies of material science at University Erlangen,
2005:   Diploma work at the chair of corrosion and surface science
               Thesis Title: „*Untersuchungen zum Wachstum selbstorganisierter Poren in Galliumphosphid*" Supervisior: Prof. Dr. Patrik Schmuki
Since October 2005:   Employed as PhD student at the Paul Scherrer Institut, Villigen
May 2009:   PhD thesis; title: "*Organic Semiconductor Interfaces with Insulators and Metals*";
               Supervisors: Prof. Dr. Jürg Osterwalder, Dr. Thomas A. Jung,

Teaching experience:
2002-2005   Student assistant at the mathematical institute tutoring exercise courses
2005-2008   Tutor in practical courses: physics for medicine students

Languages:
               German (mother tongue)
               English (fluent)
               Italian (Unicert II)
               French (basic knowledge)